

Modelling and Analysis on Helical Savonius Wind Turbine

A PROJECT REPORT

Submitted by

ABHIJITH KUSALAN (RIE17AN001)

AJAY R KRISHNAN (RIE17AN003)

ANANTHU SURESH (RIE17AN008)

NIVED SURESH LAL (RIE17AN023)

to

The APJ Abdul Kalam Technological University
In partial fulfillment of the requirements for the award of degree

of

Bachelor in Technology

In

Aeronautical engineering



Department of Aeronautical Engineering

Rajadhani Institute of Engineering and Technology
Attingal, Thiruvananthapuram.

JUNE 2021

DECLARATION

I undersigned hereby declare that the project report Modelling and Analysis on Helical Axis Wind Turbine, submitted for partial fulfilment of the requirements for the award of degree of Bachelor of Technology of the APJ Abdul Kalam Technological University, Kerala is a bonafide work done by our team directly under the supervision of Dr. ThamaraiKannan S. This submission represents our ideas in our own words and where ideas or words of others have been included, we have adequately and accurately cited and referenced the original sources. We also declare that we have adhered to ethics of academic honesty and integrity and have not misrepresented or fabricated any data or idea or fact or source in our submission. We understand that any violation of the above will be a cause for disciplinary action by the institute and/or the University and can also evoke penal action from the sources which have thus not been properly cited or from whom proper permission has not been obtained. This report has not been previously formed the basis for the award of any degree, diploma or similar title of any other University.

Trivandrum
4th June 2021

Signed By
Abhijith Kusalán
Ajay R Krishnan
Ananthu Suresh
Nived Suresh Lal

DEPARTMENT OF AERONAUTICAL

**RAJADHANI INSTITUTE OF ENGINEERING AND TECHNOLOGY, ATTINGAL,
TRIVANDRUM**



CERTIFICATE

This is to certify that the report entitled **MODELLING AND ANALYSIS ON HELICAL SAVONIUS WIND TURBINE** submitted by **Abhijith Kusalán, Ajay R Krishnan, Ananthu Suresh and Nived Suresh Lal** to the APJ Abdul Kalam Technological University in partial fulfilment of the requirements for the award of the Degree of Bachelor of Technology in Aeronautical is a bonafide record of the project work carried out by them under my guidance and supervision. This report in any form has not been submitted to any other University or Institute for any purpose.

Internal Supervisor

Dr. Thamaráikánnan S

HEAD OF THE DEPT

Dr. Thamaráikánnan S

ACKNOWLEDGEMENT

First and foremost, we concede the surviving presence and the flourishing refinement of almighty **GOD** for his concealed hand yet substantial supervision all through the seminar.

We extend our sincere gratitude to our Principal, **Dr. Suresh Babu S** for his countenance towards the successful accomplishment of the course.

We are thankful to our Vice Principal, **Dr. K. Balan** for his valuable support and guidance.

We are grateful to our Head of the Department, and our guide **Dr Thamaraikannan.S**, of the Department of Aeronautical for his timely support and valuable guidance and constant encouragement that enabled us to complete this project on time.

We also would like to thank our staff advisor **Mrs.Arshi R**, Assistant Professor, Department of Aeronautical for her valuable support and advice.

We sincerely thank all the teachers and staff members of Aeronautical Engineering Department for their valuable support, help and advice.

ABSTRACT

In this report we present our team's combined effort in the refining of an idea, which we believe is qualified enough to be a stand out final semester project with the help and mentoring of our guides. This report gives a detailed overview on our modeling practices, analysis and our efforts to make the proposed project on Modelling and Analysis on Helical Savonius Wind Turbine. The paper includes, an introduction on vertical axis wind turbines, its applications, our proposed designs, proposed methodology of analysis, Analysis data, Structural analysis, Calculations, Results and our findings along with various journals that backs up our claim for the success of our project, and various references. The future scope of our final year project is also discussed in Detail.

CONTENTS**CHAPTER 1****1.INTRODUCTION**

- 1.1. Types of wind turbines
 - 1.1.1 Horizontal Axis Wind turbines
 - 1.1.2 Vertical Axis wind Turbines
 - 1.1.2.1. Darrieus type-lift type
 - 1.1.2.2. Savonius type – drag type
- 1.2. Origin – Savonius turbines
- 1.3. Boons and cons of a drag type wind turbine
- 1.4. Objectives

CHAPTER 2**2 LITERATURE SURVEY**

- 2.1. Journal index
 - Journal 1 - *An Experimental Study on Improvement of Savonius Rotor Perform...*
 - Journal 2 - *Analysis of The Blade Profile of The Savonius Wind Turbine Usi...*
 - Journal 3 - *A Study on Increasing the Performance of Savonius Wind Rotors...*
 - Journal 4 - *Numerical Study of Savonius Wind Turbine with Additional Fin ...*
 - Journal 5 - *Design And Development Of Enlil Turbine For Highways Electric...*
 - Journal 6 - *Savonius Vertical Wind Turbine: Design, Simulation, And ...*
 - Journal 7 - *Simplified Dragonfly Airfoil Aerodynamics at Reynolds Number...*
 - Journal 8 - *Airfoil Considerations in The Design of High Performance, ...*
 - Journal 9 - *Characteristics of Wind Velocity and Temperature Change ...*
 - Journal 10 - *The Influence of Rotating Domain Size in A Rotating Frame...*

CHAPTER 3**PRELIMINARY DESIGN SKETCHES**

- 3.1. The aerofoil - Eppler's 61 (E61)
 - 3.1.1. Aerofoil properties
- 3.2 Methodology and approach
- 3.3 Geometric design
- 3.4 Structural components and parts
 - 3.4.1 Turbine shaft
 - 3.4.2 Turbine blades
 - 3.4.3 Completed 3-Dimensional geometry model
- 3.5 Cfx and cfd analysis
 - 3.5.1 Airfoil – E61
 - Meshing
 - Boundary condition
 - 3.5.2 Helical axis wind turbine
 - Geometry
 - Meshing
 - Parameters
- 3.6 Governing equations
 - K-epsilon turbulence model
 - Differential equation for mass conservation
- 3.7 Structural analysis
 - Defining Engineering Data
 - Geometry
 - Setup
 - Rotational Velocity
 - Displacement
 - Moment
 - Meshing

CHAPTER 4**4. ANALYSIS AND RESULTS**

4.1. Analysis under various wind and angular velocities

4.1.1 Low wind speed

4.1.2 Medium Wind speed

4.1.3 High wind speed

4.1.4 Conclusion

- 1) Pressure
- 2) Total deformation
- 3) Equivalent Elastic stress/Equivalent elastic...
- 4) Maximum principal stress
- 5) maximum principal strain

4.2 Analysis on the efficiency of helical Savonius wind turbine...

4.2.1 Theory

4.2.2 Efficiency analysis

- Analysis on wind speed of 2.50 m/s
- Analysis on wind speed of 5.00 m/s
- Analysis on wind speed of 7.50 m/s
- Analysis on wind speed of 10.0 m/s
- Analysis on wind speed of 12.5 m/s
- Analysis on wind speed of 15.0 m/s
- Analysis on wind speed of 17.5 m/s
- Analysis on wind speed of 20.0 m/s
- Analysis on wind speed of 22.5 m/s
- Analysis on wind speed of 25.0 m/s

4.2.3 Calculating the efficiency

CHAPTER 5**CONCLUSION****REFERENCES****LIST OF FIGURES**

Fig: No.	TITLE
Fig 1.1	Vertical Axis Wind Turbine-Darrius
Fig 1.2	Internal Parts of HAWT
Fig 1.3	Darrius Type wind turbine
Fig 1.4	Simple Savonius wind turbine
Fig 2.1	Variation of C_p according to no. of blades & velocity of...
Fig 2.2	Test section setup of rotor and stator
Fig 2.3	Analysis of power coefficient for different wind turbines
Fig 2.4	Stator Rotor ANSYS
Fig 2.5	Stator rotor wireframe mesh
Fig 2.6	Circuit of a smart wind turbine
Fig 2.7	Power Coefficient and TSR relation
Fig 2.8	Low camber aerofoil 1
Fig 2.9	Low camber aerofoil 2
Fig 2.10	C_l vs α
Fig 2.11	C_l vs C_d
Fig 2.12	Terrain wind velocity contour

Fig 2.13	Wind speed Ratio vs Tip speed Ratio
Fig 3.1	Eppler E-61 Low Reynolds number aerofoil
Fig 3.2	Basic Sketch of helical Savonius wind turbine
Fig 3.3	Eppler E61 (350mm Chord)
Fig 3.4	Cl vs Alpha
Fig 3.5	Cl vs Alpha
Fig 3.6	Cd vs Alpha
Fig 3.7	Imported Aerofoil plot
Fig 3.8	Paneled shaft
Fig 3.9	Single Blade
Fig 3.10	Completed Helical Savonius Wind turbine
Fig 3.11	Turbine shaft(solid)
Fig 3.12	Single Helical blade side view
Fig 3.13	Single Helical blade top view
Fig 3.14	Side view of VAWT 1
Fig 3.15	Side view of VAWT 2
Fig 3.16	Isometric View of VAWT
Fig 3.17	Top view of VAWT
Fig 3.18	Aerofoil Inside Fluid Enclosure (Boolean Subtracted)
Fig 3.19	Mesh data of aerofoil, using Boolean Subtraction
Fig 3.20	Boundary Nomenclature
Fig 3.21	Design modeller Rotor Part
Fig 3.22	Design modeller stator
Fig 3.23	Mesh Data of Rotor Component (Element Size 5e-02)
Fig 3.24	Mesh Data of Stator Component (Element size 1.0)
Fig 3.25	Parameter settings
Fig 3.26	Assumed Element
Fig 3.27	Moment Details
Fig 3.28	Mesh model and Meshing Window-Static structural
Fig 4.1	CFX pre setup for 10 rad/s angular velocity at 5m/s windspeed
Fig 4.2	CFX Result for pressure contour on Iso-surface
Fig 4.3	Static Structural setup window
Fig 4.4	Total deformation
Fig 4.5	Equivalent Elastic Strain
Fig 4.6	Maximum Principal Strain
Fig 4.7	Maximum principal stress
Fig 4.8	Equivalent stress
Fig 4.9	CFX Result for velocity contour on Iso-surface
Fig 4.10	Total deformation
Fig 4.11	Equivalent Elastic Strain
Fig 4.12	Equivalent stress
Fig 4.13	Maximum Principal Strain
Fig 4.14	Maximum principal stress
Fig 4.15	CFX Result for pressure contour on Iso-surface
Fig 4.16	Total deformation
Fig 4.17	Equivalent Elastic Strain
Fig 4.18	Equivalent stress

Fig 4.19	Maximum principal stress
Fig 4.20	Maximum Principal Strain
Fig 4.21	CFX Result for pressure contour on Iso-surface
Fig 4.22	Total deformation
Fig 4.23	Equivalent Elastic Strain
Fig 4.24	Equivalent stress
Fig 4.25	Maximum principal stress
Fig 4.26	Maximum Principal Strain
Fig 4.27	CFX Result for pressure contour on Iso-surface
Fig 4.28	Total deformation
Fig 4.29	Equivalent Elastic Strain
Fig 4.30	Equivalent stress
Fig 4.31	Maximum principal stress
Fig 4.32	Maximum Principal Strain
Fig 4.33	CFX Result for pressure contour on Iso-surface
Fig 4.34	Total deformation
Fig 4.35	Equivalent Elastic Strain
Fig 4.36	Equivalent stress
Fig 4.37	Maximum principal stress
Fig 4.38	Maximum Principal Strain
Fig 4.39	Graphical - Total Deformation
Fig 4.40	Graphical - Equivalent Elastic Strain
Fig 4.41	Graphical - Maximum Principal Stress
Fig 4.42	Graphical - Equivalent Stress
Fig 4.43	Graphical - Maximum Principal Strain
Fig 4.44	Pressure Contour (2.5 m/s) CFX pre
Fig 4.45	Pressure Contour (5 m/s) CFX pre
Fig 4.46	Pressure Contour (7.5 m/s) CFX pre
Fig 4.47	Pressure Contour (10 m/s) CFX pre
Fig 4.48	Pressure Contour (12.5 m/s) CFX pre
Fig 4.49	Pressure Contour (15 m/s) CFX pre
Fig 4.50	Pressure Contour (17.5 m/s) CFX pre
Fig 4.51	Pressure Contour (20 m/s) CFX pre
Fig 4.52	Pressure Contour (22.5 m/s) CFX pre
Fig 4.53	Pressure Contour (25 m/s) CFX pre
Fig 5.1	Graphical Representation of Efficiency.

LIST OF TABLES

Table 3.1	Plot - aerofoil surface line
Table 3.2	Plot - Camber
Table 4.1	Multiple Wind Velocities and Angular Velocities
Table 4.2	CFX Boundary Flow values
Table 4.3	Static Structural Analysis Results
Table 4.4	CFX Boundary Flow values
Table 4.5	Static Structural Analysis Results

Table 4.6	CFX Boundary Flow values
Table 4.7	Static Structural Analysis Results
Table 4.8	CFX Boundary Flow values
Table 4.9	Static Structural Analysis Results
Table 4.10	CFX Boundary Flow values
Table 4.11	Static Structural Analysis Results
Table 4.12	CFX Boundary Flow values
Table 4.13	Static Structural Analysis Results
Table 4.14	Data Sheet
Table 4.15	CFX Boundary Flow values
Table 4.16	CFX Boundary Flow values
Table 4.17	CFX Boundary Flow values
Table 4.18	CFX Boundary Flow values
Table 4.19	CFX Boundary Flow values
Table 4.20	CFX Boundary Flow values
Table 4.21	CFX Boundary Flow values
Table 4.22	CFX Boundary Flow values
Table 4.23	CFX Boundary Flow values
Table 4.24	CFX Boundary Flow values
Table 4.25	Multiple wind velocities with a constant angular velo
Table 4.26	Multiple turbine efficiency with constant angular velo

ABBREVIATIONS

- AC – Alternating Current.
- E61 – Eppler’s 61 Aerofoil
- Fig: - Figure of.
- HAWT – Horizontal Axis Wind Turbine.
- VAWT – Vertical Axis Wind Turbine.
- Coeff. – Coefficient.
- RPM – Revolutions Per Minute
- TSR – Tip speed Ratio

NOTATIONS

- A – Area, m²
- Cd – Drag Coefficient.
- Cl – Lift coefficient.
- C_p – Coefficient of power
- V – Velocity, m/s
- α – Angle of attack, degrees.
- ρ – Density, kg/m³
- RPM - Revolutions per minute.
- ω – Angular Velocity, rad/s or m/s.
- T – Torque, Nm
- P_T – Shaft Power, watt
- P_w – Wind Power, watt

CHAPTER 1 INTRODUCTION

A **wind turbine** is a device that converts the wind's kinetic energy into electrical energy.

Wind turbines are manufactured in a wide range of sizes, with either horizontal or vertical axes. It is estimated that hundreds of thousands of large turbines, in installations known as wind farms, now generate over 650 gigawatts of power, with 60 GW added each year. They are an increasingly important source of intermittent renewable energy, and are used in many countries to lower energy costs and reduce reliance on fossil fuels. One study claimed that, as of 2009, wind had the "lowest relative greenhouse gas emissions, the least water consumption demands and... the most favourable social impacts" compared to photovoltaic, hydro, geothermal, coal and gas.

Smaller wind turbines are used for applications such as battery charging for auxiliary power for boats or caravans, and to power traffic warning signs. Larger turbines can contribute to a domestic power supply while selling unused power back to the utility supplier via the electrical grid.

1.1 TYPES OF WIND TURBINES

Wind turbines are classified into many kinds based on significant as well as discrete and minute differences between them. But mainly wind turbines are classified into 2 major classes depending upon their orientation of shaft.

They are:

- 1) **Horizontal Axis Wind Turbines (HAWT).**
- 2) **Vertical Axis Wind Turbines (VAWT).**

1.1.1 HORIZONTAL AXIS WIND TURBINES

Horizontal axis wind turbines are the most commonly used turbines due to their strength and efficiency. The base of the towers has to be extremely strong, allowing the rotor shaft to be installed at the top of the tower which allows the turbine to be exposed to stronger winds. With the blades of the turbine being perpendicular to the wind, the rotation of the blades can generate more power compared to the vertical axis wind turbine. However, the construction of this type of turbine requires a heavy support for the tower to support the weight of the blades, gearbox and generator as well as utilizing a sizable crane to lift the components to the top of the tower.

In a situation where the wind is blowing downwards, the turbine structure may suffer from metal fatigue which could lead to a structural failure. This is resolved by designing the turbines with an upwind design. Additional yaw control is needed for the horizontal axis wind turbines in order to track the direction of the wind, to prevent damaging the turbine.

One drawback identified with downwind rotors, however, is that they have been known to 'walk' around when trying to line up with winds during low-speed conditions, diminishing low wind speed energy production.

Modern HAWTs use the aerodynamic lift force to turn each rotor blade, in a manner similar to the way an airplane flies. The lift force generally works as follows. When exposed to winds, air flows around both the upper and lower portions of a blade. As a result of the blade's curvature, however, air passes over the top of the blade more quickly (owing to a longer fetch length) than the lower portion, producing a low-pressure area on the topside. The pressure difference created between the top and bottom sides of the blade produces a force in the direction of the top of the blade.

As shown below, the lift force acts perpendicular to the 'relative wind' acting on the wind turbine blade. The force of the lift is actually stronger than the force of the wind against the blade, or the drag, which acts in parallel with the airflows. This allows turbine blades to turn at speeds greater than could be achieved relying on drag forces alone. Although some wind turbines also use the drag force to produce energy, most HAWTs are designed to minimize drag while maximizing lift.

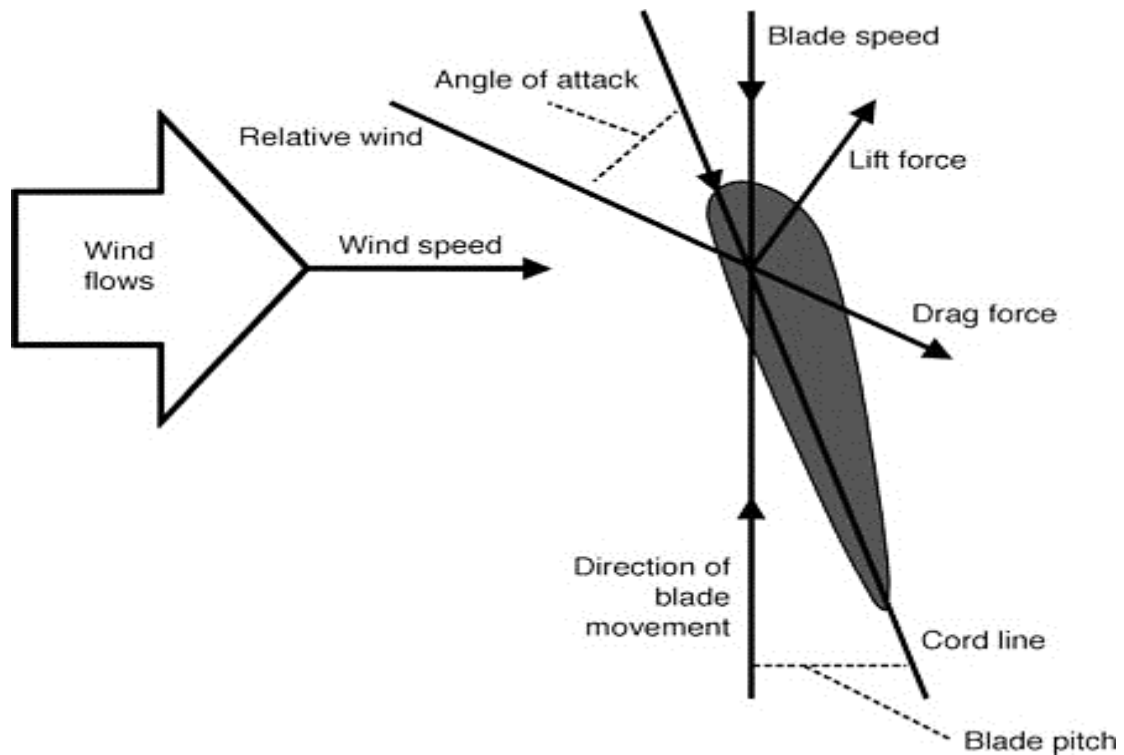


Fig 1.1: Vertical Axis Wind Turbine-Darrius

Constructional features of a typical HAWT are shown below. HAWTs work predominantly on lift principle. As the wind stream interacts with the rotor blades, lift force is generated as explained in the previous section, causing the rotor to rotate. The rotational speed varies with the design features and the size of the rotor. For a typical MW-sized turbine, this could be as low as 16 rpm. The low-speed main shaft transmits this rotation to the high-speed shaft through the gearbox (there are direct drive turbines also, which do not have a gearbox in the transmission line). The speed is enhanced by the gear trains to match with the higher speed requirement of the generator. The generator then converts the mechanical energy to electrical energy. There are a series of control systems in between for yaw alignment, power regulation, and safety.

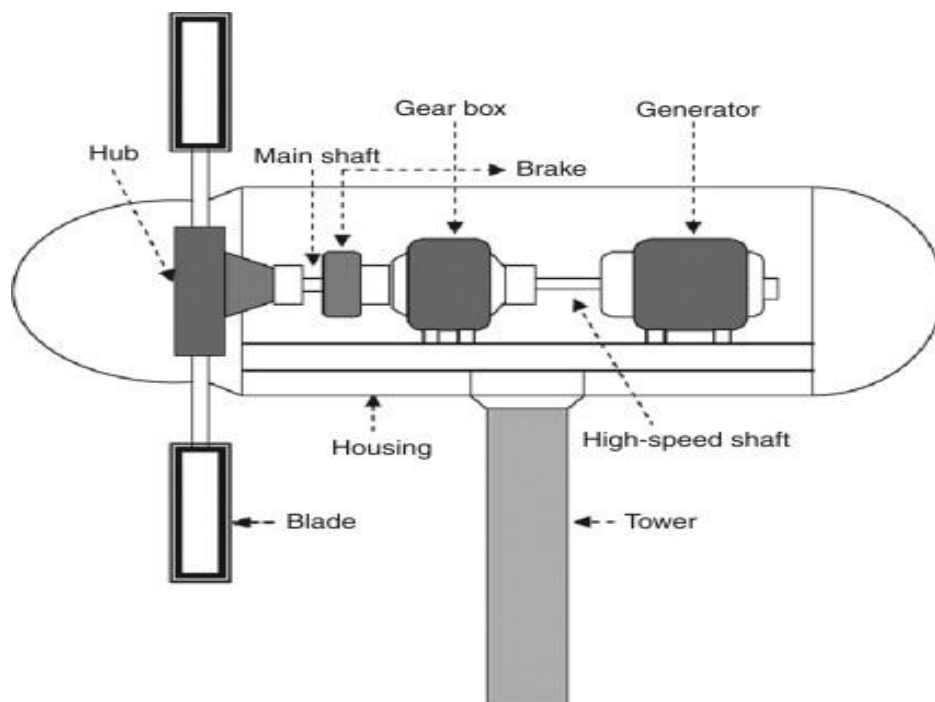


Fig 1.2: Internal parts of HAWT

1.1.2 VERTICAL AXIS WIND TURBINES

Vertical axis wind turbines are less affected by frequent wind direction changes as compared to the horizontal axis wind turbines due to the blades being rotated on the rotor shaft perpendicular to the ground. With the blades and shaft installed in this way, the turbine does not need to rotate to track wind direction. The shaft is mounted near ground level due to the difficulties of mounting the shaft and its components on the tower. An advantage of being mounted at ground level is that maintenance of the turbine is easier and can be installed at locations such as rooftops. Disadvantages to this turbine installation is that the efficiency is lower due to air drag and the lower wind speeds compared to the higher wind speeds encountered at higher elevations.

A wind turbine secures air into a hub, which then turns into a generator. The air that passes through the blades of the wind turbine is spun into the generator through rotational momentum. The VAWT, as the turbines are oftener shortened, feature the following qualities:

- Two to three blades with a vertically operating main rotor shaft – the more blades that you have on the unit, the more wind energy it will receive and the more efficiency it will offer
- Used less frequently than a horizontal wind turbine
- The position of the blades is different in the VAWT. On this model, the base of the tower holds the generator, and the blades then wrap themselves around the shaft. People use the VAWT because they can be placed closer to the ground, which makes them acceptable and effective for use at a residential location.
- With the vertical axis wind turbine, the rotor shaft is arranged in a vertical pattern
- The VAWT are easier and more affordable to maintain than horizontal units
- One complains that some users have with the VAWT is that it creates less wind energy, which may cause a number of different noises to be heard. Turbulent air flow is also a possibility that can shorten the life of the system.
- Installation of the VAWT onto the roof will cause the wind speed to double for maximum wind turbulence and wind energy usage.

There are actually a number of reasons that this decision is made. Let's take a look at some of the advantages that you can enjoy with this type of wind turbine in use at your home.

- You can build your wind turbine close to the ground so if you do not have a suitable rooftop for placement, or if you live where there are hills, ridges, etc. that prohibit the flow of air, they work wonderfully for your needs.
- Since VAWT are mounted closer to the ground they make maintenance easier, reduce the construction costs, are more bird friendly and does not destroy the wildlife.
- You do not need any mechanisms in order to operate the wind turbine
- Lower wind startup speed
- The main advantage of VAWT is it does not need to be pointed towards the wind to be effective. In other words, they can be used on the sites with high variable wind direction.
- You can use the wind turbine where tall structures are not allowed.
- VAWT's are quiet, efficient, economical and perfect for residential energy production, especially in urban environments.
- They are cost effective when compare to the HAWTs. It is still best to shop around and check prices before making a purchase, however.
- Many of the turbines are resistant to many of the different weather elements that you may experience. It is imperative to choose a unit that offers this valuable protection and extra durability when you need it the most.

In the family of Vertical Axis wind turbines there are mainly 2 types. Darrieus Type VAWT and Savonius Type VAWT.

1.1.2.1. DARRIEUS TYPE – LIFT TYPE

Darrieus Wind Turbine is commonly known as an "Eggbeater" turbine. It was invented by Georges Darrieus in 1931. A Darrieus is a high speed, low torque machine suitable for generating alternating current (AC) electricity. Darrieus generally require manual push therefore some external power source to start turning as the starting torque is very low. Darrieus has two vertically oriented blades revolving around a vertical shaft.

The Darrieus wind turbine offers the following features:

- These eggbeater shaped turbines are great at efficiency; however, they are not as reliable.
- In order to use the Darrieus wind turbine you must have an outside source of power in order to start them
- It is in your best interest to choose a wind turbine that has at least three blades.
- To support such a wind turbine, it is necessary that you have a superstructure which will connect it near the top bearing.



Fig 1.3: Darrius Type wind Turbine

1.1.2.2. SAVONIUS TYPE – DRAG TYPE

Savonius wind turbines are a type of vertical-axis wind turbine (VAWT), used for converting the force of the wind into torque on a rotating shaft. The turbine consists of a number of airfoils, usually—but not always—vertically mounted on a rotating shaft or framework, either ground stationed or tethered in airborne systems.

The Savonius turbine is one of the simplest turbines. Aerodynamically, it is a drag-type device, consisting of two or three scoops. Looking down on the rotor from above, a two-scoop machine would look like an "S" shape in cross section. Because of the curvature, the scoops experience less drag when moving against the wind than when moving with the wind. The differential drag causes the Savonius turbine to spin. Because they are drag-type devices, Savonius turbines extract much less of the wind's power than other similarly-sized lift-type turbines. Much of the swept area of a Savonius rotor may be near the ground, if it has a small mount without an extended post, making the overall energy extraction less effective due to the lower wind speeds found at lower heights.

Savonius turbines are used whenever cost or reliability is much more important than efficiency. Most anemometers are Savonius turbines for this reason, as efficiency is irrelevant to the application of measuring wind speed. Much larger Savonius turbines have been used to generate electric power on deep-water buoys, which need small amounts of power and get very little maintenance. Design is simplified because, unlike with horizontal axis wind turbines (HAWTs), no pointing mechanism is required to allow for shifting wind direction and the turbine is self-starting. Savonius and other vertical-axis machines are good at pumping water and other high torque, low rpm applications and are not usually connected to electric power grids. In the early 1980s, Risto Joutsiniemi developed a helical rotor version that does not require end plates, has a smoother torque profile and is self-starting in the same way a crossed pair of straight rotors is.

The most ubiquitous application of the Savonius wind turbine is the Flettner rotor, which is commonly seen on the roofs of vans and buses and is used as a cooling device. The ventilator was developed by the German aircraft engineer Anton Flettner in the 1920s. It uses the Savonius wind turbine to drive an extractor fan. The vents are still manufactured in the UK by Flettner Ventilator Limited.

This is the wind turbine that we are going to model and analyse.

1.2 ORIGIN – SAVONIUS TURBINES

The Savonius wind turbine was invented by the Finnish engineer Sigurd Johannes Savonius in 1922. However, Europeans had been experimenting with curved blades on vertical wind turbines for many decades before this. The earliest mention is by the Italian Bishop of Czanad, Fausto Veranzio, who was also an engineer. He wrote in his 1616 book *Machinae novae* about several vertical axis wind turbines with curved or V-shaped blades. None of his or any other earlier examples reached the state of development made by Savonius. In his Finnish biography there is mention of his intention to develop a turbine-type similar to the Flettner-type, but autorotationary. He experimented with his rotor on small rowing vessels on lakes in his country. No results of his particular investigations are known, but the Magnus effect is confirmed by König. The two Savonius patents: US1697574, were filed in 1925 by Sigurd Johannes Savonius, and US1766765, in 1928.



Fig 1.4: Simple Savonius Wind Turbine – 3 Blades.

1.3 BOONS AND CONS OF A DRAG TYPE WIND TURBINE

Advantages

VAWTs offer a number of advantages over traditional horizontal-axis wind turbines (HAWTs):

- Being Omni-directional, some forms do not need to track the wind. This means they don't require a complex mechanism and motors to yaw the rotor and pitch the blades.
- In VAWTs, gearbox replacement and maintenance are simpler and more efficient, as the gearbox is accessible at ground level, so that no cranes or other large equipment are needed on-site. This reduces costs and impact on the environment. Motor and gearbox failures generally are significant considerations in the operation and maintenance of HAWTs both on and offshore.
- Some designs of VAWTs in suitable situations can use screw pile foundations, which hugely reduces the road transport of concrete and the carbon cost of installation. Screw piles can be fully recycled at the end of their life.
- VAWTs can be installed on HAWT wind farm below the existing HAWTs; this can supplement the power output of the existing farm.

Disadvantages

- VAWTs are less reliable than HAWTs and less efficient. Whilst they might look more visually appealing, vertical axis wind turbines are known to have less efficiency compared to horizontal axis wind turbines. This is mainly due to the nature of their design and operational characteristics.
- One of the major outstanding challenges facing vertical axis wind turbine technology is dynamic stall of the blades as the angle of attack varies rapidly.
- The blades of a VAWT are fatigue-prone due to the wide variation in applied forces during each rotation. This can be overcome by the use of modern composite materials and improvements in design - including the use of aerodynamic wing tips that cause the spreader wing connections to have a static load. The vertically oriented blades can twist and bend during each turn, causing them to break apart.
- VAWTs have proven less reliable than HAWTs, although modern designs of VAWTs have overcome many of the issues associated with early designs.

1.4 OBJECTIVES

The major objectives that we plan on achieving through this project are:

- 1) To make a new type of Savonius Wind turbine, by incorporating an aerofoil cross section.
- 2) To design and model the new type of Wind turbine in a 3-Dimensional model format, using CATIA VR-19 software.
- 3) To simulate the designed model under various conditions to obtain the moment forces acting on the aerofoil, using ANSYS 2020 CFX platform.
- 4) To calculate the efficiency of the simulated turbine model using the Shaft power- Wind Power ratio equation.
- 5) To Analyse the structural loads acting on the Wind Turbine under various conditions using ANSYS 2020 Static Structural Platform.

CHAPTER 2 LITERATURE SURVEY

JOURNAL INDEX

SL No:	Name	Page
1	<i>An experimental study on improvement of Savonius rotor performance.</i>	Page 18
2	<i>Analysis of the blade profile of the Savonius wind turbine Using computational fluid dynamics</i>	Page 19
3	<i>A study on increasing the performance of Savonius wind rotors</i>	Page 20
4	<i>Numerical study of Savonius wind turbine with additional Fin-blade using computational fluid dynamic</i>	Page 21
5	<i>Design and Development of ENLIL Turbine for Highways Electrification</i>	Page 22
6	<i>Savonius vertical wind turbine: design, simulation, and physical testing</i>	Page 23
7	<i>Simplified dragonfly airfoil aerodynamics at Reynolds numbers below 8000</i>	Page 24
8	<i>Airfoil considerations in the design of high performance, low Reynolds number propellers</i>	Page 25
9	<i>Characteristics of Wind Velocity and Temperature Change near an Escarpment-Shaped Road Embankment</i>	Page 26
10	<i>The influence of rotating domain size in a rotating frame of reference approach for simulation of rotating impeller in a mixing vessel.</i>	Page 27

JOURNAL 1

An experimental study on improvement of Savonius rotor performance.

- **Authors:** N.H.Mahmoud, El-Haroun E.Wahba M, H.Nasef.
- **Year:** 2012

In this work different geometries of Savonius wind turbine are experimentally studied in order to determine the most effective operation parameters. It was found that, the two blades rotor is more efficient than three and four ones. The rotor with end plates gives higher efficiency than those of without end plates.

Double stage rotors have higher performance compared to single stage rotors. The rotors without overlap ratio (β) are better in operation than those with overlap. The results show also that the power coefficient increases with rising the aspect ratio (α). The conclusions from the measurements of the static torque for each rotor at different wind speeds verify the above summarized results of this work.

The mechanical power for the tested Savonius rotor is determined by measuring the mechanical torque on the rotating shaft and rotational speed at different values of wind speed.

The wind speed is measured by a propeller type digital anemometer. While the shaft rotational speed is measured using a digital dc tachometer.

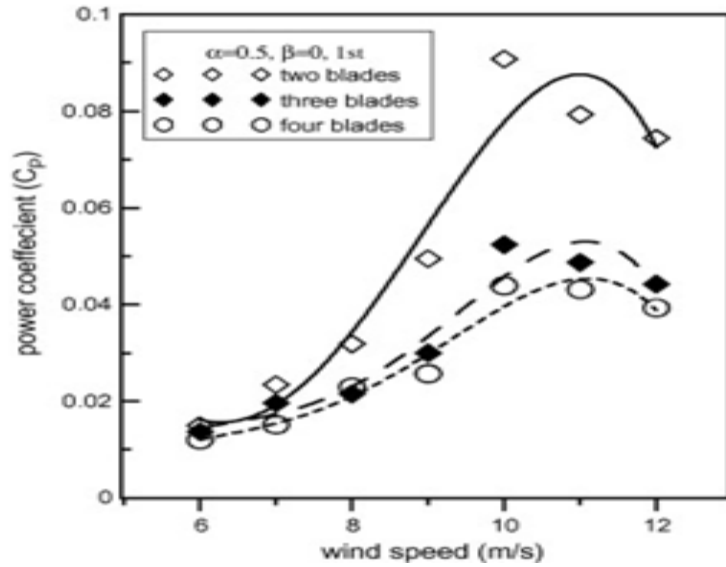


Fig 2.1: This Graphical representation shows the variation of C_p according to number of blades and velocity of wind.

JOURNAL 2

Analysis of the blade profile of the Savonius wind turbine using computational fluid dynamics

- **Authors:** S P Venkitesan, S. Senthamizh Selvan, Yugandhar Sai
- **Year:** May 15 2019

This study characterizes the performance of the Savonius type vertical axis wind turbine (VAWT). The performance of the Savonius type VAWT can be characterized by power and coefficient of power.

The main parameter considered for analyzing the Savonius-type VAWT is the tip speed ratio (TSR). The mesh independency test and time independency test are carried out, in which the medium mesh and three degree of time step for rotation are selected.

The Savonius wind turbine is analyzed at various TSR ranging from 0.2 to 5.0, in which TSR is 4.4, the performance of the turbine is high. Considering 4.4 TSR as the optimum one, the analysis of the Savonius type VAWT is carried out under various wind speed ranging from 1 to 10 m/s. From the analysis, the validation between numerical analysis and theoretical analysis is carried out and the efficiency of the Savonius type VAWT is increased to 50%.

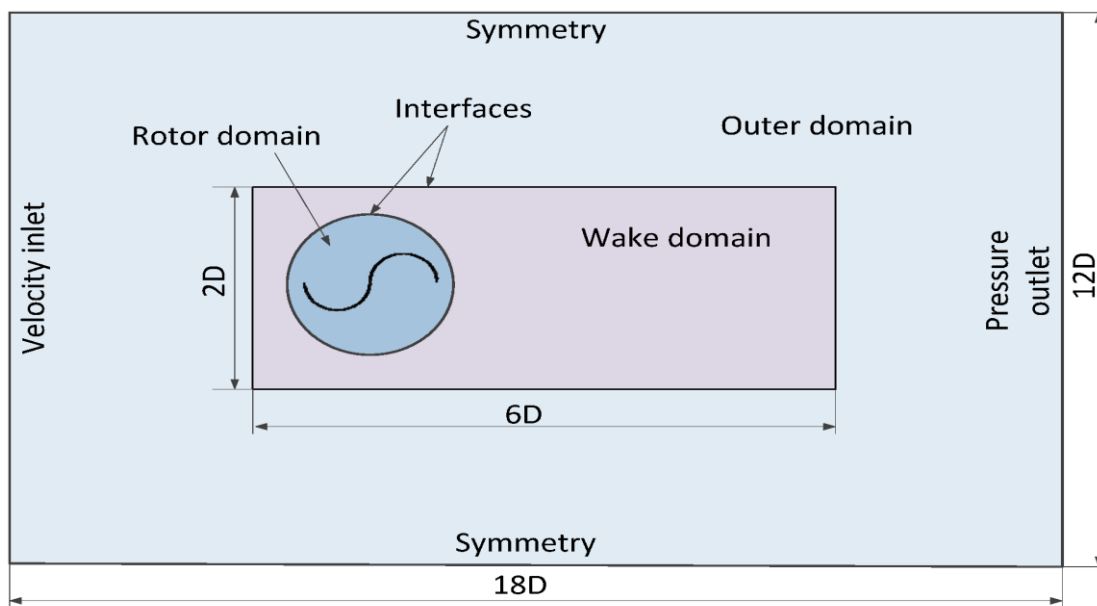


Fig 2.2: Test section setup of rotor and stator.

JOURNAL 3**A study on increasing the performance of Savonius wind rotors**

- **Authors:** Burçin Deda Altan & Mehmet Atılgan
- **Year:** 20 May 2012

Savonius wind rotors with a vertical axis are not much preferred and used due to their lower aerodynamic performance than that of the other high-speed wind rotors.

The present study is intended to increase the rotor performance of the Savonius wind rotor with theoretical method by focusing on a curtain arrangement as a wind deflector with a simple construction, which has been designed to increase the performance of the Savonius wind rotor.

This curtain arrangement has been placed in front of the rotor so as to prevent the negative torque that occurs on the convex surface of the Savonius wind rotor and causes the performance of the rotor to be low. Thus, it has become possible to make a more efficient use of the wind energy increasing the low performance level of the Savonius wind rotors.

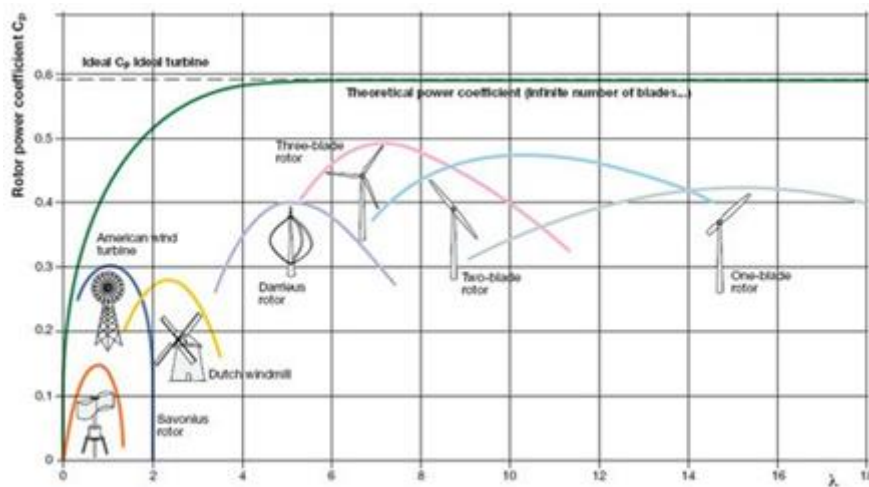


Fig 2.3: Analysis of power coefficient for different wind turbines.

JOURNAL 4**Numerical study of Savonius wind turbine with additional fin blade using computational fluid dynamic**

- **Authors:** B Anggara, I Widiastuti and H Saputro
- **Year:** 18 April 2018

Savonius wind turbine is the wind energy conversion systems which has good potential for small-scale electrical energy source. However, standard design Savonius rotor has a relatively low efficiency and rotation speed. The aim of this research is to study modification of wind turbine design of Savonius type S by adding variation of fin in its turbine blades.

It utilized computational fluid dynamic (CFD) using a commercial Finite Element (FEA) software. Savonius rotor employed in this research has a 1.1 m rotor diameter in 1.4 m height. The 3D model of Savonius rotor was developed by a CAD Software, SolidWorks. The wind speed utilized for simulation purpose were 3 to 5 m/s with k-epsilon turbulent model.

Simulation was performed using ANSYS to generate mesh of the flow domain all of blade variant. Dynamic mesh model was used in this simulation, which then exported to FLUENT in evaluating the fluid flow for determining the aerodynamic coefficient such as drag, torque and power coefficient.

This model simulated a fluid flow striking the blade and wind condition around the rotate blade. Results from this study is expected to provide an alternative evaluation of Savonius wind turbine performance in various conditions with different design parameters.

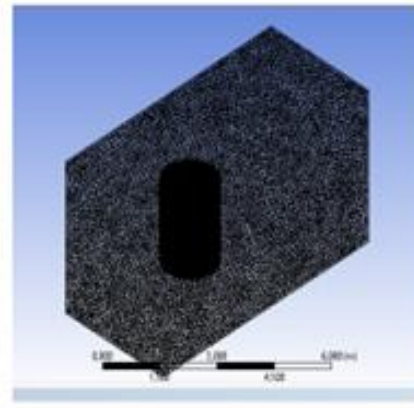
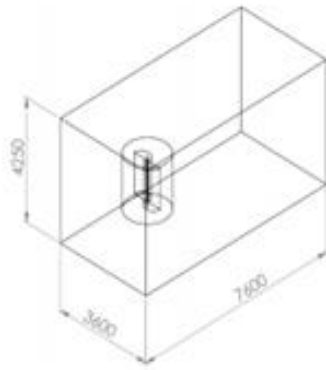


Fig 2.4: Stator Rotor ANSYS Fig 2.5: Stator rotor wireframe mesh

JOURNAL 5

Design and Development of ENLIL Turbine for Highways Electrification

- Authors: P.Karthikeyan, P.Dineshkumar, R.Gokul, G.Tamilvanan
- Year: March 2019

ENLIL is a vertical axis wind turbine that transforms highways into renewable energy sources by using the dynamics of the city. Enlil will generate energy by using the winds created by the vehicles as well as the natural winds.

This turbine uses the wind pressure generated by the fast-moving vehicles on roads such as big trucks and busses that helps to rotate its blade. It is designed with vertical long blades such that it will use the utmost quantity of wind energy.

Enlil turbine covers the lesser space on the ground and is simple to handle and can easily be assembled and disassembled which makes it more durable. Solar Panel is also fixed at the top of the turbine to generate electricity. In this paper the design of an axial flow permanent magnet synchronous generator is discussed which converts the mechanical energy from the blades to electrical output of approximately 100 watts.

The turbine is designed vertically with long blades. Solar panels are fixed at the top of the turbine to generate extra electricity. The product is still in its developmental phase. The Deveci Tech team is still improving their design to make it more efficient and well-built before it hits the roads

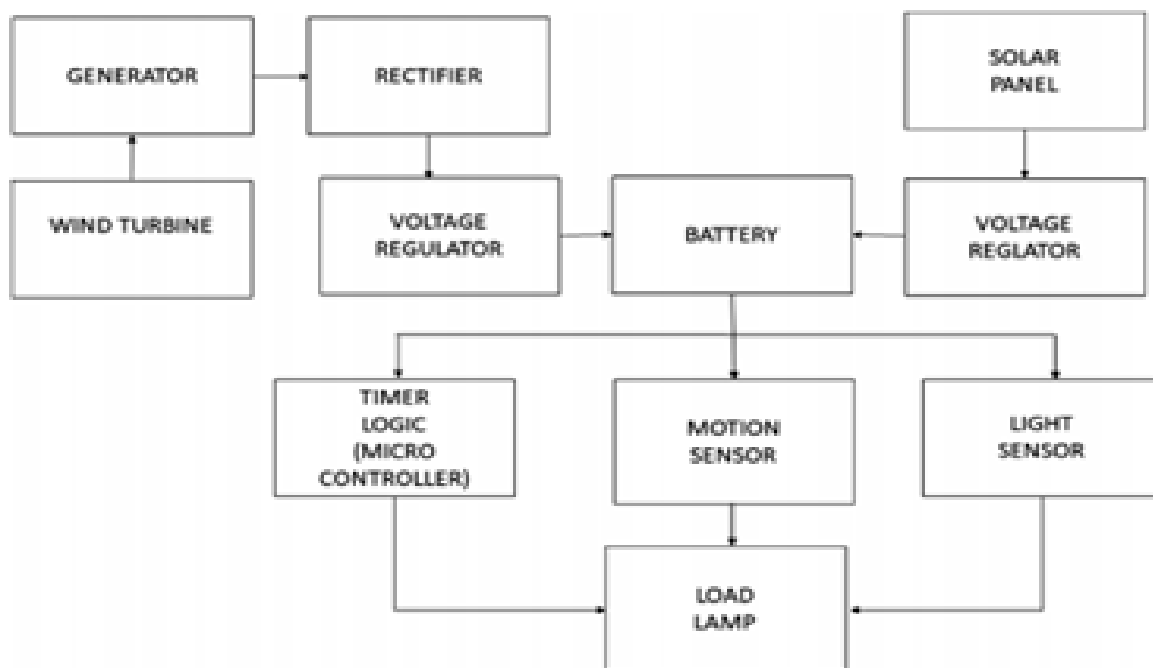


Fig 2.6: Circuit of a smart wind turbine

JOURNAL 6**SAVONIUS VERTICAL WIND TURBINE: DESIGN, SIMULATION, AND PHYSICAL TESTING**

- **AUTHORS:** Eddahmani Aymane, Dr. Hassan Darhmaoui, Dr. Naeem Sheikh
- **YEAR:** May 2017.

This project consists of designing, and testing the performance of a Savonius Vertical Wind Turbine.

The project compares the performance of two designs: a classic barrel Savonius design, and the innovative design of Icewind, an Icelandic startup that makes Vertical Axis Wind Turbines (VAWTs). A Computer Aided Design (CAD) tool is used to make a basic barrel Savonius rotor. Then, the Icewind design is reverse engineered from materials. Computer simulations, both 2D and 3D, are run to understand the characteristics of a Savonius rotor, and to obtain its pressure profile when subjected to a wind flow. A physical model of both designs is built to physically test and compare the performance of the two designs under different conditions.

Tip Speed Ratio The tip speed ratio (λ) is the ratio of the speed of the tip of the blades to the speed of the wind:

$$\lambda = v_{tip} / v_{wind}.$$

As the tip speed ratio varies, so does the power coefficient and hence the efficiency of the turbine. An optimal value that will result in the maximum C_p is desired.

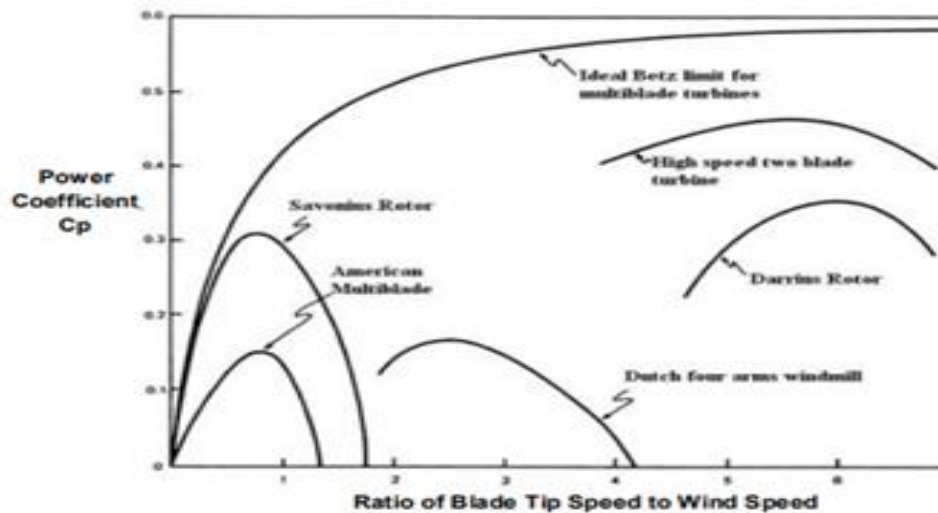


Fig 2.7: Power coefficient and TSR relation.

JOURNAL 7**Simplified dragonfly airfoil aerodynamics at Reynolds numbers below 8000**

- **Authors:** David-Elie Levy and Avraham Seifert
- **Year:** 2009

In this study, a simplified dragonfly airfoil is numerically analyzed in a steady free-stream flow. The aerodynamic performance (such as mean and fluctuating lift and drag), are first compared to a “traditional” low Reynolds number airfoil: the Eppler-E61.

The numerical results demonstrate superior performances of the corrugated airfoil. A series of low-speed wind and water tunnel experiments were performed on the corrugated airfoil, to validate the numerical results.

The findings indicate quantitative agreement with the mean wake velocity profiles and shedding frequencies while validating the two dimensionalities of the flow.

A flow physics numerical study was performed in order to understand the underlying mechanism of corrugated airfoils at these Reynolds numbers. Airfoil shapes based on the flow field characteristics of the corrugated airfoil were built and analyzed. Their performances were compared to those of the corrugated airfoil, stressing the advantages of the latter. It was found that the flow which separates from the corrugations and forms span wise vortices intermittently reattaches to the aft-upper arc region of the airfoil.

This mechanism is responsible for the relatively low intensity of the vortices in the airfoil wake, reducing the drag and increasing the flight performances of this kind of corrugated airfoil as compared to traditional low Reynolds number airfoils such as the Eppler E-61.

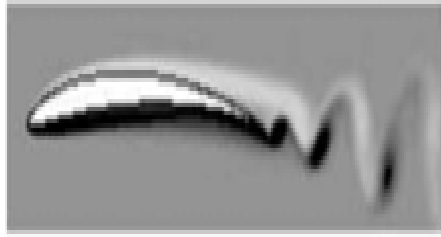


Fig 2.8: Low camber airfoil-1



Fig 2.9: Low camber airfoil-2

JOURNAL 8

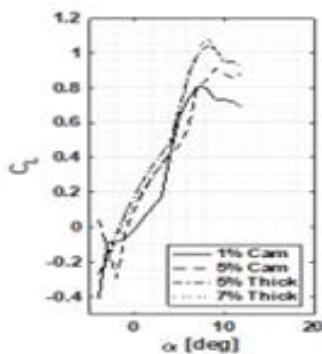
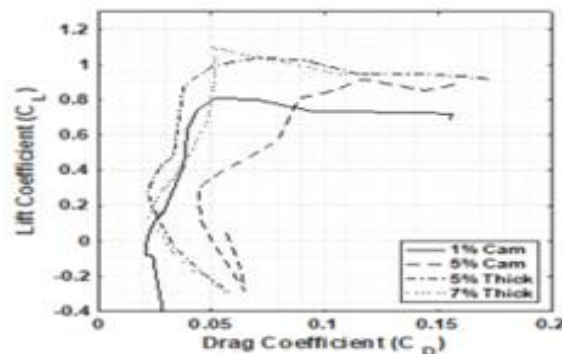
AIRFOIL CONSIDERATIONS IN THE DESIGN OF HIGH PERFORMANCE, LOW REYNOLDS NUMBER PROPELLERS

- Authors: Umunna J Reuben, Koju Hiraki , Miyamoto Shohe.
- Year: September 2018

A propeller was designed using 2D airfoil data obtained from a panel method numeric code. The propeller was designed to operate at 75% chord-based Reynolds number of 20k. At low Reynolds numbers <40k, there are no publicly available 2D airfoil force data largely because of inherent difficulty in their measurement.

Theoretical prediction of the propeller's peak efficiency was 0.67 while experiment results was 0.58. To improve the propeller efficiency by using better performing airfoils, six airfoils of varying thickness and camber were studied. Three of the six airfoils were chosen and used in the design of three propellers - a single airfoil for each propeller design.

The propellers were designed to operate at Reynolds number of 30k at 0.75 radius and the 2D airfoil force data used for the designs were obtained from a numeric code. Theoretical predictions of efficiency were all > 81% in each of the designed propellers.

Fig 2.10: C_l vs α Fig 2.11: C_l vs C_d

JOURNAL 9

Characteristics of Wind Velocity and Temperature Change near an Escarpment-Shaped Road Embankment

- Authors: Young-Moon Kim, Ki-Pyo You, and Jang-Youl You
- Year: 20 July 2014

Artificial structures such as embankments built during the construction of highways influence the surrounding airflow. Various types of damage can occur due to changes in the wind velocity and temperature around highway embankments. However, no study has accurately measured micrometeorological changes (wind velocity and temperature) due to embankments.

This study conducted a wind tunnel test and field measurement to identify changes in wind velocity and temperature before and after the construction of embankments around roads. Changes in wind velocity around an embankment after its construction were found to be influenced by the surrounding wind velocity, wind angle, and the level difference and distance from the embankment.

When the level difference from the embankment was large and the distance was up to $3H$, the degree of wind velocity declines was found to be large. In changes in reference wind velocities around the embankment, wind velocity increases were not proportional to the rate at which wind velocities declined. The construction of the embankment influenced surrounding temperatures. The degree of temperature change was large in locations with large level differences from the embankment at daybreak and during evening hours when wind velocity changes were small.

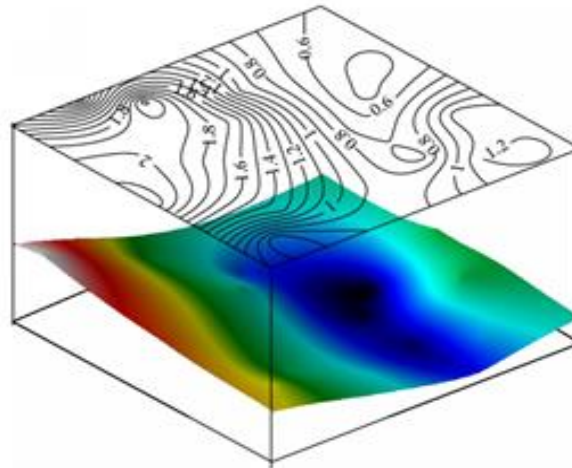


Fig 2.12: Terrain Wind Velocity Contour.

JOURNAL 10

The influence of rotating domain size in a rotating frame of reference approach for simulation of rotating impeller in a mixing vessel.

- **Authors:** Matej Zadavec and Matjaz Hriberšek
- **Year:** August 2007

This paper presents simulation of rotating impeller in a mixing vessel by means of Computational Fluid Dynamics (CFD).

A special emphasis is devoted to the study of influence of the choice of numerical model for simulation of rotation of impeller when mixing a Newtonian fluid in a vessel equipped with Rushton impeller, and operating under turbulent flow conditions.

In order to determine the best simulation approach experimental validation of the selected problem is done by means of Particle Image Velocimetry (PIV) system.

When using the rotating frame of reference approach, the stirring vessel geometry has to be split into a stationary and rotating part, and the question arises where to position the interface between both regions in order to avoid numerical errors, originating in numerical approximations at the interface. To answer this question, a comparison between the CFD based numerical results and experimental results, was made.

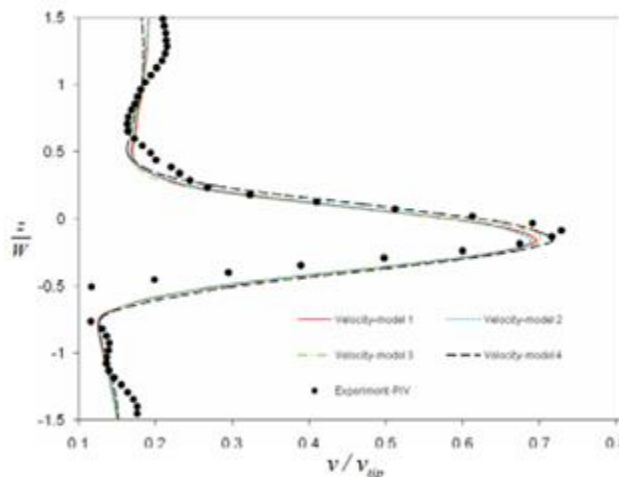


Fig 2.13: Wind speed Ratio vs Tip speed Ratio

CHAPTER 3 PRELIMINARY DESIGN SKETCHES

The basic idea is to make a Savonius wind turbine with 2 helical blades. For the blades we chose a particular type of aerofoil and tried to incorporate it into the design and analyse it.

The aerofoil we selected for the same purpose is the Eppler-E61 with a chord length of 350mm.

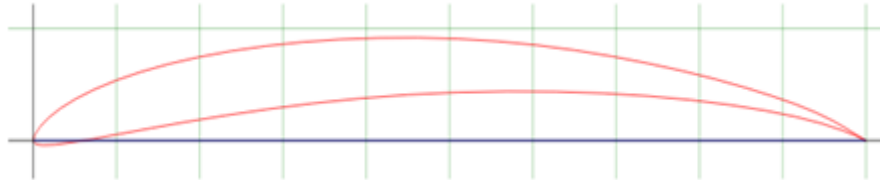


Fig: 3.1: Eppler E-61 Low Reynolds number aerofoil.

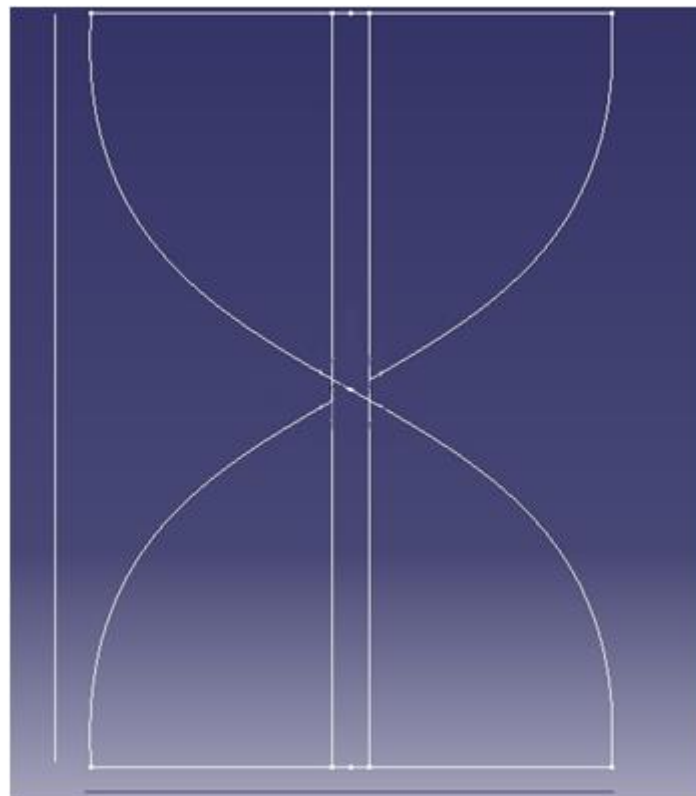


Fig: 3.2: Basic Sketch of Helical Savonius Wind Turbine.

3.1 THE AEROFOIL – EPPLER'S 61 (E61)

The Eppler Airfoil Design and Analysis Code combines a conformal-mapping method for the design of airfoils with prescribed velocity-distribution characteristics, a panel method for the analysis of the potential flow about given airfoils, and an integral boundary-layer method. Basically, Eppler E61 is a low Reynolds number type of Airfoil which specializes in low wind speed low altitude low speed flight. In theory the airfoil should be able to perform really well in a drag type wind turbine under medium and high velocity.

The second reason for choosing this airfoil in particular is that of its thin nature and low camber. It can catch and generate large amount of drag and utilize them to turn effectively. The thin surface also makes it a low weight substitute for a structural material. The only drawback is it might become fragile because of the amount of stress and strain it might have to endure continuously.

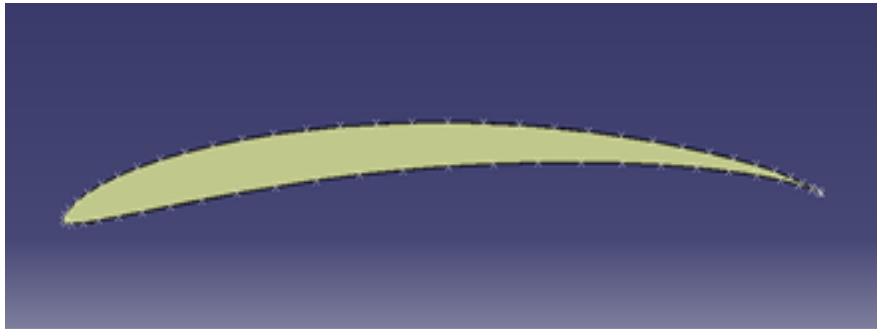


Fig 3.3; Eppler E61 (350mm Chord)

3.1.1 AEROFOIL PROPERTIES

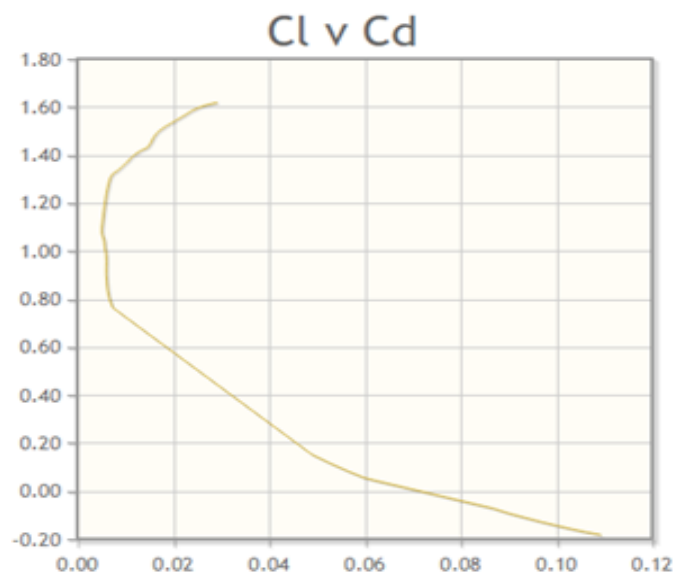


Fig 3.4: Here the Cl v Cd plot is a C shaped curve with values ranging from 0.11 to .005 for Cd and -0.20 to 1.61 for Cl

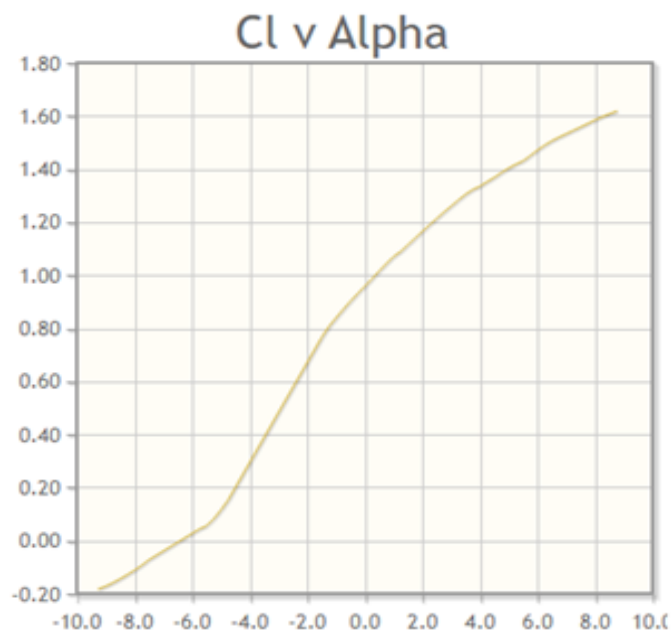


Fig 3.5: Cl vs Alpha or Angle of attack is a rising slope with least value of -.20 for Cl at -9.2 degrees alpha and max value of 1.61 Cl at 8.8-degree alpha

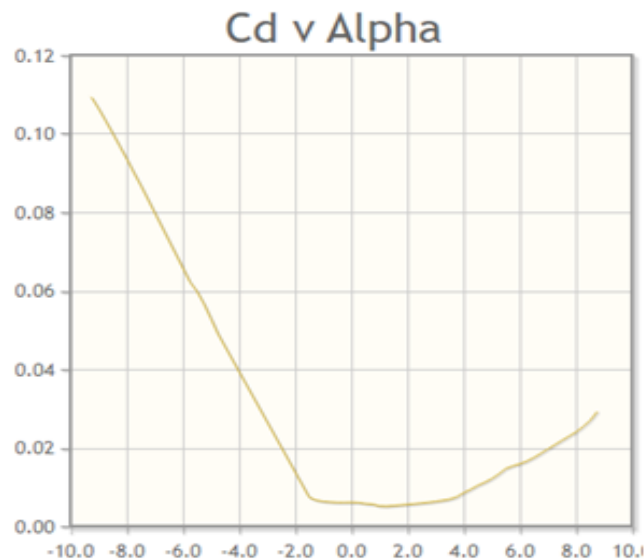


Fig 3.6: Here the Cd vs Alpha Curve is a slanted slope with a curved unstable end. The Coeff of Drag decreases steadily up to an alpha of -1.8 degrees and an evenly increases to 10-degree alpha

3.2 METHODOLOGY AND APPROACH

With the progress of the science of aerodynamics, there are variety of techniques and tools to accomplish this time-consuming job of designing and simulating. A variety of tools and software based on aerodynamics and numerical methods have been developed in the past decades. The desire for more accurate lift and drag predictions for transonic flows-along with a more detailed analysis of the flow field for all flow types-have resulted in the increased use of computational fluid dynamics (CFD).

The basic designing and modelling of the entire structural component of the wind turbine, basically the turbine blades are designed on CATIA V5 R19. There are numerous programs which are available as its market substitute but the versatility and ease of use of CATIA is unparalleled. The 3-Dimensional model thus generated can be used in any type of CFX or CFD analysis program tool.

In this project the turbine analysis is done using computational fluid dynamics techniques. There are different CFD and CFX software available in the market. Among them ANSYS is the one in which we have got some working experience. Its market availability, easier user interface and accurate solutions made ANSYS workbench 2020 as our working software. ANSYS has so many different domain software with its package. ANSYS CFX and ANSYS Fluent is suitable for aerodynamic simulations and fluid problems.

The structural analysis of the model can be conducted using ANSYS 2020 itself, using ANSYS Static Structural and the values obtained from CFX and CFD simulations can be used to obtain the structural analysis data.

3.3 GEOMETRIC DESIGN

During the design phase of our project, we have successfully completed a solid geometric design on CATIA V5 R19. The model consists of 2 helical shaped blades with Eppler E61 airfoil cross sections with a Tip-to-Tip span of 350 mm and a shaft of 5 cm diameter and a length of 1 m. The design procedure is as shown below:

The design procedure began with the importing of Airfoil coordinates (Eppler E61) from a CVS file into the product part window of CATIA. To import the coordinates a Spline generation Macros was used. A circle of 5 cm radius is drawn with the leading-edge point as its center. Thus, we get a cross sectional area of our desired wind turbine blades as shown in Fig: 3.3.1.

The circle is extruded to a length of 1m using the pan option in part design as shown in Fig 3.3.2. Using the Helix tool, form the wireframe and surfaces window, a path for the helical a blade is made from a camber point or airfoil from the top edge to the bottom edge of the shaft with a height of 1000mm, pitch of 2000mm and 0.5 revolutions. Using Ribs option in CATIA, the airfoil cross section is extruded to follow the path of the spiral as shown in Fig 3.3.3.

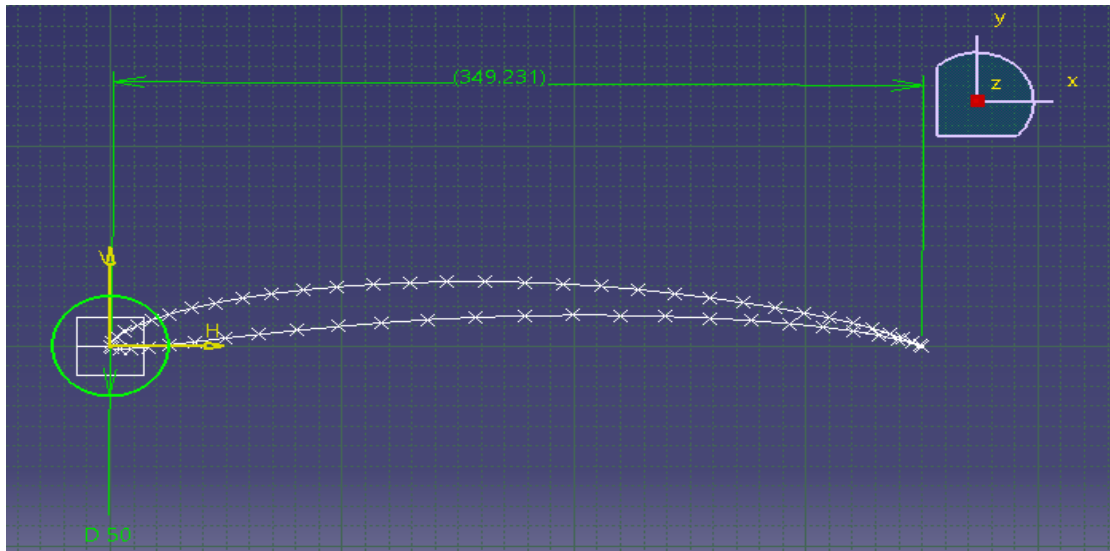


Fig 3.7: Imported Airfoil Plot

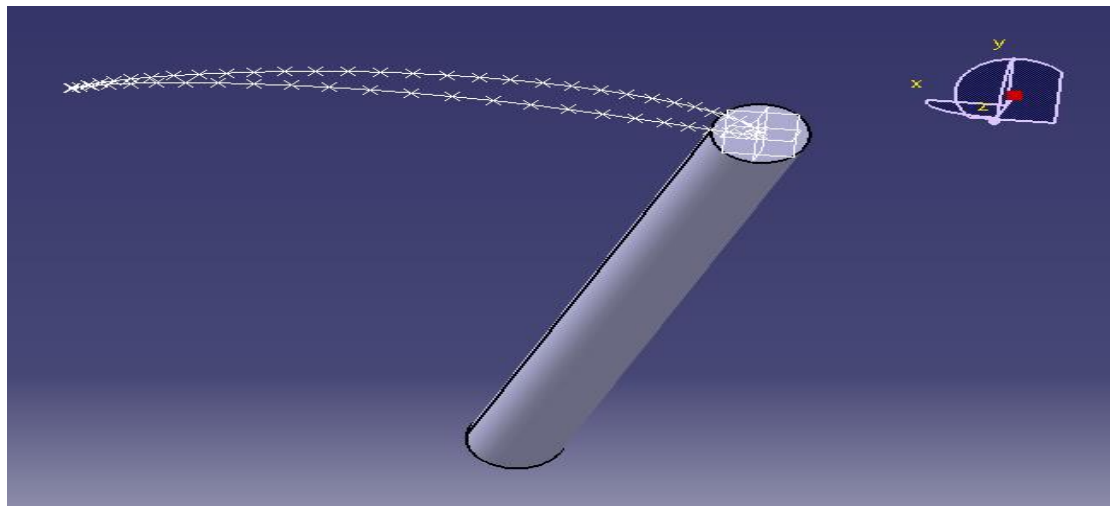


Fig 3.8: Paned Shaft

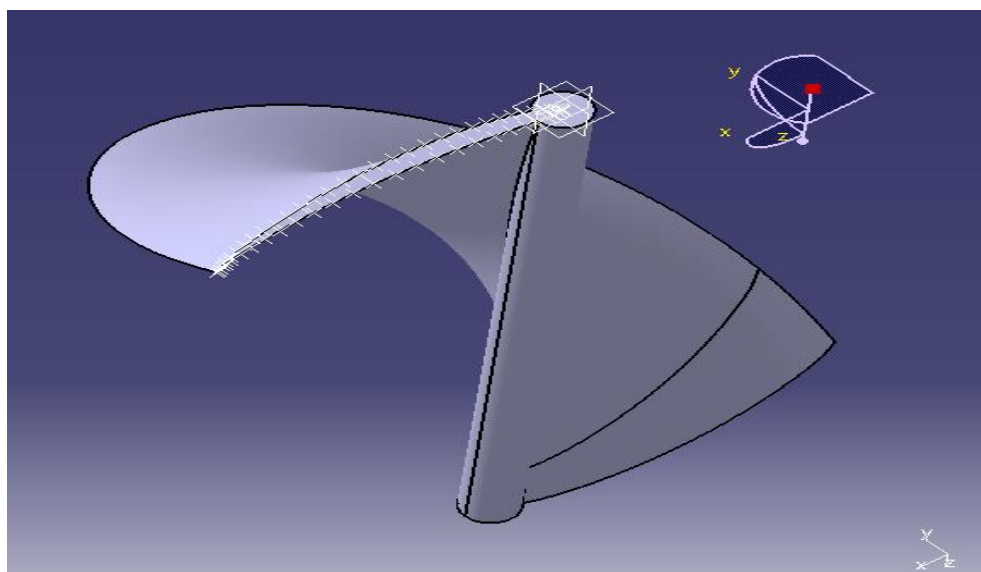


Fig 3.9: Single Blade

This is the basic single blade design. In order to replicate the same, we use the circular tool with an angular difference of 180 degrees apart. The final 3-Dimensional model almost shaped like a hour glass is formed as shown in Fig: 3.3.4

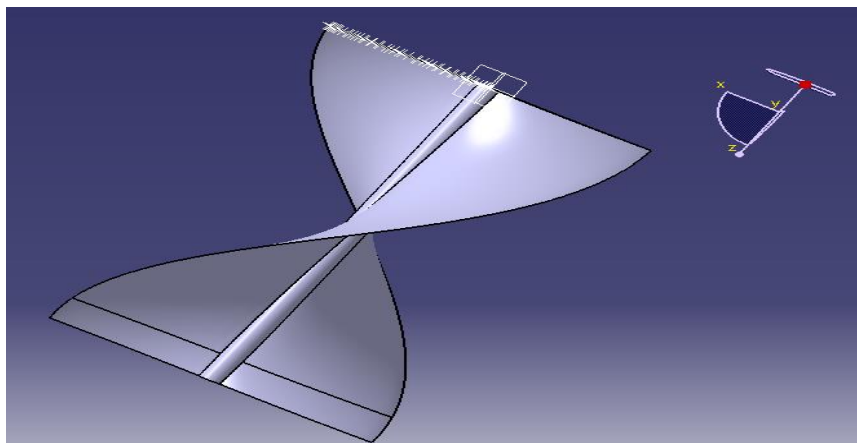


Fig 3.10 Completed Helical Savonius Wind Turbine

The plot values of the entire E61 airfoil are gives below. The points can be imported into a Design and Modelling software can be done using a generative Design Macro program.

X(mm)	Y(mm)	4.095	-1.4735
350	0	9.198	-1.295
348.9745	0.434	16.324	-0.588
346.087	1.7325	25.4555	0.5565
341.6665	3.766	36.547	2.0755
335.923	6.2195	49.5145	3.857
328.8285	8.785	64.239	5.8065
320.2745	11.361	80.5595	7.8155
310.289	13.972	98.287	9.7755
298.991	16.604	117.2045	11.585
286.5135	19.201	137.074	13.132
272.986	21.7175	157.591	14.301
258.566	24.094	178.409	15.043
243.411	26.285	199.2025	15.3615
227.682	28.2135	219.6845	15.267
211.5365	29.8095	239.561	14.7665
195.097	31.0135	258.5555	13.8915
178.4895	31.7905	276.3915	12.6665
161.84	32.137	292.8135	11.144
145.292	32.0705	307.5765	9.3695
129.01	31.6085	320.4565	7.427
113.1515	30.7615	331.247	5.3655
97.8705	29.5435	339.675	3.297
83.3105	27.9755	345.5375	1.5225
69.6115	26.082	348.908	0.3815
56.896	23.8945	350	0
45.276	21.4445		
34.8495	18.781		
25.7005	15.9495		
17.892	13.0165		
11.473	10.045		
6.475	7.119		
2.9085	4.3505		
0.7735	1.862		
0.0035	-0.1015		
0.9975	-1.1515		

Table 3.1: Plot - airfoil Surface

X(mm)	Y(mm)
0.7735	1.862
2.9085	1.500171
6.475	2.864376
11.473	4.487856
17.892	6.312513
25.7005	8.269777
34.8495	10.31201
45.276	12.3596
56.896	14.3644
69.6115	16.27492
83.3105	18.04758
97.8705	19.63648
113.1515	20.97941
129.01	22.05633
145.292	22.83537
161.84	23.29472
178.4895	23.41737
195.097	23.15606
211.5365	22.55705
227.682	21.63956
243.411	20.43707
258.566	18.99239
272.986	17.30895
286.5135	15.46454
298.991	13.50274
310.289	11.46621
320.2745	9.407724
328.8285	7.306274
335.923	5.21868
341.6665	3.2301
346.087	1.53449
348.9745	0.396134
350	0

Table 3.2: Plot - Camber line

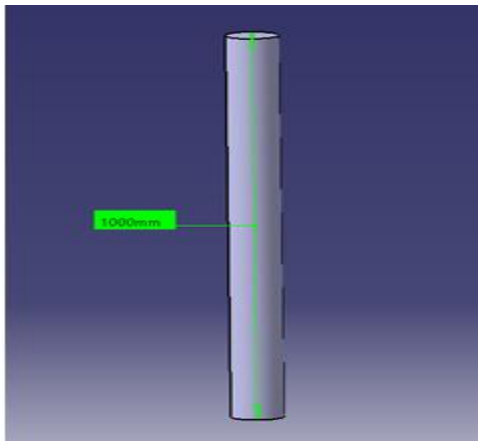
The camber line can be used to accurately plot the dissecting line through the midsection of the turbine blade. The camber also helps to find the point of intersection of the shaft and airfoil cross section.

3.4 STRUCTURAL COMPONENTS AND PARTS

There are mainly 3 major structural components for the proposed design of the wind turbine, in which two are essential and one is optional.

3.4.1. TURBINE SHAFT

The turbine shaft is a singular hollow or solid pole (depends upon the size of the wind turbine), which holds the blades in place through the middle and acts as a driving unit which helps in transferring the rotatory motion to the generator.

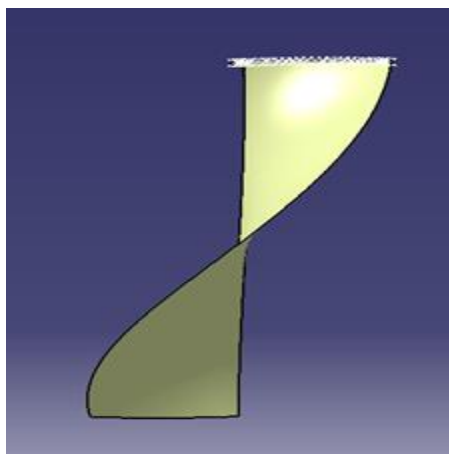


Properties	Dimensions
Shape	Cylinder
Radius	50mm
Length	1000mm
Material	Steel, Aluminum, Iron.

Fig 3.11: Turbine shaft (solid)

3.4.2 TURBINE BLADES

These are the integral part of any turbine which enables the transfer of kinetic energy of the flowing wind into a rotational energy which can be utilized by the generator, here for the proposed Savonius model, the blades are in the shape of a swirl or a helical structure flowing around the shaft for maximum integrity. The cross section of the blades is Eppler E61 model airfoil shaped. Which is a low Reynolds number thin airfoil.



Properties	Dimensions
Shape	Helical
Profile	Thin
Cross section	Eppler E61
Span (single)	350 mm
Span (tip to tip)	700mm
Pitch	2000mm
Revolutions	0.5
Material	ABS/Aluminum.

Fig 3.12: Single Helical Blade Side view

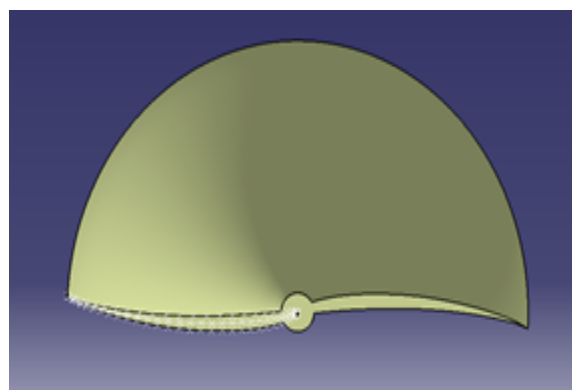


Fig 3.13: Single Helical Blade Top view

3.4.3 COMPLETED 3-DIMENSIONAL GEOMETRY MODEL

The 3-dimensional model is completed with defining the material and surface finish of the model.

Various views of the model are as shown below.

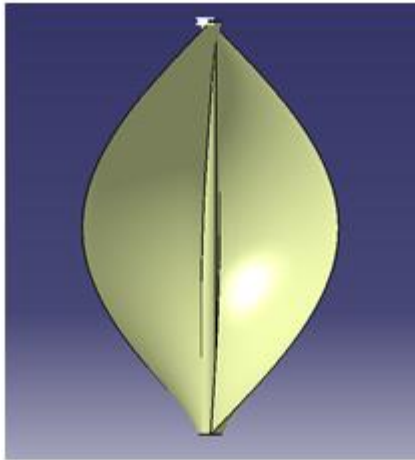


Fig 3.14: Side View of VAWT 1

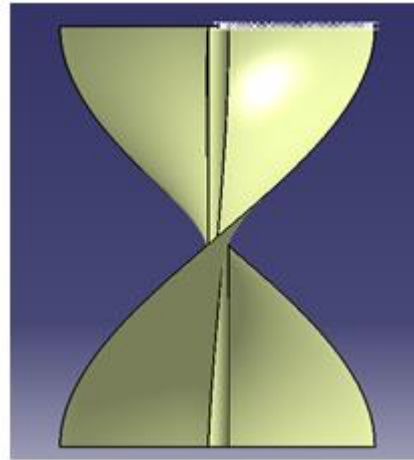


Fig 3.15: Side View of VAWT 2

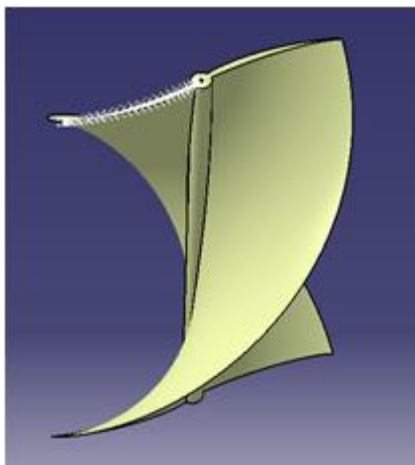


Fig 3.16: Isometric View of VAWT

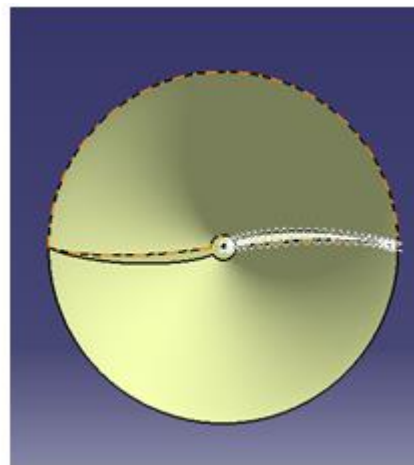


Fig 3.17: Top View of VAWT

3.5 CFX AND CFD ANALYSIS

3.5.1 AIRFOIL - E61

The analysis of aerofoil is a 2-D analysis in a stationary plane. For this analysis the aerofoil is given a flow direction from trailing edge to leading edge rather than from leading edge to trailing edge.

3.5.1.1 MESHING

The partial differential equations that govern fluid flow and heat transfer are not usually amenable to analytical solutions, except for very simple cases. Therefore, in order to analyse fluid flows, flow domains are split into smaller subdomains (made up of geometric primitives like hexahedral and tetrahedral in 3 dimension and quadrilaterals and Triangles in 2D). The governing equations are then discretised and solved inside each of these subdomains. Typically, one of three methods is used to solve the approximate version of the system of equations: finite volumes, finite elements or finite differences. Care must be taken to ensure proper continuity of solution across the common interfaces between two subdomains, so that the approximate solutions inside various portions can be put together to give a complete picture of fluid flow in the entire domain. The subdomains are often called elements or cells, and the collection of all elements or cells is called a mesh or grid.

The meshing of the 3-D model is done using ANSYS 2020 Workbench Meshing. The aerofoil coordinates are imported using an ANSYS compatible (.cvs) file format. An enclosure is given and the aerofoil is subtracted from the fluid enclosure surface using Boolean Subtraction.

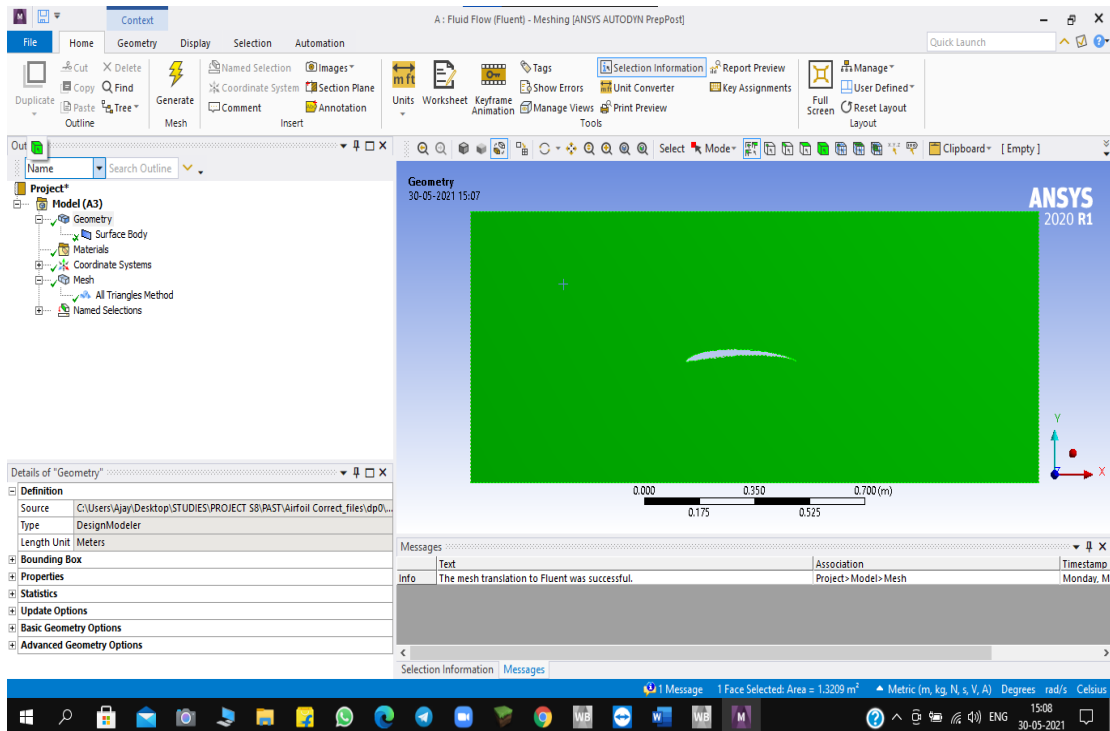


Fig 3.18: Aerofoil inside Fluid enclosure (Boolean Subtracted)

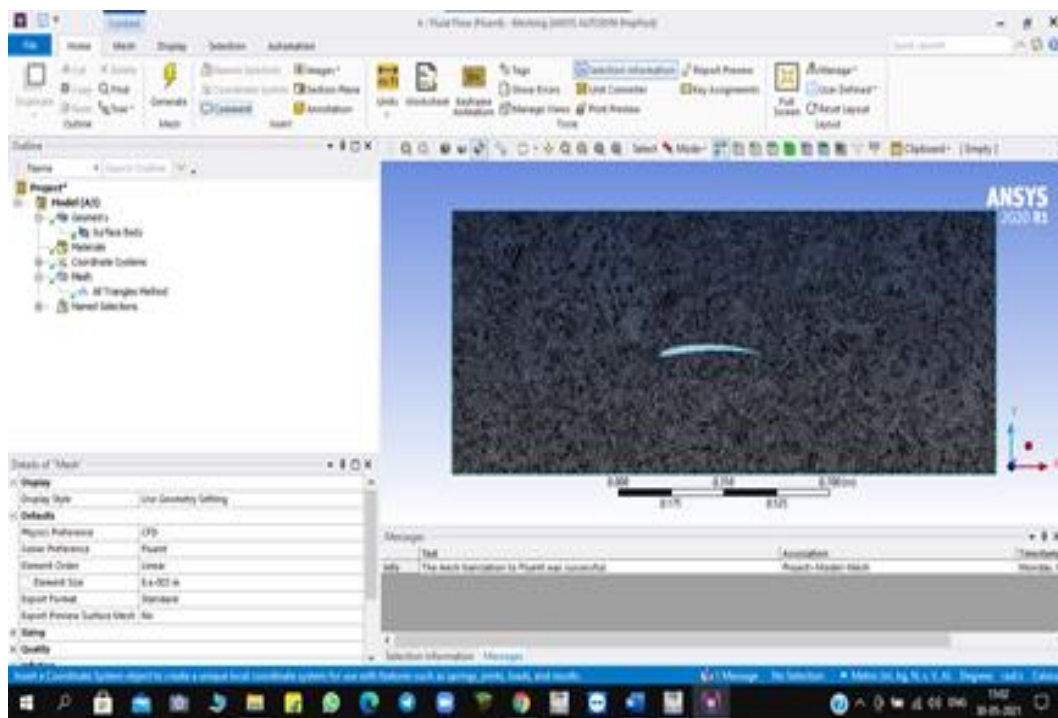


Fig 3.19: Mesh data of Aerofoil, using Boolean Subtraction.

3.5.1.2 BOUNDARY CONDITIONS

As we know that the most important part of any Computational Fluid Dynamics (CFD) problem is the definition of its boundary conditions. Therefore, it is required that the user understands and uses the boundary conditions correctly, wisely and effectively and also understands its role in the numerical algorithm. If the boundary conditions are not specified correctly, then the solution might result in blunders and if they are not utilized wisely, then the problem-solving time may increase manifold. Various types of boundary conditions are used in CFD for different conditions and purposes. The boundary conditions here are given just before the solving process. The solver is run on, Double precision mode.

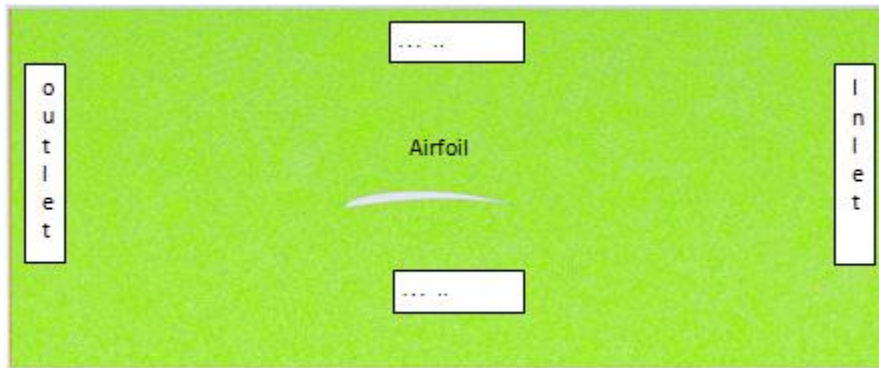


Fig 3.20: Boundary Nomenclature

BASIC BOUNDARY CONDITIONS	
Solid Material	Aluminium
Fluid Material	Air
Computation carried out from	Inlet
Enclosure Length	1803 mm
Enclosure width	735 mm
Aerofoil Chord Length	350 mm
Solving Type	Iterations (500)
Time Scaling	Steady

INLET BOUNDARY CONDITIONS	
Inlet Type	Velocity based
Computation carried out from	Inlet
Density	1.225 Kg/m ³
Temperature	288.16K
Viscosity	Laminar
Velocity	20 m/s
Viscosity	1.7894e-05

OUTLET BOUNDARY CONDITIONS	
Outlet Type	Pressure based
Computation carried out from	Inlet
Density	1.225 Kg/m ³
Temperature	288.16K
Viscosity	Laminar
Velocity	0 m/s
Computed Values	Relative to Inlet

3.5.2 HELICAL AXIS WIND TURBINE

3.5.2.1 GEOMETRY

The geometry setup for the CFX analysis is different from that of a normal one. Since the rotor should turn independently and the analysis should be about the performance of flow of wind and its action on the rotating turbine blade. Therefore, the geometry is done in two parts.

a) **Rotor Part:** The rotor part is the Rotating part consisting of the entire Turbine Blades, shaft and a cylindrical enclosure. The entire geometry is done in Design Modeller window since it is 3-D in nature. The Rotor blades are Boolean Subtracted without preserving the body and the enclosure material is changed to fluid because of the absence of any real body.

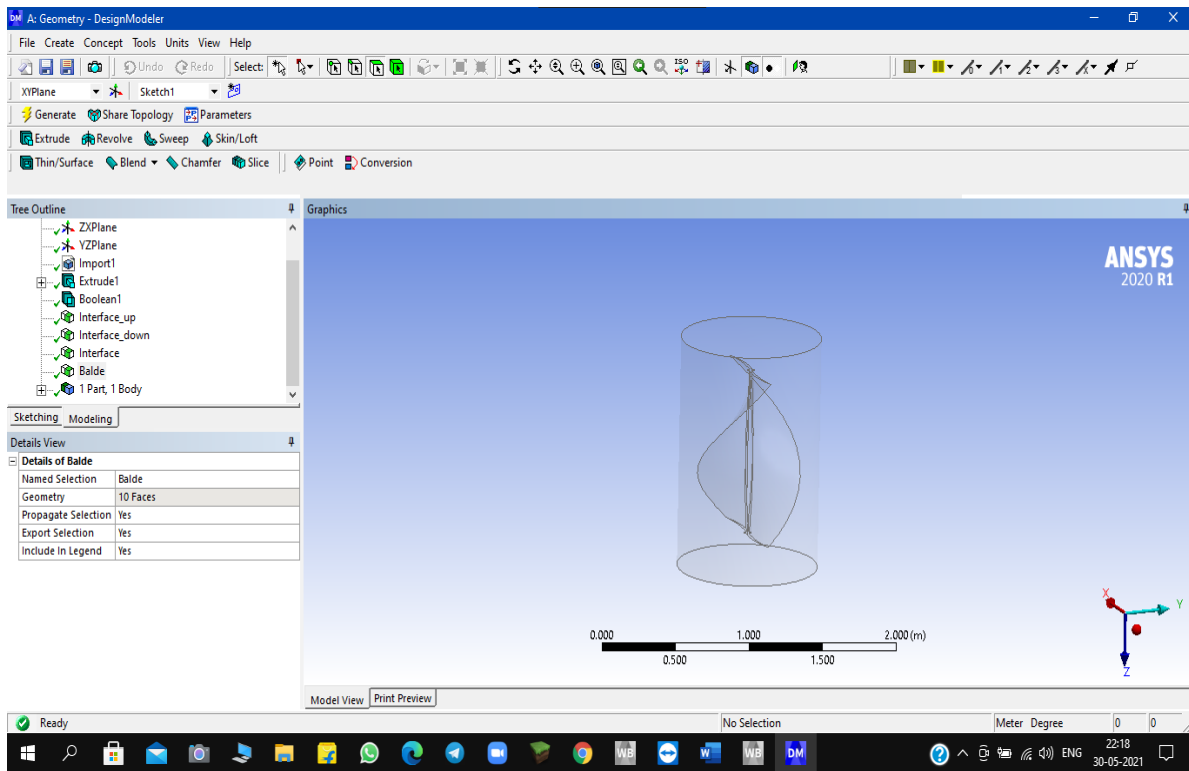


Fig 3.21: Design Modeller Rotor Part.

ROTOR PART DIMENSIONS	
Turbine Blade Width	0.7 m
Turbine Blade Height	1.0 m
Enclosure Height	1.2m
Enclosure Diameter	0.957m

b) Stator Part: The stator part, as the name suggests is the stationary part where the simulations of the rotor take effect. The Stator part acts as an enclosure or a slot for the entire rotor part. The stator part is completely fluid and is large enough to enclose the rotor interface surface. It is cuboid in nature and has a cylindrical cavity relatively in the middle but more leaning towards the inlet, for the Rotor part.

STATOR PART DIMENSIONS	
Enclosure Width	4.16 m
Enclosure Height	3.4 m
Enclosure Length	7.9 m
Cavity Diameter	0.9572 m
Cavity Height	1.2 m

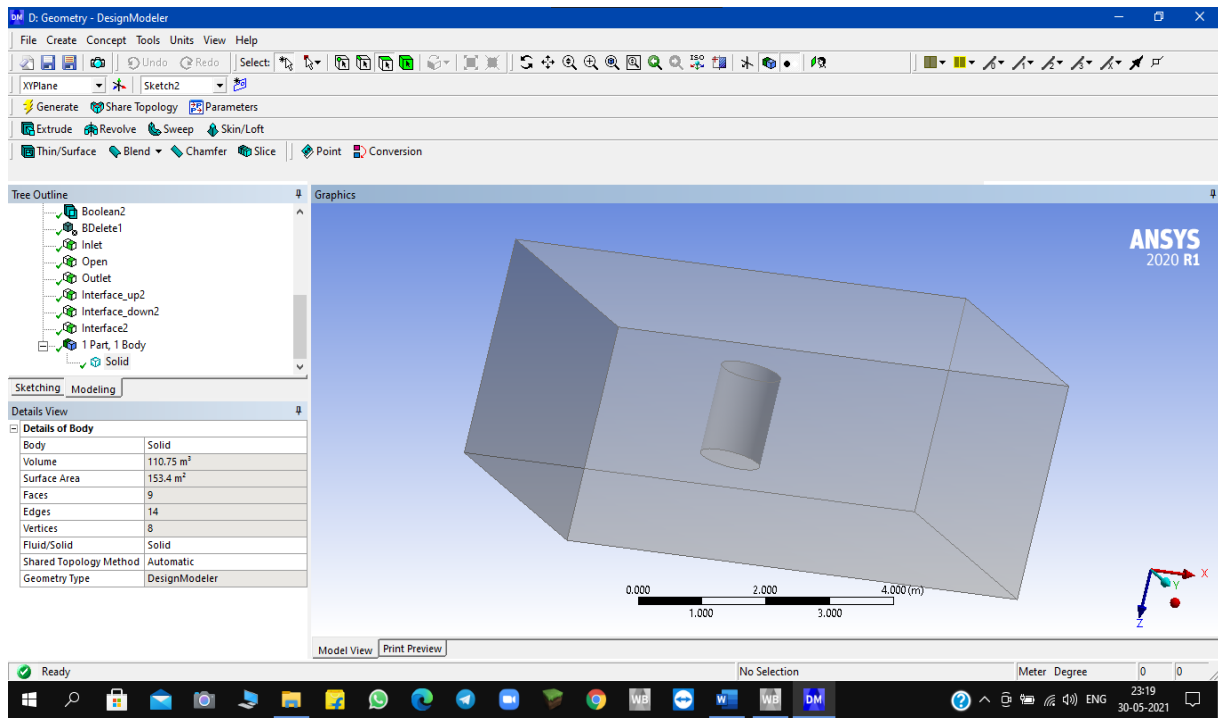


Fig 3.22: Design Modeller Stator

3.5.2.2 MESHING:

In order to analyse fluid flows, flow domains are split into smaller subdomains (made up of geometric primitives like hexahedral and tetrahedral in 3 dimension and quadrilaterals and Triangles in 2D). The governing equations are then discretised and solved inside each of these subdomains. Typically, one of three methods is used to solve the approximate version of the system of equations: finite volumes, finite elements or finite differences. The subdomains are often called elements or cells, and the collection of all elements or cells is called a mesh or grid. The rotor part and the stator parts are Meshed using ANSYS 2020 Meshing stand-alone system. Both the parts are meshed in multiple Stand-alone system and are analyzed in a combined manner.

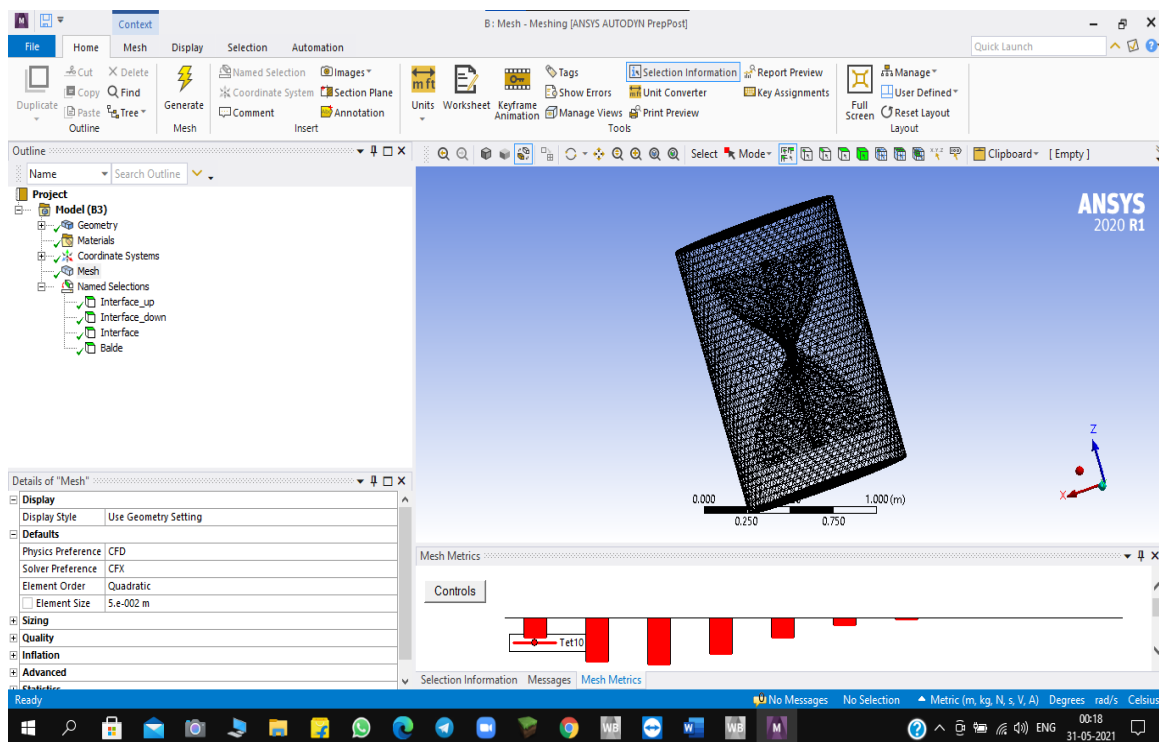


Fig 3.23: Mesh Data of Rotor Component (Element Size 5e-02)

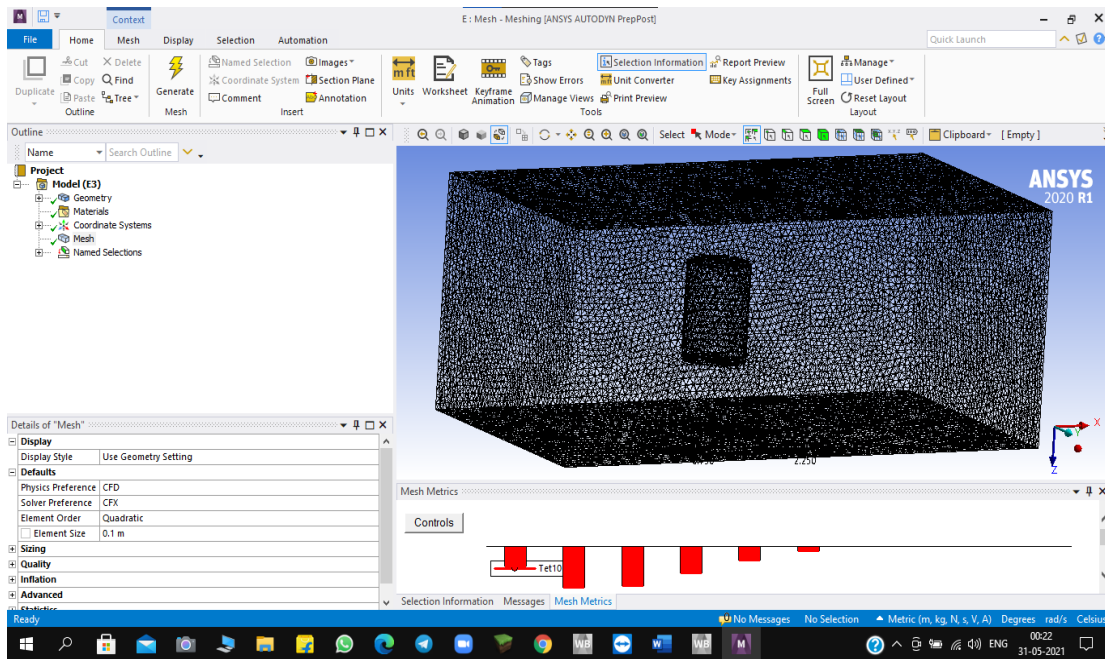


Fig 3.24: Mesh Data of Stator Component (Element Size 1.0)

3.5.1.3. PARAMETERS

The meshed Rotor part has to be parameterized in order to be in motion. The parameter that we use here is an input parameter, mainly Mesh curvature. The mesh curvature should be kept minimum size as 0.

Outline of All Parameters				
	A	B	C	D
1	ID	Parameter Name	Value	Unit
2	[-] Input Parameters			
3	[-] Mesh (B1)			
4	[P] P1	Mesh Curvature Min Size	0	m
*	[P] New input parameter	New name	New expression	
6	[+] Output Parameters			
*	[P] New output parameter		New expression	
8	Charts			

Fig 3.25: Parameter settings

3.5.2.3 BOUNDARY CONDITION AND SETUP

The boundary condition and setup for both Rotor and Stator stand-alone systems are linked together to create a single interface setup which makes the rotor to interact with the whole stator part without any ill effects. Within the Simulation set up window, one must define the characteristics of the stator, rotor and the interface.

a) **ROTOR:** The rotor part is the rotating part so the characteristic values and initial values of the rotor domain should be defined along with the rotor domain boundary. The rotor domain, having a cylindrical enclosure has 3 interfaces in mesh with that of the stator, the interfaces should be well defined along with their initial values. Within the rotor interface, one must also define the proper geometry of the turbine blade. The turbine blades here should be assigned characteristic details of a rotating wall, whereas the interfaces should be stationary to the stator.

b) **STATOR:** The stator part should be defined the same way as the rotor, and the major inlet outlet and global wall areas should be defined. The openings to the atmosphere must also be defined correctly. Along with all these information, the interface interacting with the rotor interface should also be defined, they pose utmost importance as their actions affect the entire simulations and the flow of fluid into the chamber.

c) **INTERFACE REGION:** This part defines all the interfaces individual characteristics independent of their part and locations. The interface region characteristics should be well defined along with their type as interfaces, the interface Mixing model types should be defined as transient rotor type and the model connection type should be General model type.

3.6 GOVERNING EQUATIONS

There are multiple equations of fluid motion and turbulence in place for a CFX and CFD analysis.

1) **K-epsilon (k-ε) turbulence model** is the most common model used in Computational Fluid Dynamics (CFD) to simulate mean flow characteristics for turbulent flow conditions. It is a two-equation model that gives a general description of turbulence by means of two transport equations (PDEs). The original impetus for the K-epsilon model was to improve the mixing-length model, as well as to find an alternative to algebraically prescribing turbulent length scales in moderate to high complexity flows.

- The first transported variable is the turbulent kinetic energy (k).
- The second transported variable is the rate of dissipation of turbulent kinetic energy (ε).
- The exact k-ε equations contain many unknown and unmeasurable terms. For a much more practical approach, the standard k-ε turbulence model (Launder and Spalding, 1974) is used which is based on our best understanding of the relevant processes, thus minimizing unknowns and presenting a set of equations which can be applied to a large number of turbulent applications.

$$\frac{\partial(\rho k)}{\partial t} + \frac{\partial(\rho k u_i)}{\partial x_i} = \frac{\partial}{\partial x_j} \left[\frac{\mu_t}{\sigma_k} \frac{\partial k}{\partial x_j} \right] + 2\mu_t E_{ij} E_{ij} - \rho \epsilon$$

u_i Represents velocity component in corresponding direction

E_{ij} Represents component rate of deformation

μ_t Represents eddy viscosity

$$\mu_t = \rho C_\mu \frac{k^2}{\epsilon}$$

2) **The Differential Equation for mass conservation:** Let consider an infinitely small elemental control volume having dimensions dx, dy, dz in X, Y, Z directions respectively.

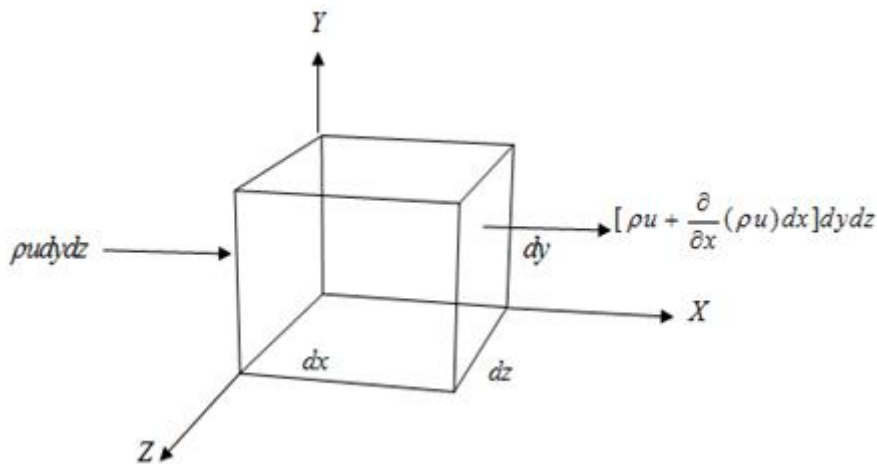


Fig 3.26: Assumed Element

The flow through each side of the element is approximately one dimensional hence the approximate mass conservation relation is used here,

$$\int_{cv} \frac{\partial \rho}{\partial t} dV + \sum_i (\rho_i A_i V_i)_{out} - \sum_i (\rho_i A_i V_i)_{in} = 0$$

3.7 STRUCTURAL ANALYSIS

Structural analysis is done mainly in terms of the results obtained from the ANSYS CFX results. The main results are the obtained directional moment. The structural analysis consists of obtaining the effect of actions on all or part of the structure in order to check the ultimate limit states and serviceability limit states. Such an analysis must be conducted for the different design situations using adequate structural models that consider the influence of all relevant variables.

In order to conduct the analysis, both the geometry of the structure and the actions and support conditions are idealized by means of an adequate mathematical model, which must also roughly reflect the stiffness conditions of the cross-sections, members, joints and interaction with the ground. The structural models must allow to consider the effects of movements and deformations in those structures or part thereof, where second-order effects increase the effects of the actions significantly. In certain cases, the model must incorporate the following into its stiffness conditions:

- The non-linear response of the material outside the elastic analysis.
- The effects of shear lag in sections with wide flanges.
- The effects of local buckling in compressed sheet panels.
- The effects of the catenary (using a reduced modulus of elasticity, for example) and of displacement on structures with cables.
- The shear deformability of certain structural members.
- The stiffness of the joints.
- Interaction between the ground and the structure.

Where it is necessary to conduct dynamic analyses, the structural models must also consider the properties of mass, stiffness, resistance and damping of each structural member, as well as the mass of other, non-structural, members. Where it is appropriate to perform a quasi-static approximation of the structure's dynamic effects in accordance with the codes or regulations in force, such effects may be included in the static values of the actions, or dynamic amplification factors equivalent to such static actions could even be applied. In some cases (e.g., vibrations caused by wind or earthquake), the effects of the actions may be obtained from linear elastic analyses using the modal superposition method.

Here the structural analysis is conducted by giving the following data:

- Defining Engineering Data: The degree of structural load bearing and capacity of any member should only be as good as the materials used. The material that we have used here in this project is, Aluminum Alloy which is a predefined engineering general material in ANSYS 2020.
- Geometry: The geometry of the Helical Savonius turbine should be imported into the design modeler without the enclosure. The field setup should be done on this model.
- Setup: The setup part is the pillar of Structural analysis, where we give the boundary conditions are defined. For this the following constrains are provided into the model.
 - Rotational Velocity: The velocity at which the turbine blade spins. The velocity is placed at the shaft. Since the turbine blade is vertical in nature, the velocity acts about Z axis.
 - Displacement: The shaft is fixed for this analysis, so the displacement of the shaft in free space should be kept zero.ie;
 - X axis – 0
 - Y axis – 0
 - Z axis – 0

Moment: The moment is defined as in physics, **moment of force** (often just **moment**) is a measure of its tendency to cause a body to rotate about a specific point or axis. Here the moments are given as components with respect to x and y axis. The moment values are obtained directly from the ANSYS CFX simulations

Details of "Moment 2"	
Scope	
Scoping Method	Geometry Selection
Geometry	4 Faces
Definition	
Type	Moment
Define By	Components
Coordinate System	Global Coordinate System
<input type="checkbox"/> X Component	0. N·m (ramped)
<input type="checkbox"/> Y Component	0. N·m (ramped)
<input type="checkbox"/> Z Component	0. N·m (ramped)
Suppressed	No
Behavior	Deformable
Advanced	

Fig 3.27: Moment Details

Here the components of moment are given and the Scope of the moment or the area on which the moment acts are defined. For the Helical Savonius Wind Turbine model, the moment is assumed to act directly on the shaft.

- **Meshing:** Meshing is similar to that of meshing in CFX. The Mesh here is directly associated with the solver where once you try to solve the structural analysis giving the valid constrains and equations, one can get the mesh and the solution simultaneously.

A detailed window of the meshed Turbine blade and meshing window is given below, once solved you can view the different solutions associated with the structural analysis on the mesh model itself.

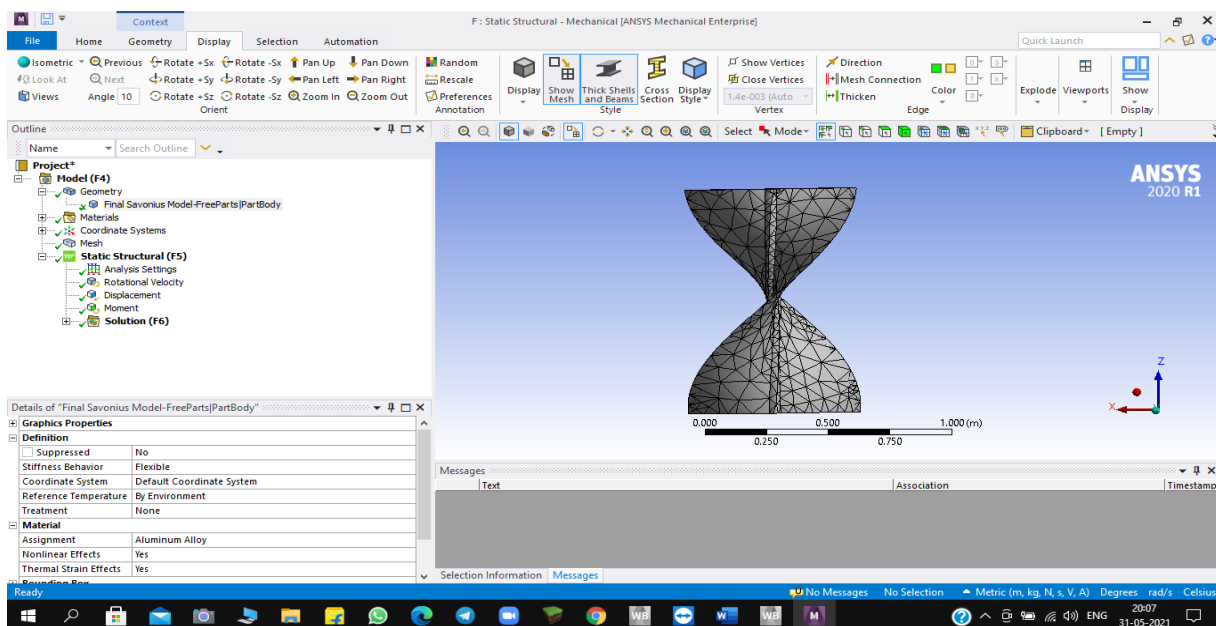


Fig 3.28: Mesh model and Meshing window - Static structural.

CHAPTER 4 ANALYSIS AND RESULTS

The major objective of our analysis is to find the characteristic properties and behavior of our Helical Savonius Wind Turbine under various conditions and properties of atmosphere.

4.1 ANALYSIS UNDER VARIOUS WIND AND ANGULAR VELOCITIES

The designed turbine blade model was analyzed under different angular velocities and different wind velocities. The test setup was done for the following Wind speeds and their respective angular velocities.

DATA ANALYSIS ON HELICAL SAVOUNIUS WIND TURBINE		
SL NO	WIND SPEED	ω
1	5 ms ⁻¹	LOW WIND SPEED
		10
		20
2	15 ms ⁻¹	MEDIUM WIND SPEED
		40
		50
3	25 ms ⁻¹	HIGH WIND SPEED
		70
		80

Table 4.1: Multiple Wind Velocities and Angular velocities

4.1.1 LOW WIND SPEED (5m/s)

- **Angular Velocity 10 rad/s**

Under the setup condition of the ANSYS CFX pre window, the cartesian velocity components are set to 5m/s to simulate wind speed, for both stator and rotor.

Under the same setup condition, the Rotor domain motion is set for -10 rad/s for simulating the blade rotation at desired speed through the desired direction.

Shown below are the analysis and result data for CFX pre ANSYS 2020:

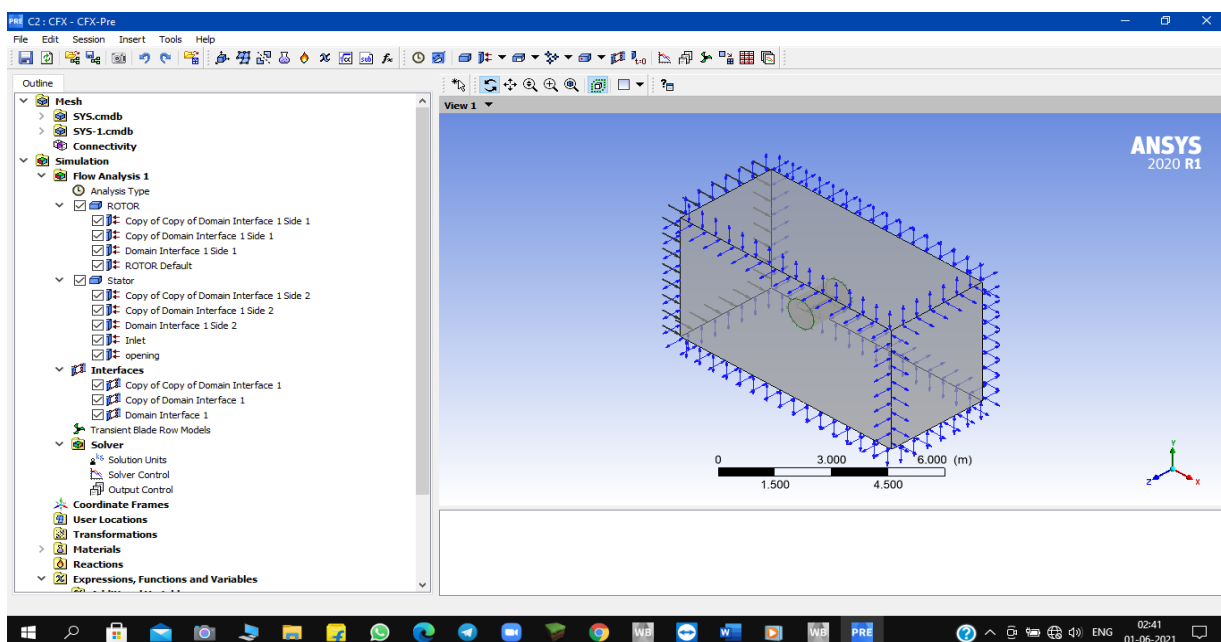


Fig 4.1: CFX pre setup for 10 rad/s angular velocity at 5m/s windspeed

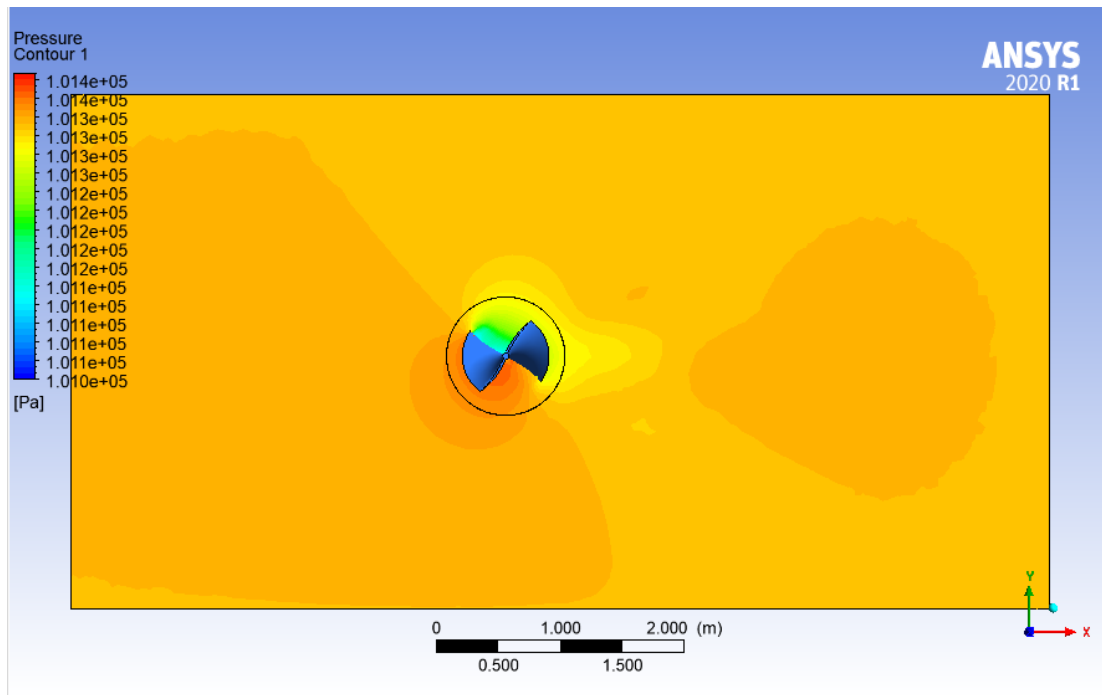


Fig 4.2: CFX Result for pressure contour on Iso-surface

Maximum Pressure	1.014e+05 Pa
Minimum Pressure	1.010e+05 Pa
Wind speed	5 m/s
Angular Velocity	-10 rad/s

LOCATION	TYPE	MASS FLOW	MOMENTUM		
			x	y	z
Inlet (Stator)	Boundary	1.6765e+2	1.4352e+6	4.1140e-8	1.6059e-8
ROTOR Default (ROTOR)	Boundary	0.0000e+0	6.7467e+1	2.6970e+0	-2.8691e-2
opening (Stator)	Boundary	-1.6764e+2	-1.4352e+6	7.5000e-1	2.0717e+0
Copy of Copy of Domain Interface 1 Side 1 (ROTOR)	Domain Interface	-7.9886e-1	6.8026e+0	-4.3561e+0	-7.2405e+4
Copy of Copy of Domain Interface 1 Side 2 (Stator)	Domain Interface	7.9884e-1	7.0857e+0	-1.8272e-2	7.2011e+4
Copy of Domain Interface 1 Side 1 (ROTOR)	Domain Interface	-7.7643e-1	6.4216e+0	-5.8597e+0	7.2601e+4
Copy of Domain Interface 1 Side 2 (Stator)	Domain Interface	7.7642e-1	7.8397e+0	3.0042e-1	-7.2388e+4
Domain Interface 1 Side 1 (ROTOR)	Domain Interface	1.5758e+0	-1.2786e+1	7.4385e+1	-1.5554e+0
Domain Interface 1 Side 2 (Stator)	Domain Interface	-1.5760e+0	-6.4382e+1	-4.5408e+1	1.5464e+0

Table 4.2: of CFX Boundary Flow values

• **STRUCTURAL ANALYSIS**

In the Static structural window, the values we obtain from the CFX pre analysis is considered. The obtained momentum is given to the momentum constrain in Static structural Setup.

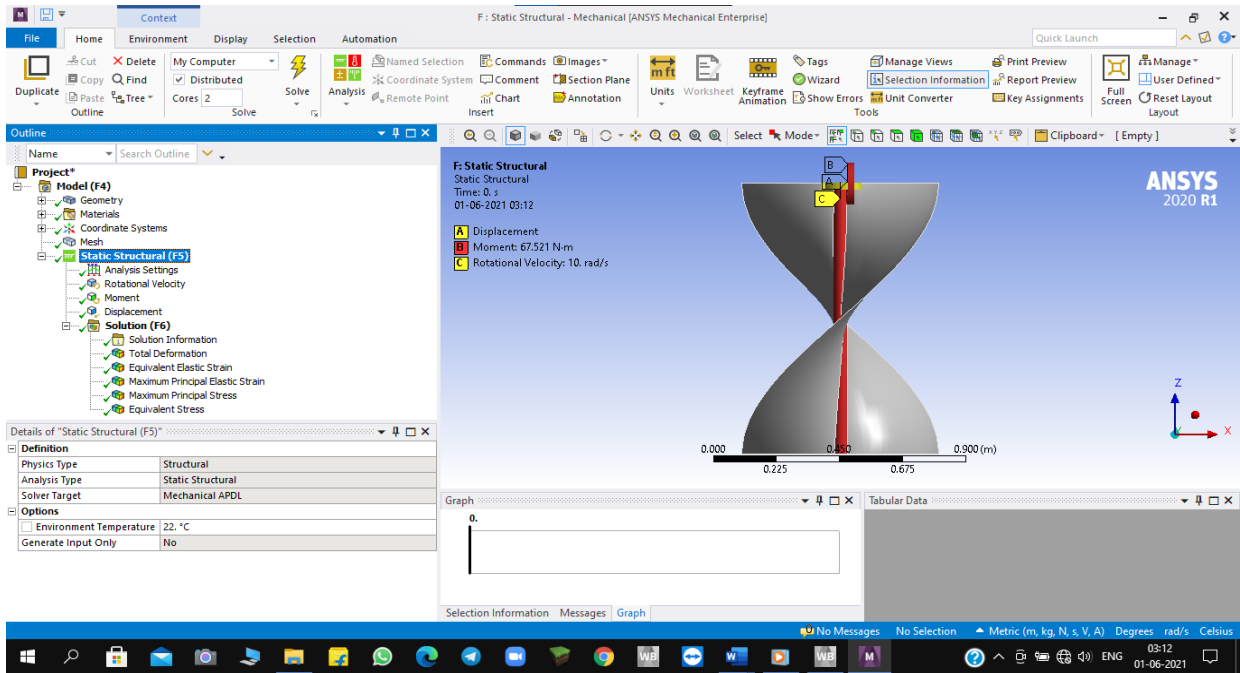


Fig 4.3: Static Structural Setup Window

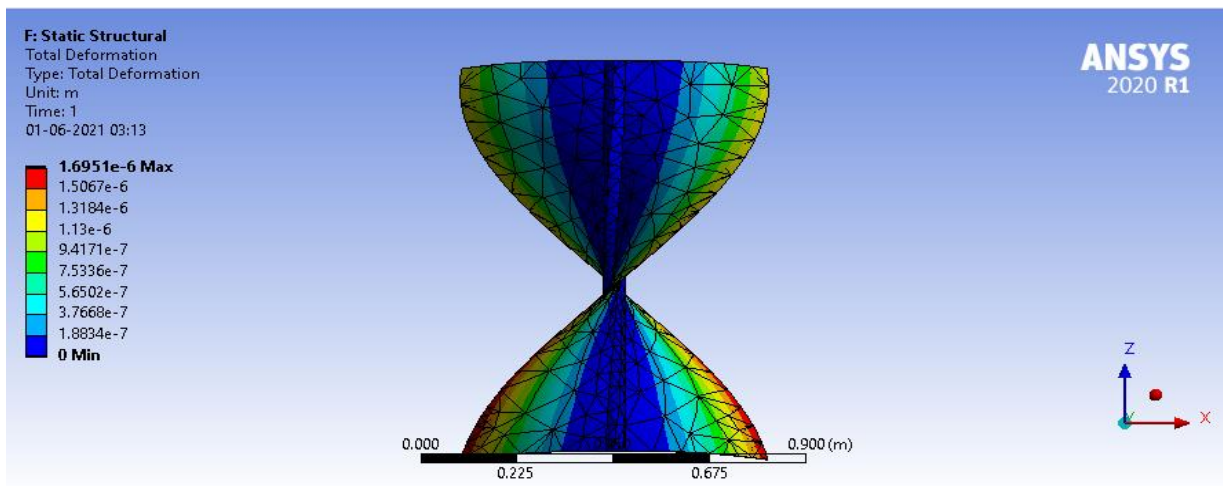


Fig4.4: Total Deformation

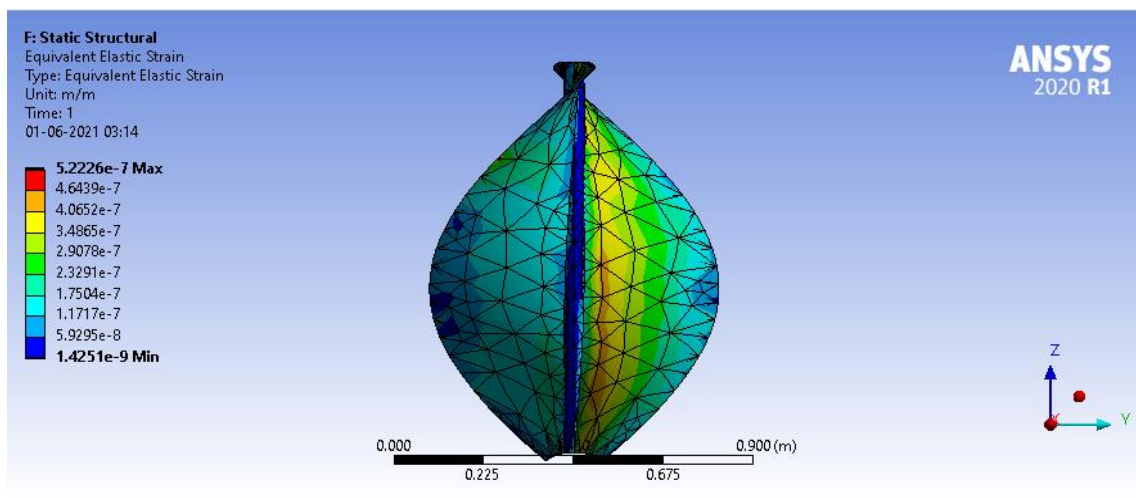


Fig 4.5: Equivalent Elastic Strain

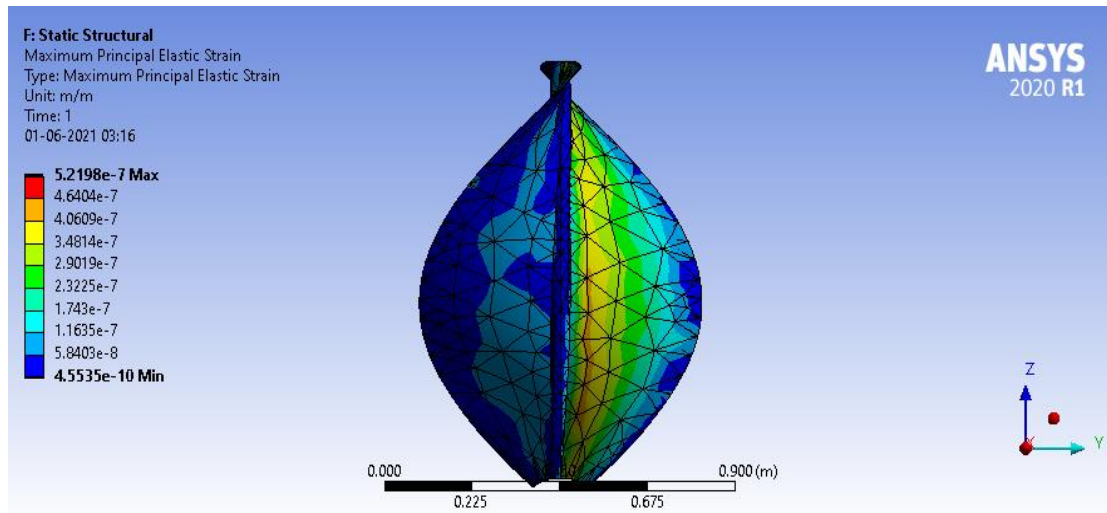


Fig 4.6: Maximum Principal Strain

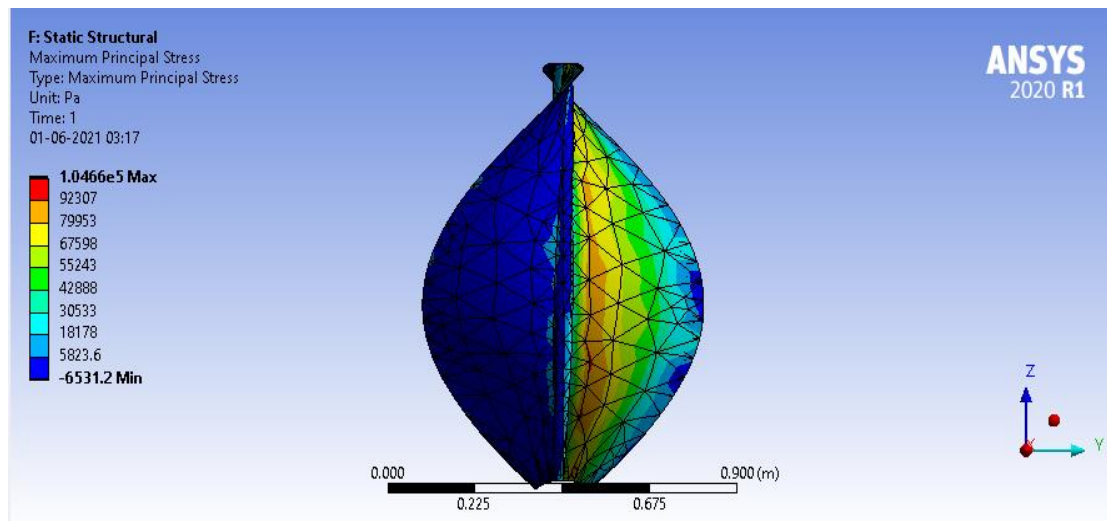


Fig 4.7: Maximum Principal Stress

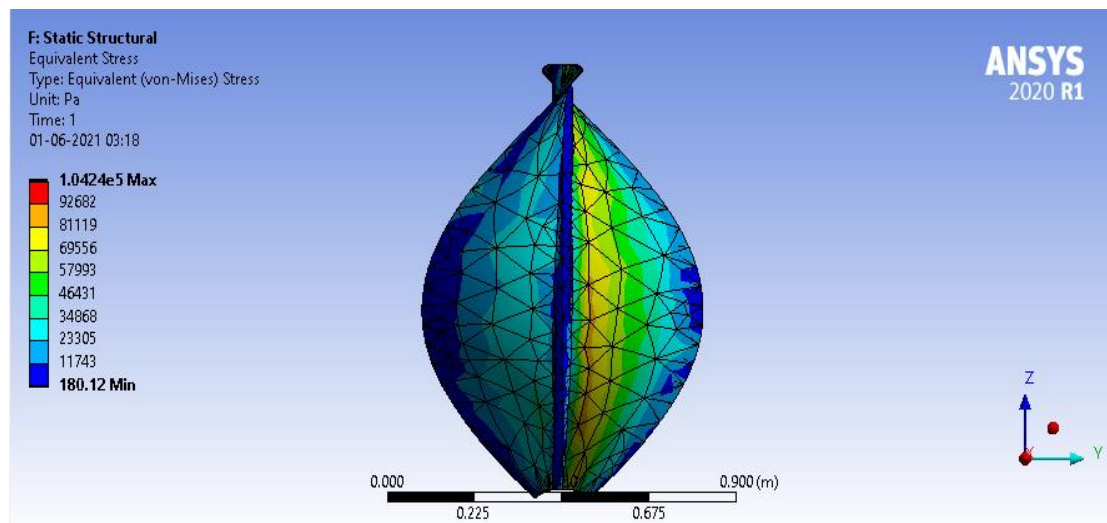


Fig 4.8: Equivalent Stress

Sl. No	SOLUTION	MIN VALUE(Pa)	MAX VALUE(Pa)
1	Total Deformation	0	1.6951e-6
2	Equivalent Elastic Strain	1.4251e-9	5.2226e-7
3	Maximum Principal Stress	-6531.2	1.0466e5
4	Maximum Principal Strain	4.5535e-10	5.2198e-7
5	Equivalent Stress	180.12	1.0424e5

Table 4.3: of Static Structural Analysis Results

• **Angular Velocity 20 rad/s**

Under the setup condition of the ANSYS CFX pre window, the cartesian velocity components are set to 5m/s to simulate wind speed, for both stator and rotor.

Under the same setup condition, the Rotor domain motion is set for -20 rad/s for simulating the blade rotation at desired speed through the desired direction.

Maximum Pressure	1.014e+05 Pa
Minimum Pressure	1.010e+05 Pa
Wind speed	5 m/s
Angular Velocity	-20 rad/s

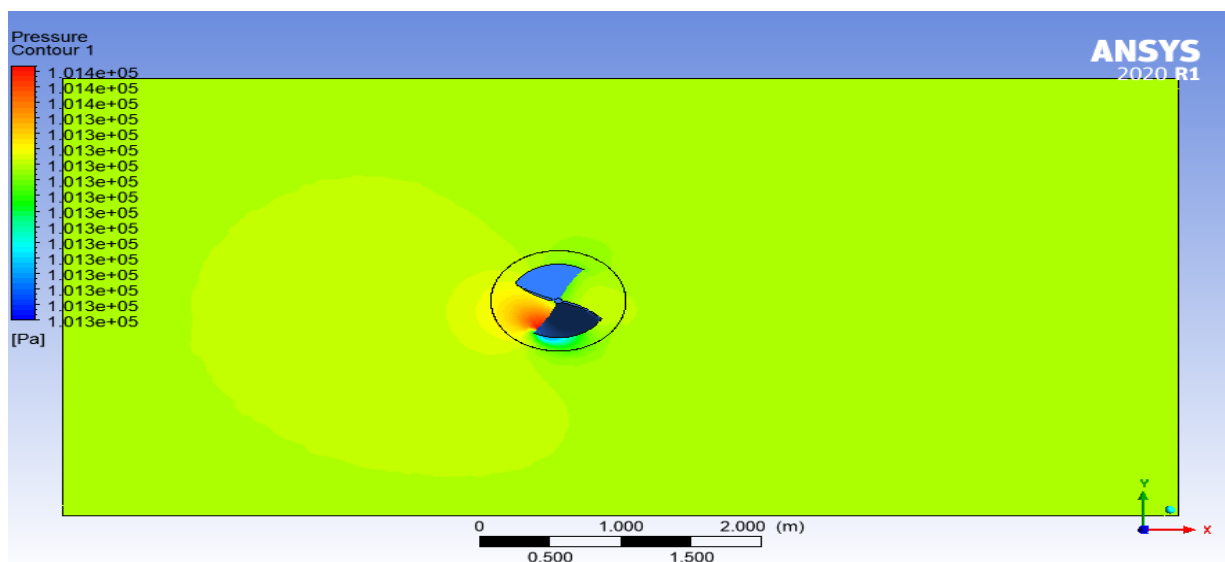


Fig 4.9: CFX Result for velocity contour on Iso-surface.

LOCATION	TYPE	MASS FLOW	MOMENTUM		
			x	y	z
Inlet (Stator)	Boundary	8.3822e+1	1.4339e+6	4.3919e-8	-3.9583e-8
ROTOR Default (ROTOR)	Boundary	0.0000e+0	2.5552e+1	-1.1499e+0	5.7674e+0
opening (Stator)	Boundary	-8.3823e+1	-1.4339e+6	6.2500e-1	2.1508e+0
Copy of Copy of Domain Interface 1 Side 1 (ROTOR)	Domain Interface	-5.0126e-1	4.0129e+0	-3.6452e+0	-7.2404e+4
Copy of Copy of Domain Interface 1 Side 2 (Stator)	Domain Interface	5.0129e-1	2.0135e+0	3.9038e-1	7.2010e+4
Copy of Domain Interface 1 Side 1 (ROTOR)	Domain Interface	1.1344e-1	-1.6753e+0	-1.3825e+0	7.2602e+4
Copy of Domain Interface 1 Side 2 (Stator)	Domain Interface	-1.1344e-1	-6.2533e-1	1.2321e-2	-7.2390e+4
Domain Interface 1 Side 1 (ROTOR)	Domain Interface	3.8732e-1	3.8005e+1	7.3893e+1	-5.4169e+0
Domain Interface 1 Side 2 (Stator)	Domain Interface	-3.8717e-1	-1.7752e+1	-1.1867e+1	5.4086e+0

Table 4.4: of CFX Boundary Flow values

• **STRUCTURAL ANALYSIS**

In the Static structural window, the values we obtain from the CFX pre analysis is considered. The obtained momentum is given to the momentum constrain in Static structural Setup.

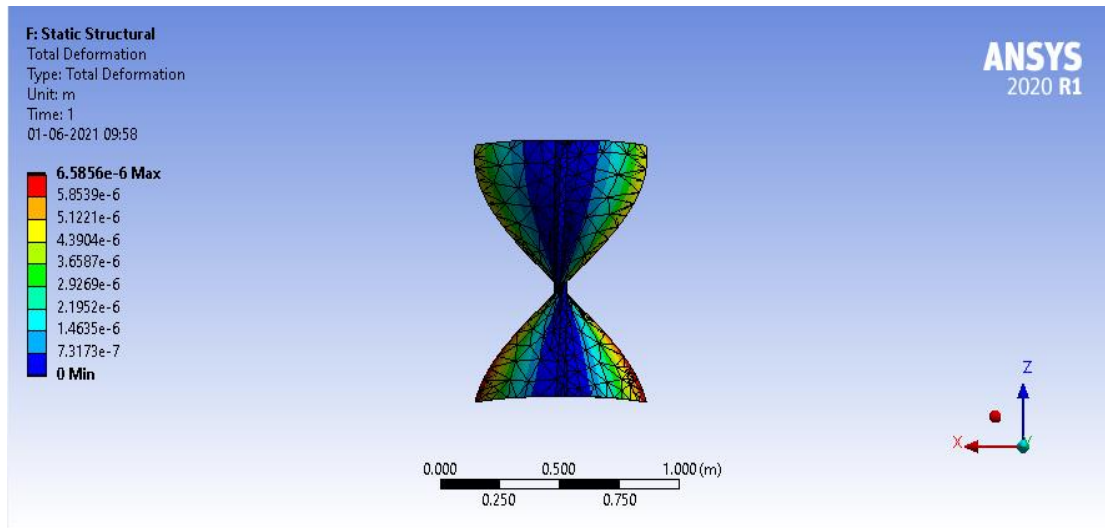


Fig 4.10: Total Deformation

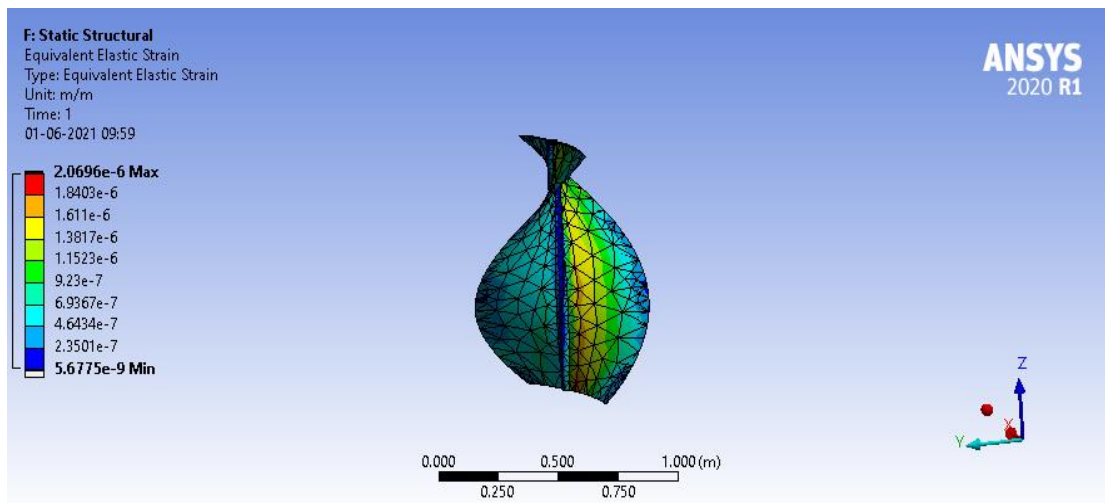


Fig 4.11: Equivalent Elastic Strain

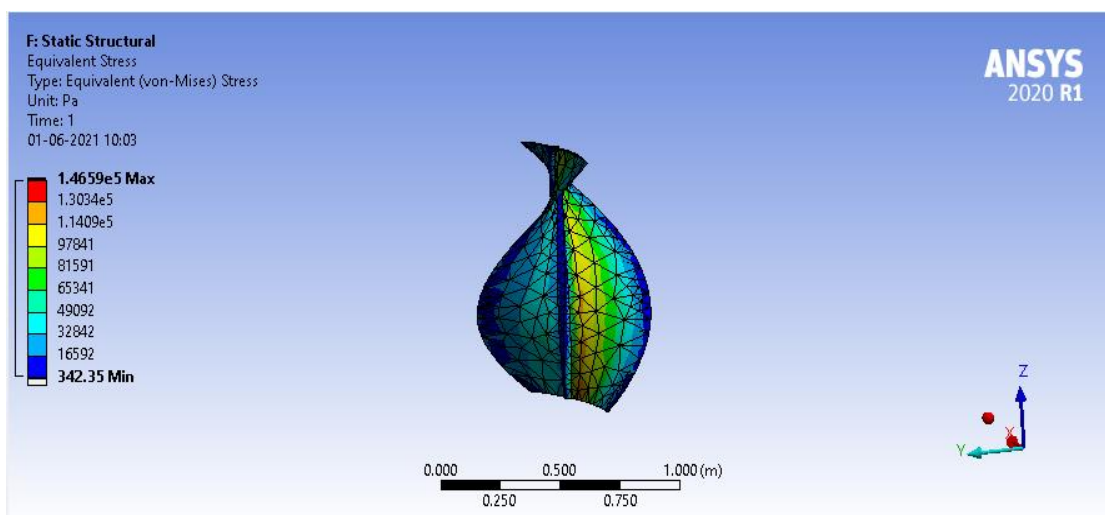


Fig 4.12: Equivalent Stress

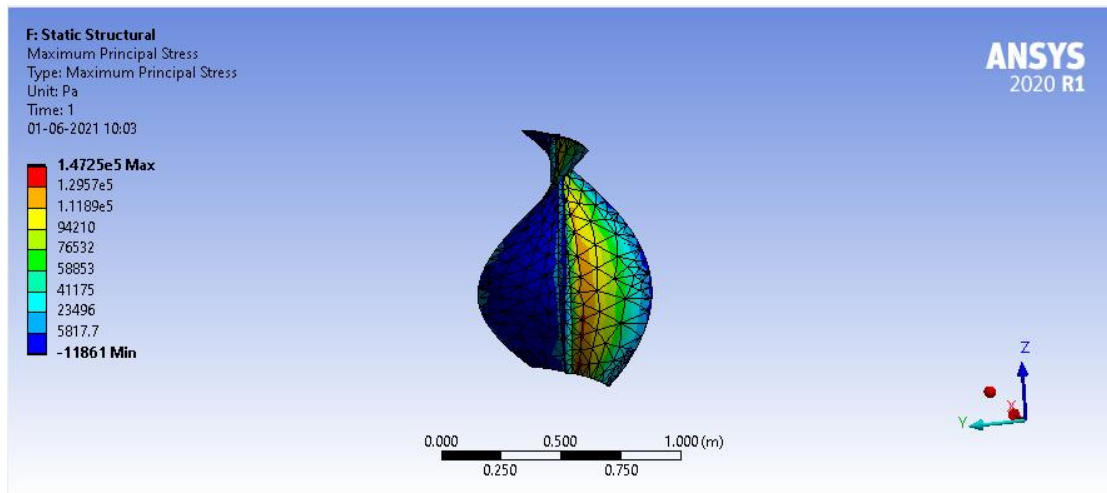


Fig 4.13: Maximum Principal Stress

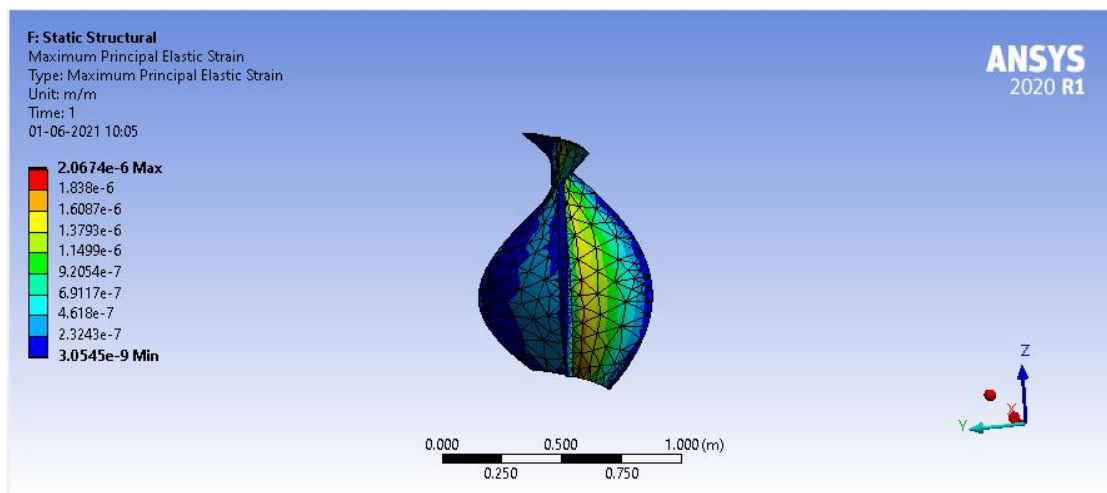


Fig 4.14: Maximum Principal Elastic Strain

Sl. No	SOLUTION	MIN VALUE(Pa)	MAX VALUE(Pa)
1	Total Deformation	0	6.5856e-6
2	Equivalent Elastic Strain	5.6775e-9	2.0696e-6
3	Maximum Principal Stress	-11861	1.4725e5
4	Maximum Principal Strain	3.0545e-9	2.0674e-6
5	Equivalent Stress	342.35	1.4659e5

Table 4.5: of Static Structural Analysis Results

4.1.2 MEDIUM WIND SPEED (15m/s)

• **Angular Velocity 40 rad/s**

Under the setup condition of the ANSYS CFX pre window, the cartesian velocity components are set to 5m/s to simulate wind speed, for both stator and rotor.

Under the same setup condition, the Rotor domain motion is set for -40 rad/s for simulating the blade rotation at desired speed through the desired direction.

Maximum Pressure	1.014e+05 Pa
Minimum Pressure	1.007e+05 Pa
Wind speed	5 m/s
Angular Velocity	-40 rad/s

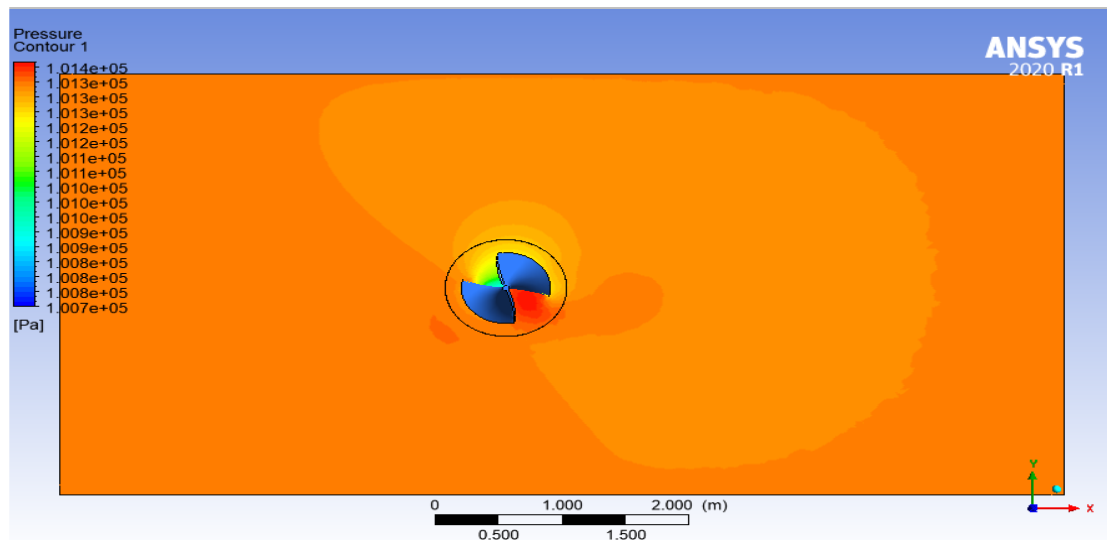


Fig 4.15: CFX Result for pressure contour on Iso-surface.

LOCATION	TYPE	MASS FLOW	MOMENTUM		
			x	y	z
Inlet (Stator)	Boundary	2.5147e+2	1.4373e+6	4.1338e-8	-7.6758e-9
ROTOR Default (ROTOR)	Boundary	0.0000e+0	1.9708e+2	-5.8053e+0	2.1874e+1
opening (Stator)	Boundary	-2.5147e+2	-1.4373e+6	6.2500e-1	2.0521e+0
Copy of Copy of Domain Interface 1 Side 1 (ROTOR)	Domain Interface	-1.5244e+0	3.0845e+1	-1.7723e+1	-7.2409e+4
Copy of Copy of Domain Interface 1 Side 2 (Stator)	Domain Interface	1.5244e+0	1.7614e+1	3.4189e+0	7.2014e+4
Copy of Domain Interface 1 Side 1 (ROTOR)	Domain Interface	-1.6726e-1	-3.2496e+0	-1.1751e+1	7.2591e+4
Copy of Domain Interface 1 Side 2 (Stator)	Domain Interface	1.6725e-1	2.1590e+0	1.9488e-1	-7.2379e+4
Domain Interface 1 Side 1 (ROTOR)	Domain Interface	1.6890e+0	1.6918e+2	4.5733e+2	-3.6386e+1
Domain Interface 1 Side 2 (Stator)	Domain Interface	-1.6890e+0	-1.5459e+2	-9.2615e+1	3.6330e+1

Table 4.6: of CFX Boundary Flow values

• **STRUCTURAL ANALYSIS**

In the Static structural window, the values we obtain from the CFX pre analysis is considered. The obtained momentum is given to the momentum constrain in Static structural Setup.

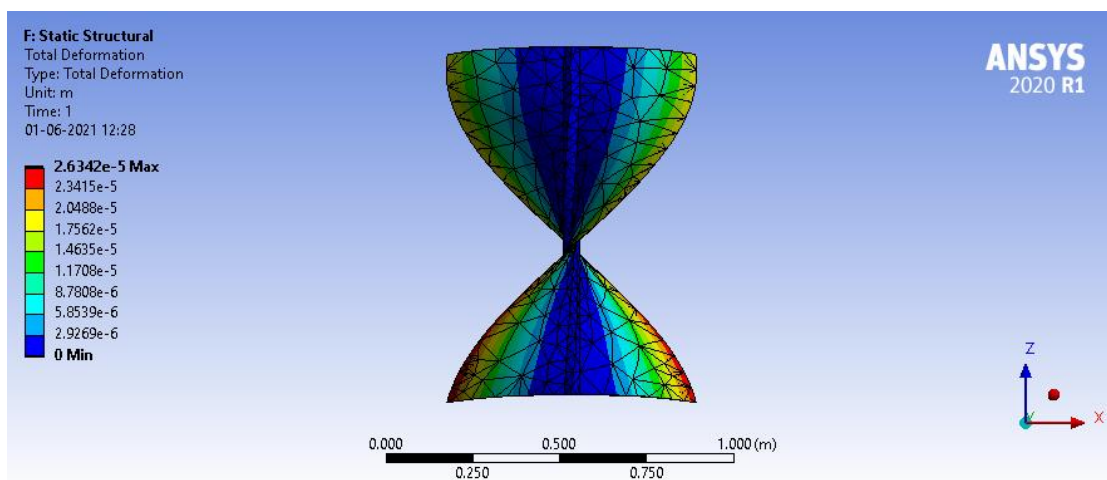


Fig 4.16: Total Deformation

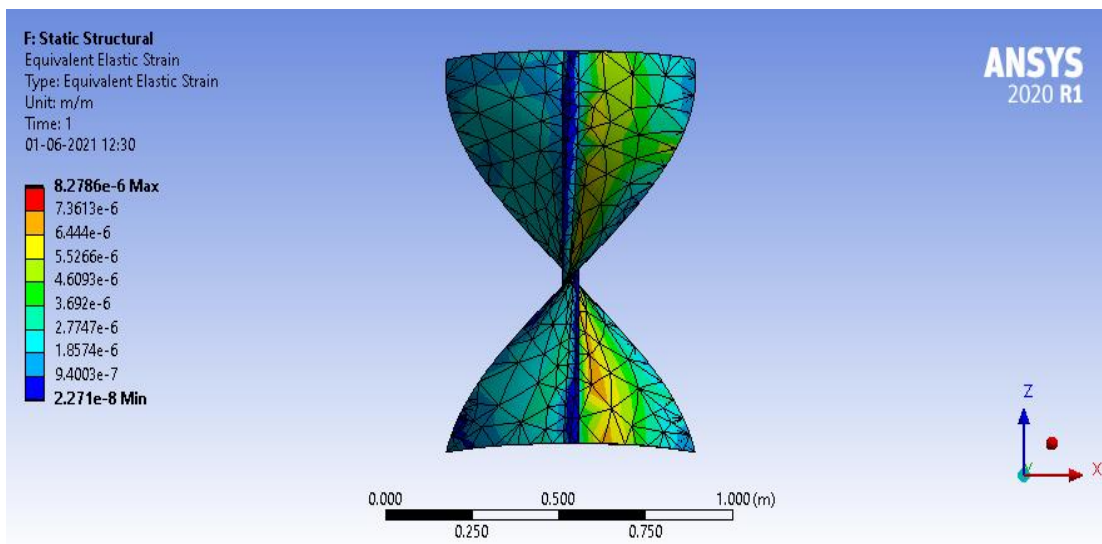


Fig 4.17: Equivalent Elastic Strain

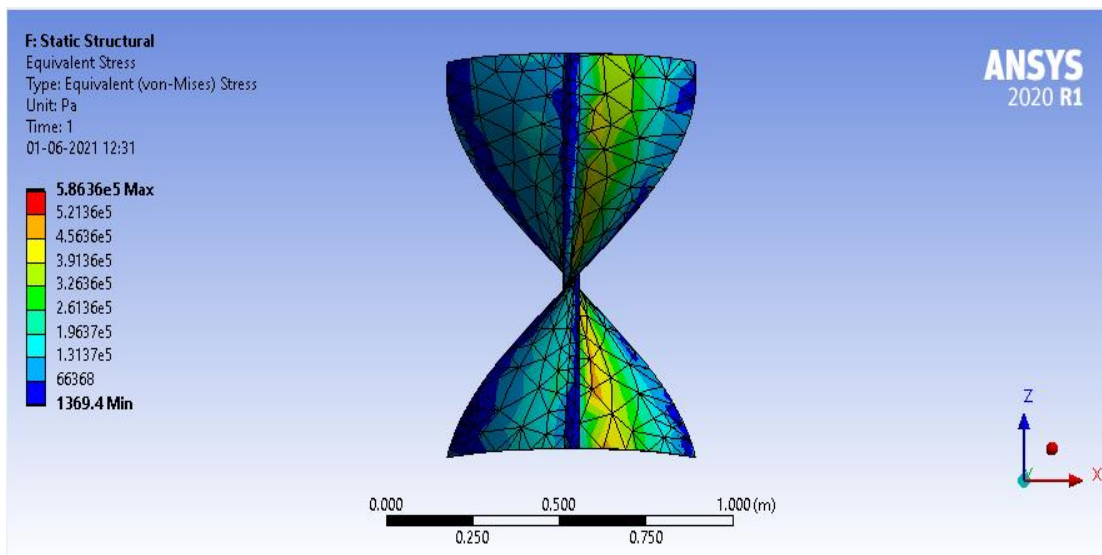


Fig 4.18: Equivalent Stress

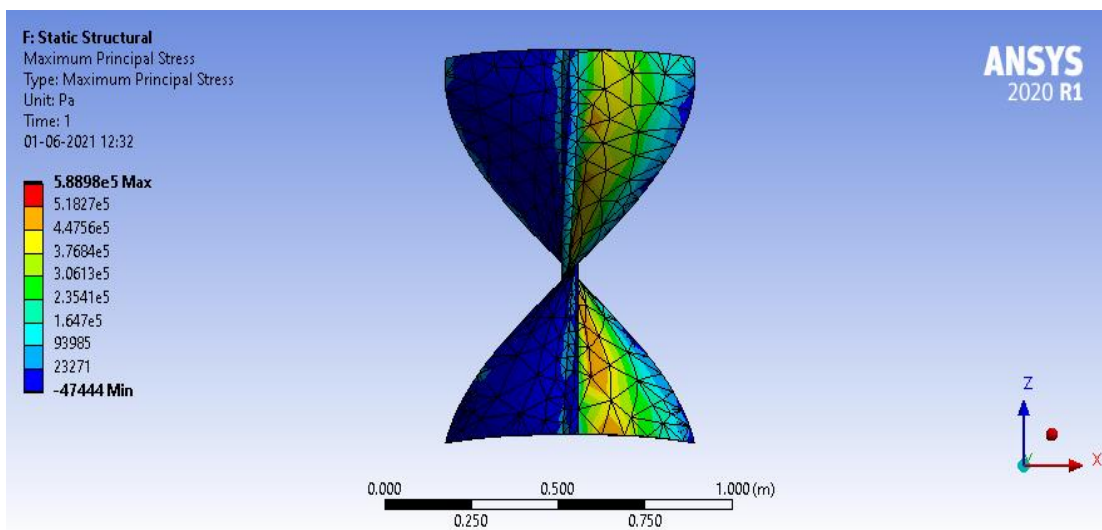


Fig 4.19: Maximum Principal Stress

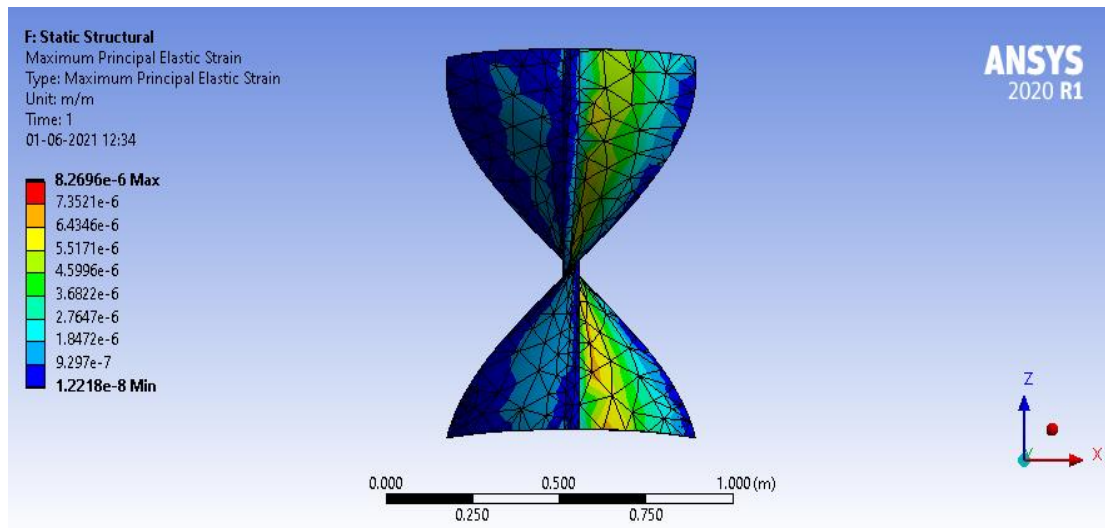


Fig 4.20: Maximum Principal Elastic strain

Sl. No	SOLUTION	MIN VALUE(Pa)	MAX VALUE(Pa)
1	Total Deformation	0	2.6342e-5
2	Equivalent Elastic Strain	2.271e-8	8.2786e-6
3	Maximum Principal Stress	-47444	5.8898e5
4	Maximum Principal Strain	1.2218e-8	8.269e-6
5	Equivalent Stress	1369.4	5.8636e5

Table 4.7: of Static Structural Analysis Results

• **Angular Velocity 50 rad/s**

Under the setup condition of the ANSYS CFX pre window, the cartesian velocity components are set to 15m/s to simulate wind speed, for both stator and rotor.

Under the same setup condition, the Rotor domain motion is set for -50 rad/s for simulating the blade rotation at desired speed through the desired direction.

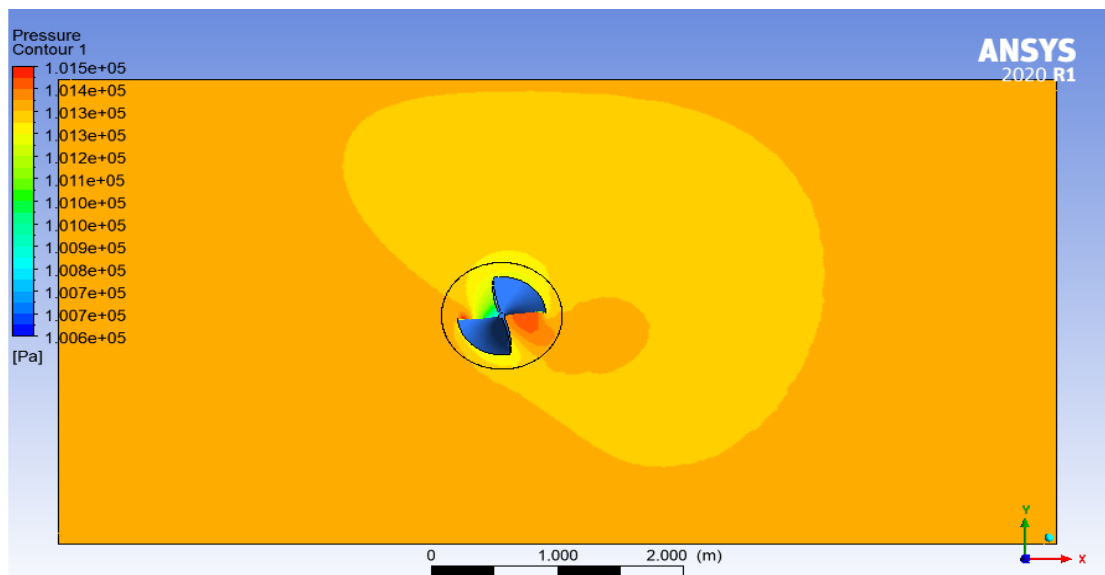


Fig 4.21: CFX Result for pressure contour on Iso-surface.

Maximum Pressure	1.014e+05 Pa
Minimum Pressure	1.006e+05 Pa
Wind speed	15 m/s
Angular Velocity	-50 rad/s

LOCATION	TYPE	MASS FLOW	MOMENTUM		
			x	y	z
Inlet (Stator)	Boundary	2.5147e+2	1.4373e+6	3.5384e-8	-1.6447e-8
ROTOR Default (ROTOR) opening (Stator)	Boundary	0.0000e+0	2.1099e+2	1.1910e+1	3.5600e+1
Copy of Copy of Domain Interface 1 Side 1 (ROTOR)	Domain Interface	-2.5147e+2	-1.4373e+6	6.2500e-1	2.1782e+0
Copy of Copy of Domain Interface 1 Side 2 (Stator)	Domain Interface	-1.5618e+0	3.7564e+1	-2.0214e+1	-7.2409e+4
Copy of Copy of Domain Interface 1 Side 2 (Stator)	Domain Interface	1.5618e+0	1.6777e+1	3.9392e+0	7.2015e+4
Copy of Domain Interface 1 Side 1 (ROTOR)	Domain Interface	9.7588e-2	-8.1859e+0	-1.3027e+1	7.2588e+4
Copy of Domain Interface 1 Side 2 (Stator)	Domain Interface	-9.7594e-2	-1.9082e+0	1.6029e-1	-7.2377e+4
Domain Interface 1 Side 1 (ROTOR)	Domain Interface	1.4617e+0	1.8013e+2	5.8827e+2	-4.2426e+1
Domain Interface 1 Side 2 (Stator)	Domain Interface	-1.4617e+0	-1.5906e+2	-9.7058e+1	4.2372e+1

Table 4.8: of CFX Boundary Flow values

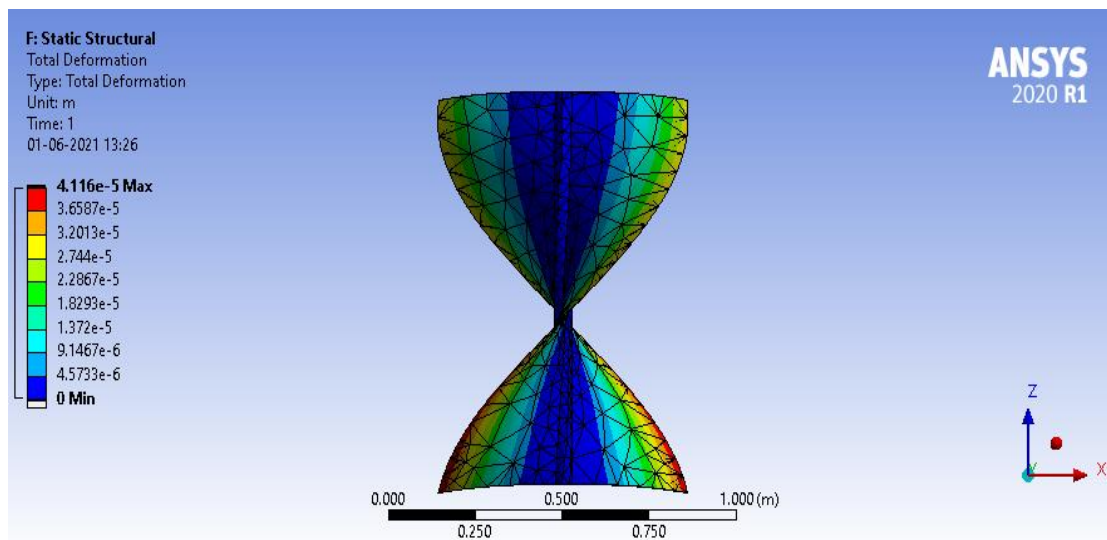


Fig 4.22: Total Deformation

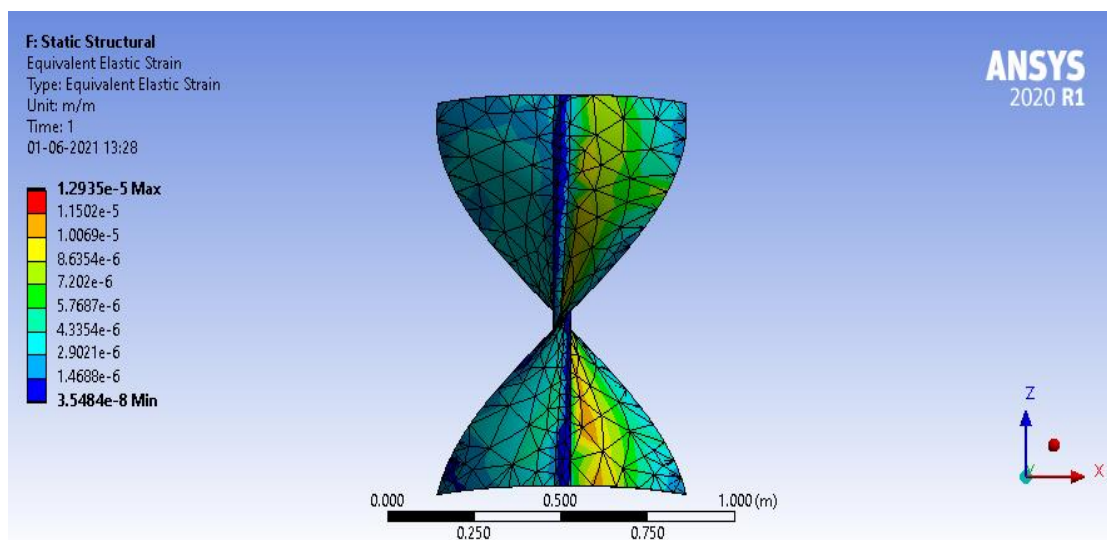


Fig 4.23: Equivalent Strain

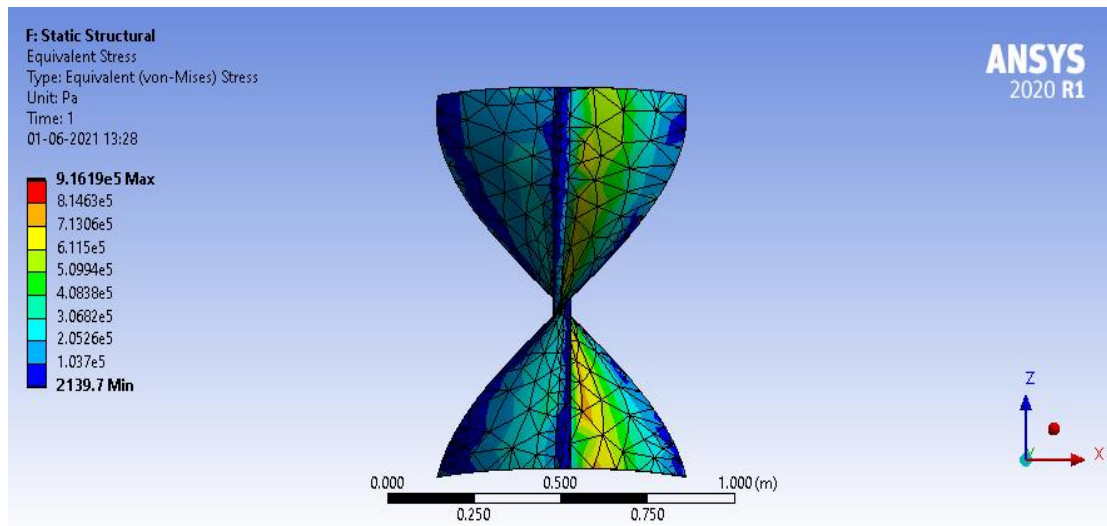


Fig 4.24: Equivalent Stress

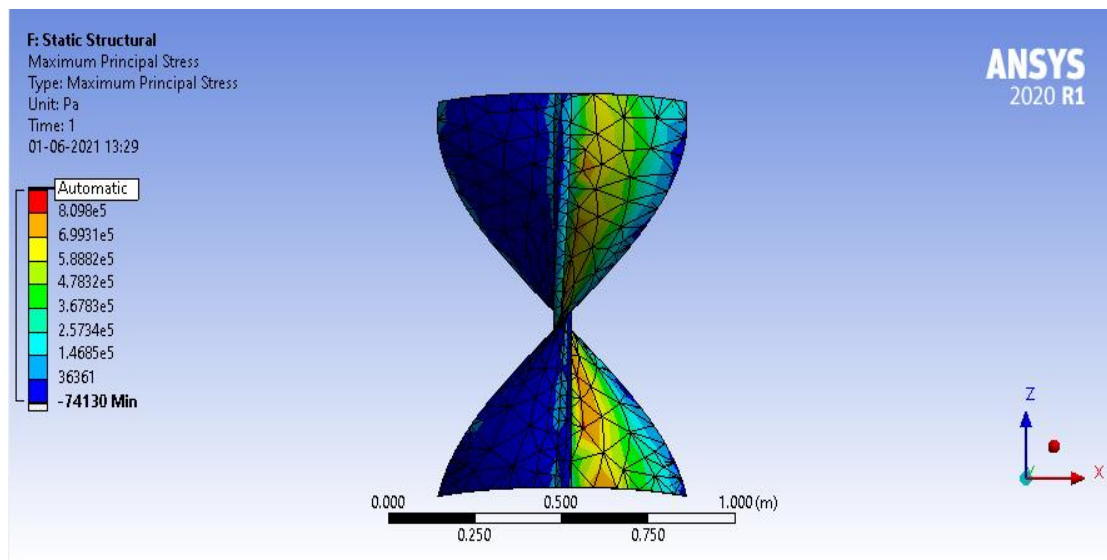


Fig 4.25: Maximum Principal Stress

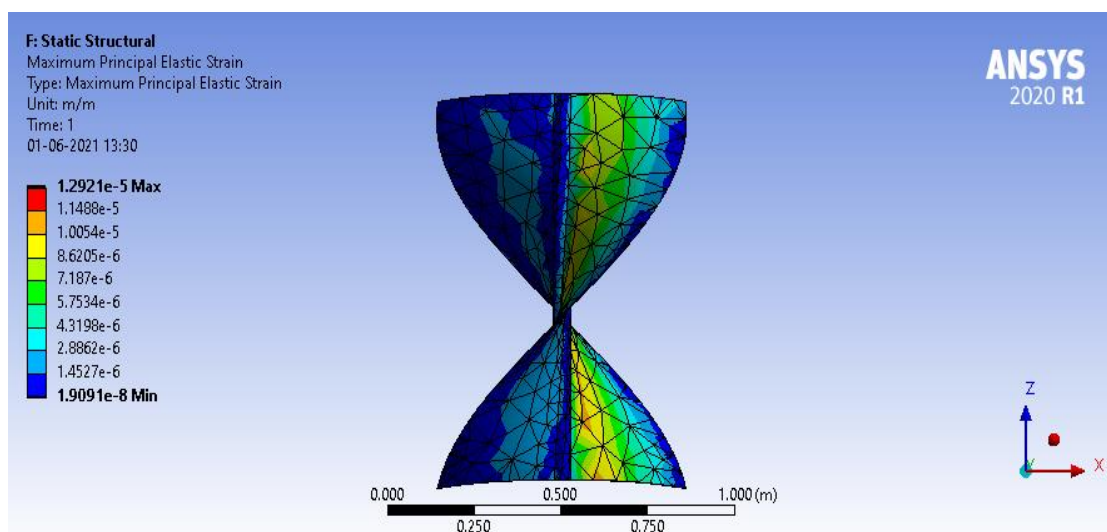


Fig 4.26: Maximum Principal Strain

Sl. No	SOLUTION	MIN VALUE(Pa)	MAX VALUE(Pa)
1	Total Deformation	0	4.116e-5
2	Equivalent Elastic Strain	3.5484e-8	1.2935e-5
3	Maximum Principal Stress	-74130	9.2029e5
4	Maximum Principal Strain	1.9091e-8	1.2921e-5
5	Equivalent Stress	2139.7	9.1619e5

Table 4.9: of Static Structural Analysis Results

4.1.3 HIGH WIND SPEED (25m/s)

• Angular Velocity 70 rad/s

Under the setup condition of the ANSYS CFX pre window, the cartesian velocity components are set to 25m/s to simulate wind speed, for both stator and rotor.

Under the same setup condition, the Rotor domain motion is set for -70 rad/s for simulating the blade rotation at desired speed through the desired direction.

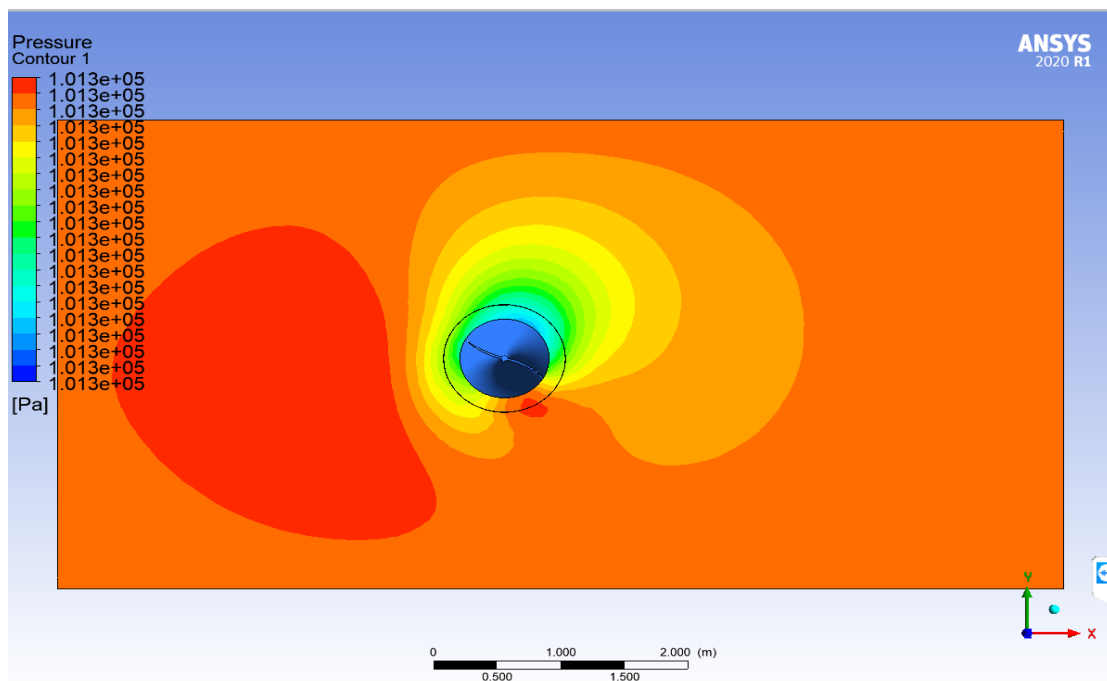


Fig 4.27: CFX Result for pressure contour on Iso-surface.

LOCATION	TYPE	MASS FLOW	MOMENTUM		
			x	y	z
Inlet (Stator)	Boundary	4.1911e+2	1.4440e+6	3.5089e-8	-1.2575e-8
ROTOR Default (ROTOR)	Boundary	0.0000e+0	5.5561e+2	-1.8900e+1	6.9821e+1
opening (Stator)	Boundary	-4.1911e+2	-1.4441e+6	7.5000e-1	1.5460e+0
Copy of Copy of Domain Interface 1 Side 1 (ROTOR)	Domain Interface	-2.5409e+0	8.7576e+1	-5.3200e+1	-7.2419e+4
Copy of Copy of Domain Interface 1 Side 2 (Stator)	Domain Interface	2.5409e+0	4.8840e+1	9.7324e+0	7.2023e+4
Copy of Domain Interface 1 Side 1 (ROTOR)	Domain Interface	-1.7297e-1	-1.2917e+1	-3.2616e+1	7.2567e+4
Copy of Domain Interface 1 Side 2 (Stator)	Domain Interface	1.7296e-1	3.2737e+0	5.2325e-1	-7.2355e+4
Domain Interface 1 Side 1 (ROTOR)	Domain Interface	2.7097e+0	5.1877e+2	1.3301e+3	-1.0355e+2
Domain Interface 1 Side 2 (Stator)	Domain Interface	-2.7097e+0	-4.3044e+2	-2.6056e+2	1.0340e+2

Table 4.10: of CFX Boundary Flow values

• **STRUCTURAL ANALYSIS**

In the Static structural window, the values we obtain from the CFX pre analysis is considered. The obtained momentum is given to the momentum constrain in Static structural Setup.

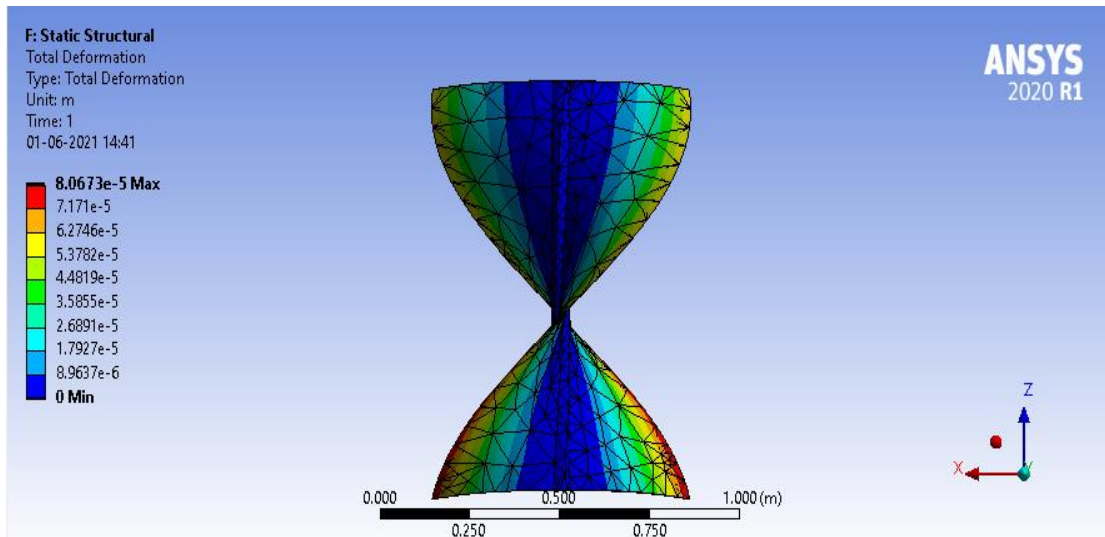


Fig 4.28: Total Deformation

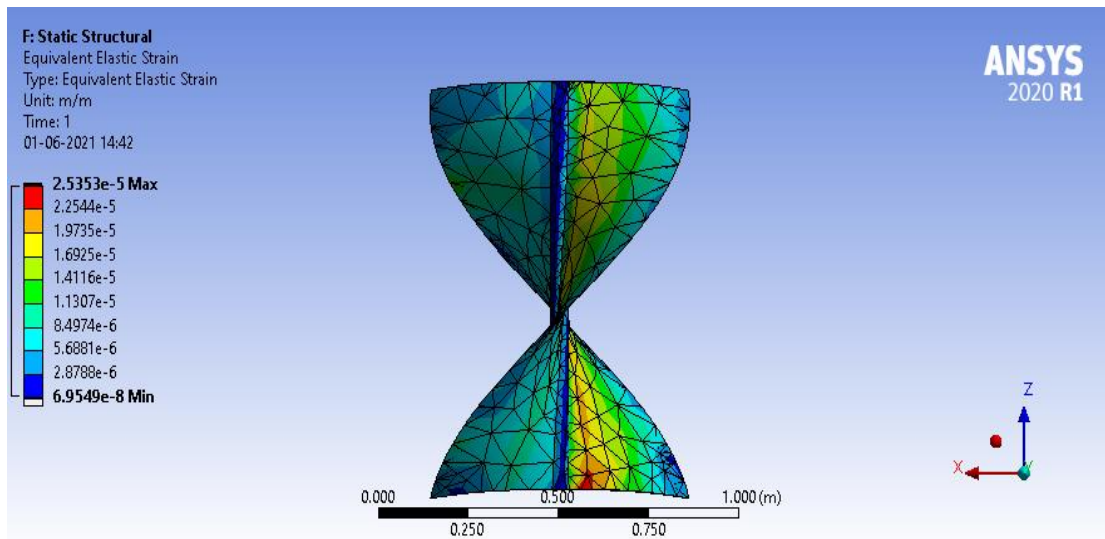


Fig 4.29: Equivalent Strain

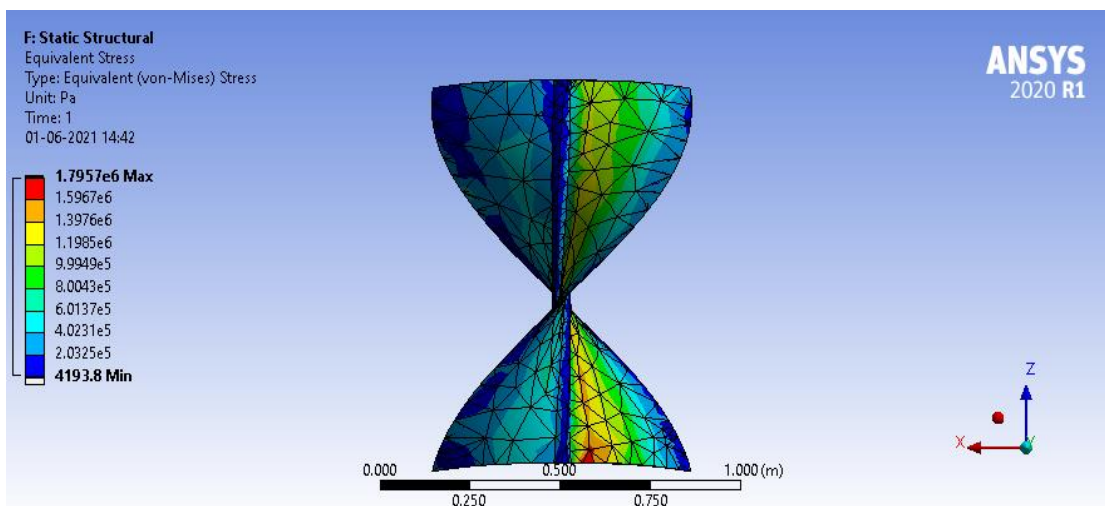


Fig 4.30: Equivalent Stress

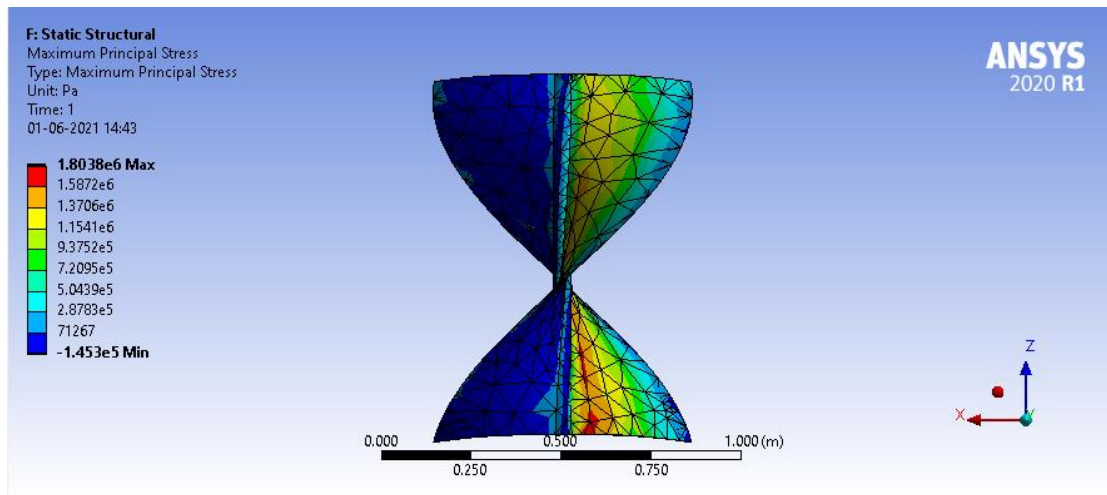


Fig 4.31: Maximum Principal Stress

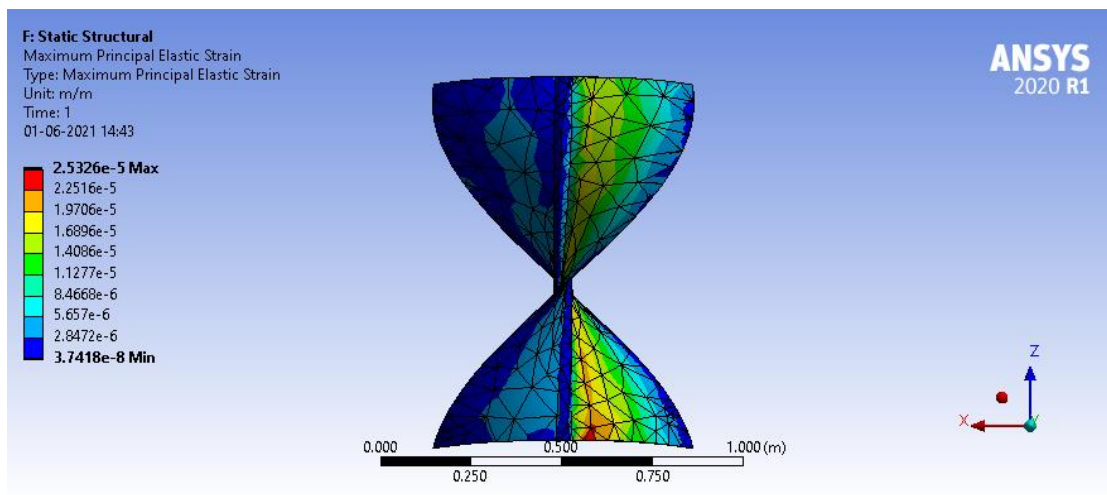


Fig 4.32: Maximum Principal Strain

Sl. No	SOLUTION	MIN VALUE(Pa)	MAX VALUE(Pa)
1	Total Deformation	0	8.0673e-5
2	Equivalent Elastic Strain	3.5484e-8	2.5353e-5
3	Maximum Principal Stress	-1.453e5	1.8038e6
4	Maximum Principal Strain	3.7418e-8	2.5326e-5
5	Equivalent Stress	4193.8	1.7957e6

Table 4.11: of Static Structural Analysis Results

• **Angular Velocity 80 rad/s**

Under the setup condition of the ANSYS CFX pre window, the cartesian velocity components are set to 25m/s to simulate wind speed, for both stator and rotor.

Under the same setup condition, the Rotor domain motion is set for -80 rad/s for simulating the blade rotation at desired speed through the desired direction.

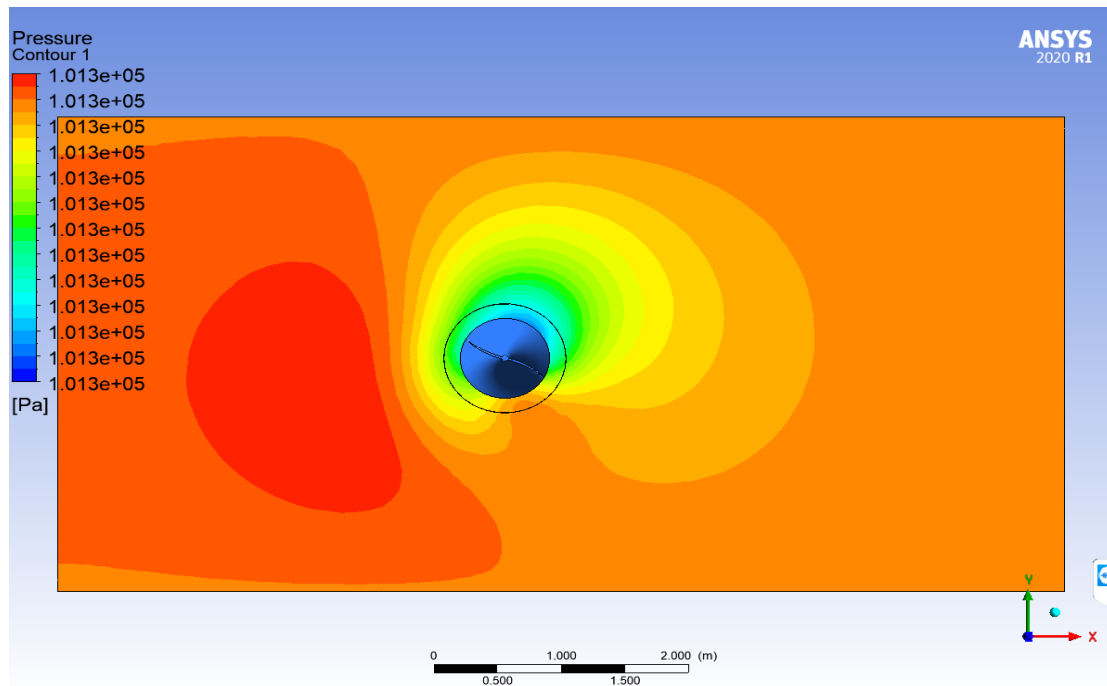


Fig 4.33: CFX Result for pressure contour on Iso-surface.

LOCATION	TYPE	MASS FLOW	MOMENTUM		
			X	Y	Z
Inlet (Stator)	Boundary	4.1911e+2	1.4440e+6	2.3152e-8	-1.5087e-8
ROTOR Default (ROTOR)	Boundary	0.0000e+0	5.8137e+2	-2.4041e+1	9.5281e+1
opening (Stator)	Boundary	-4.1911e+2	-1.4441e+6	7.5000e-1	1.2992e+0
Copy of Copy of Domain Interface 1 Side 1 (ROTOR)	Domain Interface	-2.5311e+0	9.2378e+1	-6.5572e+1	-7.2418e+4
Copy of Copy of Domain Interface 1 Side 2 (Stator)	Domain Interface	2.5311e+0	4.8889e+1	9.9372e+0	7.2023e+4
Copy of Domain Interface 1 Side 1 (ROTOR)	Domain Interface	1.0864e-1	-2.3580e+1	-3.2849e+1	7.2565e+4
Copy of Domain Interface 1 Side 2 (Stator)	Domain Interface	-1.0864e-1	-3.9372e+0	4.5776e-1	-7.2353e+4
Domain Interface 1 Side 1 (ROTOR)	Domain Interface	2.4190e+0	6.6558e+2	1.5058e+3	-1.1285e+2
Domain Interface 1 Side 2 (Stator)	Domain Interface	-2.4190e+0	-4.3288e+2	-2.7091e+2	1.1269e+2

Table 4.12: of CFX Boundary Flow values

• **STRUCTURAL ANALYSIS**

In the Static structural window, the values we obtain from the CFX pre analysis is considered. The obtained momentum is given to the momentum constrain in Static structural Setup.

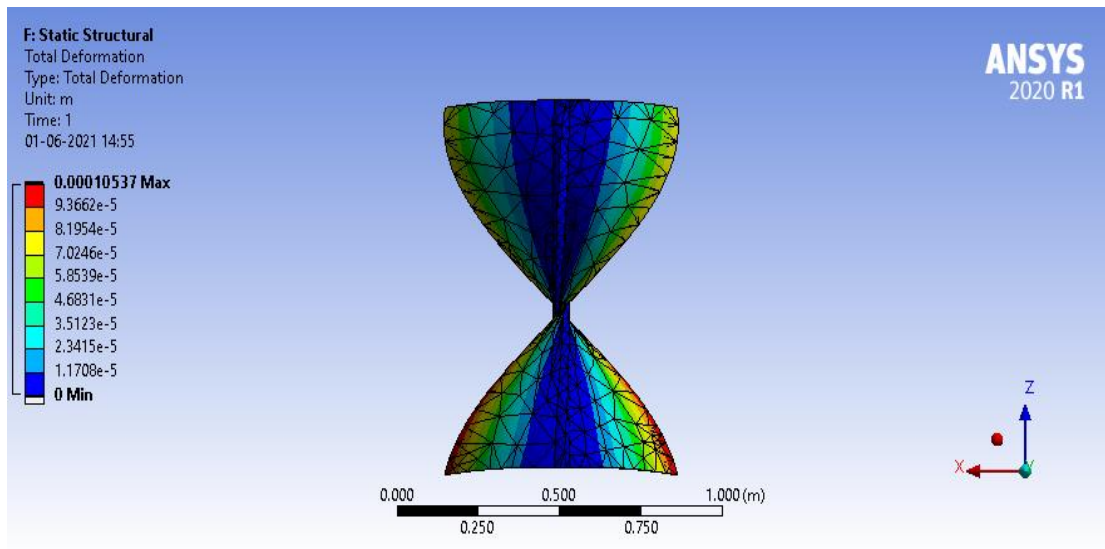


Fig 4.34: Total Deformation

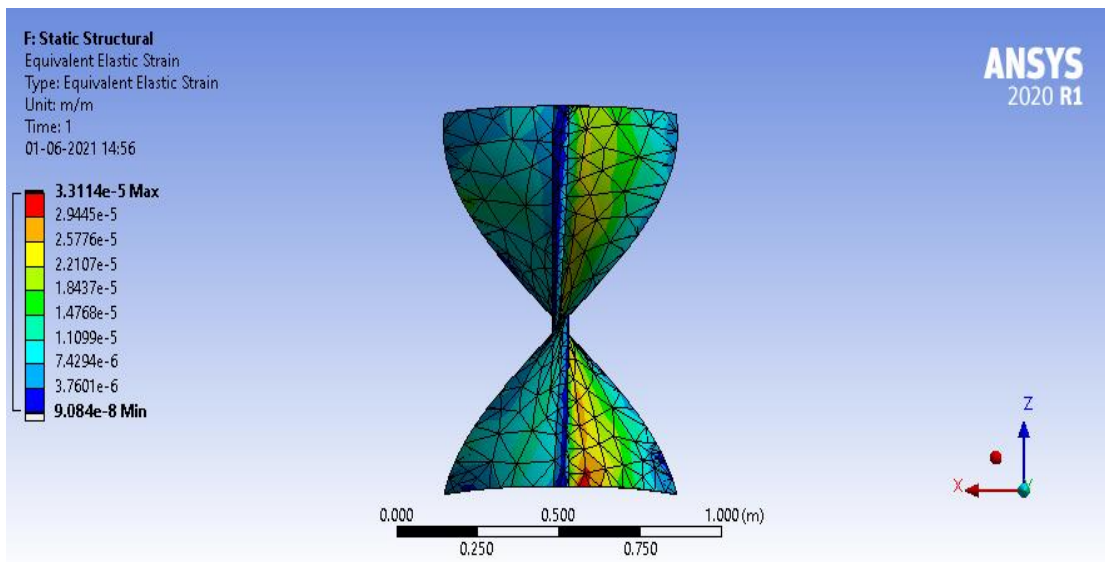


Fig 4.35: Elastic Strain

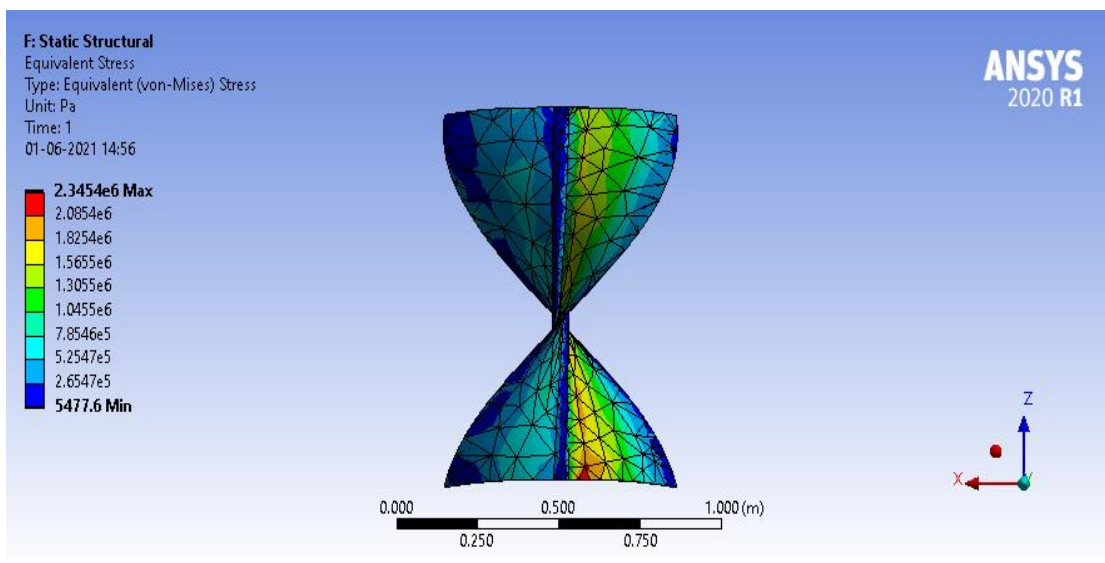


Fig 4.36: Equivalent Stress

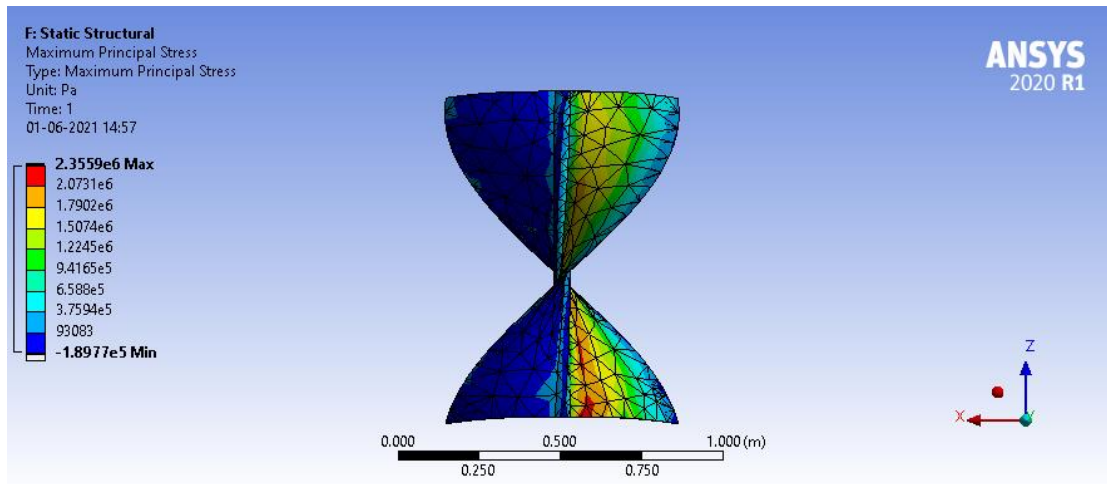


Fig 4.37: Maximum Principal Stress

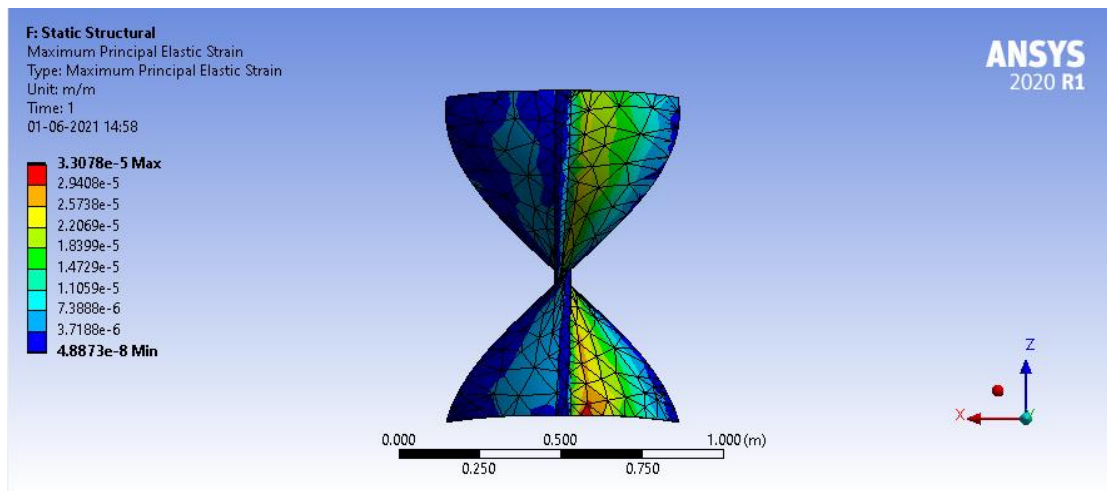


Fig 4.38: Maximum Principal Strain

Sl. No	SOLUTION	MIN VALUE(Pa)	MAX VALUE(Pa)
1	Total Deformation	0	0.10537e-3
2	Equivalent Elastic Strain	9.084e-8	3.3114e-5
3	Maximum Principal Stress	-1.8977e5	2.3559e6
4	Maximum Principal Strain	4.8873e-8	3.3078e-5
5	Equivalent Stress	5477.6	2.3454e6

Table 4.13: of Static Structural Analysis Results

4.1.1 CONCLUSION

The data analysis on the HELICAL SAVONIUS WIND TURBINE revealed much information about the design. The major characteristic behavior that affects the turbine are namely, Pressure, Total Deformation, Equivalent Elastic Stress, Maximum Principal Stress, Maximum Principal Strain and Equivalent Stress.

The characteristics of the wind turbine in detail are given below:

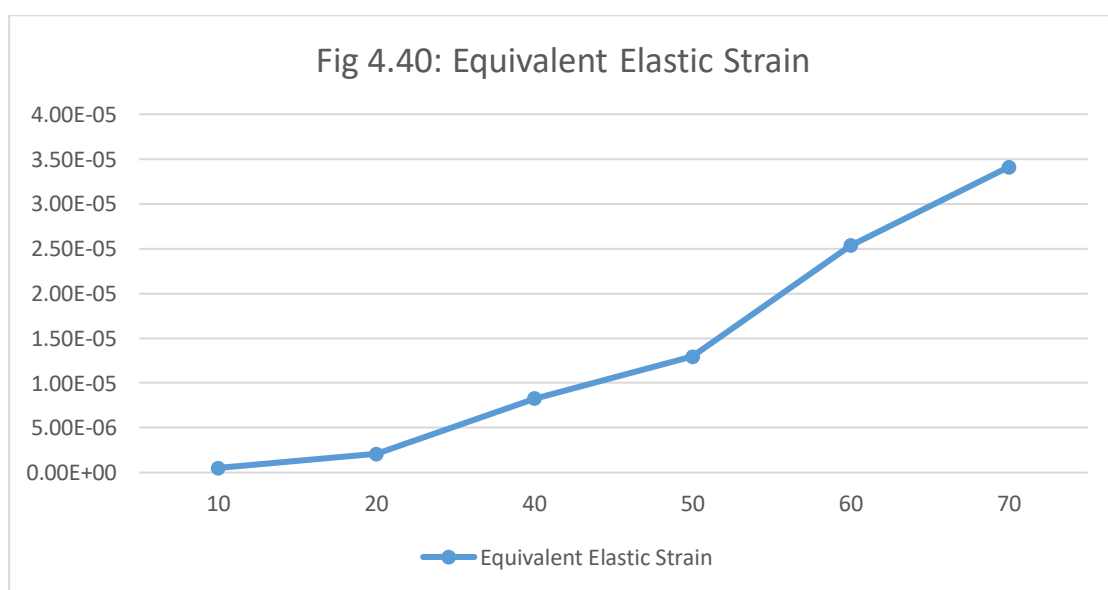
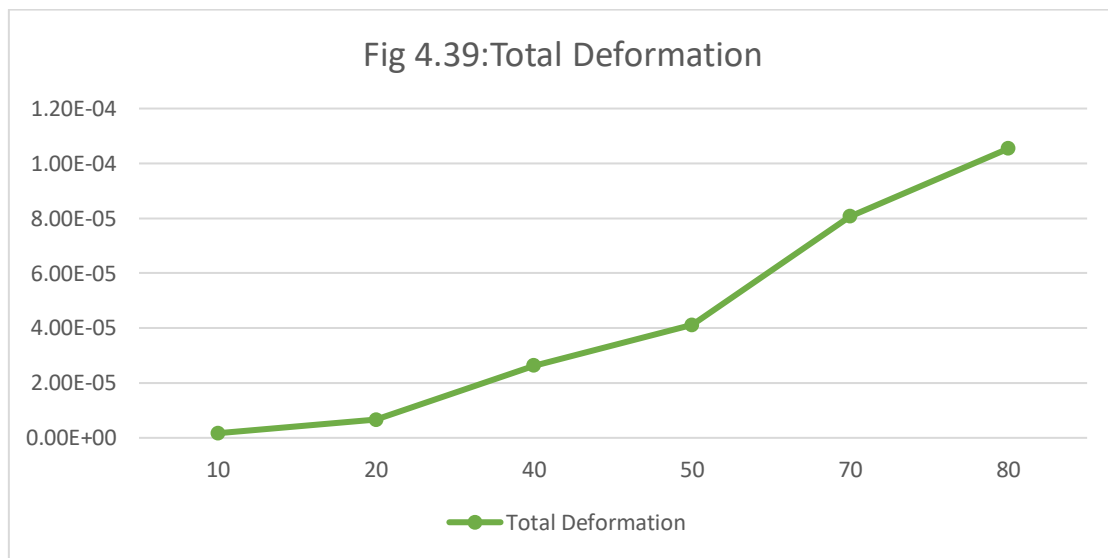
- 1) **Pressure:** The pressure of the system decreases with increase in velocity and it tends to increase significantly when the wind comes in contact with the wind turbine. The Steady drop in wind will not be equal to zero else there creates a blunt body with sharp edge dynamics. The pressure in front of the turbine is greater than that in the back of the airfoil due to the obstruction of the turbine itself. Since there is not a significant drop in pressure around the turbine while rotation, we can assume that it has a safe way of rotating without extreme obstruction to the wind flow.
- 2) **Total Deformation:** In physics, deformation is the continuum mechanics transformation of a body from a reference configuration to a current configuration. ... In a continuous body, a deformation field results from a stress field induced by applied

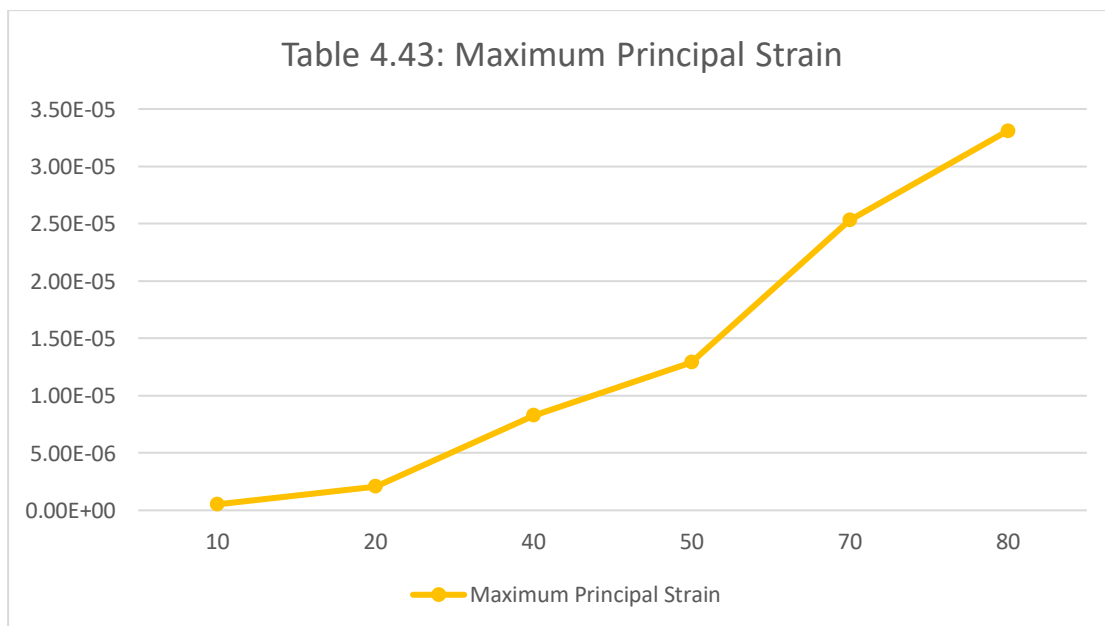
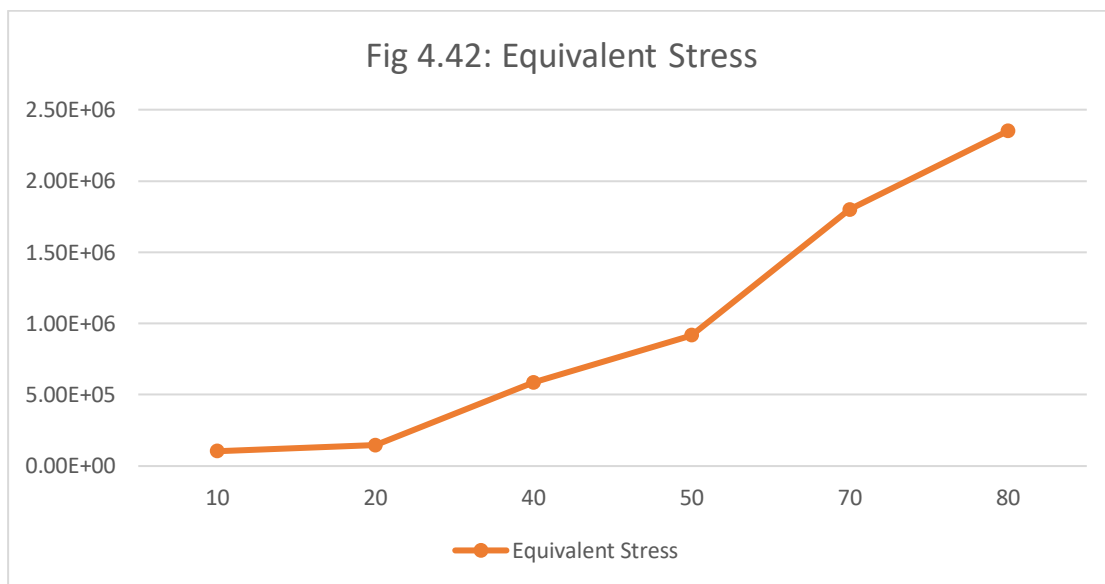
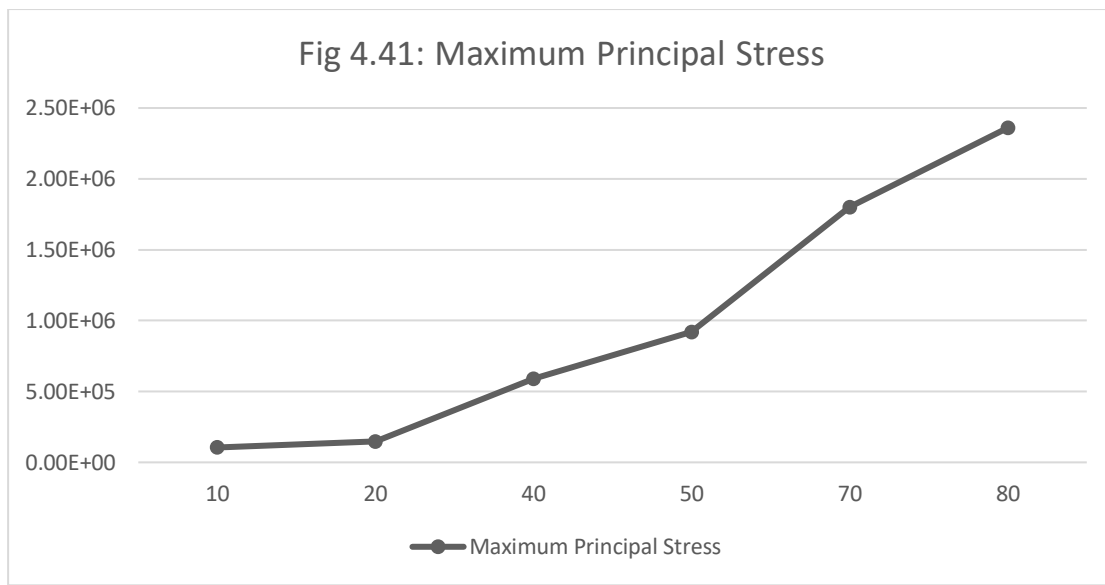
forces or is due to changes in the temperature field inside the body. This is also what the word literally means: a change in form or shape. An alteration of form for the worse. Hence, the strain energy of the material becomes a major factor in designing the springs. Here we can see clearly from the given total deformation Figures that all the figures tend to deform at the same area around the edges with different values for different conditions. The case of Total deformation suggests that in time, as the wind mill tends to wear off, the deformation is likely to happen in the edges of the, turbine so one must be cautious when designing the material as they might break and loose the aerodynamic performance. The amount of deformation is directly proportional to the loads acting on them. On the central part, mainly the shaft the deformation is almost equal to zero, because off the assumption that it is stationary for the time being. Hence the farther away from the shaft the greater the deformation.

3) **Equivalent Elastic Stress/ Equivalent Elastic strain:** The equivalent elastic strain is defined as the limit for the values of Strain/Stress up to which the object will rebound and come back to the original shape upon the removal of the load. Here we can see that the strain is concentrated upon the left region or blade of the Helical Savonius Wind turbine, that is because of the direction of angular velocity or the direction it spins, the Strain develops to oppose the change in characteristics almost in the middle of the wing section. Which makes it subjected to bending and sometimes crack could develop from that part.

4) **Maximum Principal Stress:** is the maximum normal stress a body can have at its some point. It represents purely normal stress. If at some point principal stress is said to have acted it does not have any shear stress component. Here we can see that the maximum amount of principal stress is acting near the shaft, but on the blade wing. The stress can also be seen acting on a single side, due to the direction of rotation.

5) **Maximum Principal Strain:** Maximum and minimum normal strain possible for a specific point on a structural element. Shear strain is 0 at the orientation where principal strain occurs. Here it acts on par with that of Maximum principal stress.





From these depictions of the Structural Analysis data, we can conclude that there is a direct relationship between Total Deformation, Equivalent Elastic Stress, Maximum Principal Stress, Maximum Principal Strain and Equivalent Stress. As the Wind speed and Angular Velocity increases, the values of all the variables given above also increases.

4.2. ANALYSIS ON THE EFFICIENCY OF HELICAL SAVONIUS WIND TURBINE UNDER CONSTANT ANGULAR VELOCITY.

Efficiency has multiple definitions, all of them valid. We can define efficiency as:

- the ability to avoid wasting energy when performing a particular work
- the ratio between the useful work performed by a device and the total energy consumed as input

The main objective of this study is to know how efficient this wind turbine would be in converting the potential wind energy to that of a rotating mechanical energy and up to what extent does this wind energy will be transferred through the shaft.

To conduct the analysis on the efficiency of the model, the angular velocity of the turbine is fixed at a constant speed of 10 rad/s and the Wind velocity is stepped up from 2.5m/s to 25m/s sequentially, with an increment of 2.5m/s in wind velocity.

The Boundary flow data from each of the analysis is taken and the data over the rotor section is taken to view the moment over X direction.

4.2.1 Theory

The basic idea in finding the efficiency is that, the efficiency of the wind turbine is relative to that of the wind energy and the shaft power, i.e. The Coefficient of power, C_p . The C_p is directly proportional to Efficiency. The efficiency calculated here is ideal, with Coefficient of Performance = 1;

$$C_p \propto \text{Shaft Power} / \text{Wind Power}$$

- Wind Power:

$$P_w = \frac{1}{2} \rho A V^3$$

- Shaft Power:

$$P_T = T\omega.$$

So, the Ideal Coefficient of Power, is given by the equation,

$$\text{Power co-efficient, } C_p = T\omega / \left(\frac{1}{2} \rho A V^3 \right)$$

C_p = Coefficient of Power

T = Torque

ω = Angular velocity

ρ = Fluid Density

A = Surface Swept Area

V = Wind velocity

SL NO	ANGULAR VELOCITY	WIND SPEED (m/s)
1	10 rad/s (95.493 RPM)	2.5
2		5
3		7.5
4		10
5		12.5
6		15
7		17.5
8		20
9		22.5
10		25

Table:4.14 Data Sheet

4.2.2 Efficiency Analysis

Under the setup condition of the ANSYS CFX pre window, the cartesian velocity components are set to 2.5m/s to simulate wind speed, for both stator and rotor. The angular velocity is kept at a constant 10 rad/s.

➤ Analysis on wind speed of 2.5 m/s

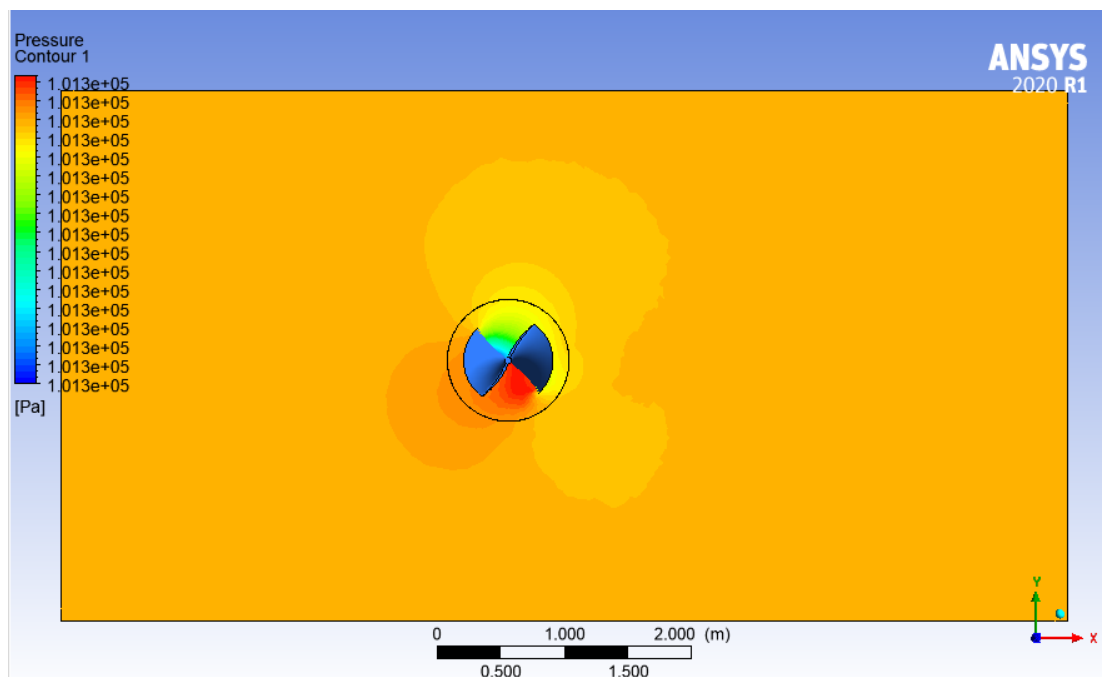


Fig 4.44: Pressure Contour (2.5 m/s) CFX pre

Maximum Pressure	1.014e+05 Pa
Minimum Pressure	-1.017e+05 Pa
Wind speed	2.5 m/s

LOCATION	TYPE	MASS FLOW	MOMENTUM		
			X	Y	Z
Inlet (Stator)	Boundary	4.1911e+1	1.4336e+6	2.9583e-7	-1.7189e-7
ROTOR Default (ROTOR)	Boundary	0.0000e+0	1.2314e+0	4.6754e+0	8.7180e-1
opening (Stator)	Boundary	-4.1911e+1	-1.4336e+6	6.2500e-1	2.1512e+0
Copy of Copy of Domain Interface 1 Side 1 (ROTOR)	Domain Interface	-3.4632e-1	8.8436e-1	8.0494e-1	-7.2795e+4
Copy of Copy of Domain Interface 1 Side 2 (Stator)	Domain Interface	3.4630e-1	-9.0813e-2	-1.7844e-1	7.2392e+4
Copy of Domain Interface 1 Side 1 (ROTOR)	Domain Interface	5.0717e-2	2.7025e-1	-3.6755e-1	7.2794e+4
Copy of Domain Interface 1 Side 2 (Stator)	Domain Interface	-5.0821e-2	-1.3977e-1	2.3511e-3	-7.2391e+4
Domain Interface 1 Side 1 (ROTOR)	Domain Interface	2.9533e-1	-1.6881e+1	1.0224e+1	-1.2773e+0
Domain Interface 1 Side 2 (Stator)	Domain Interface	-2.9545e-1	-4.4844e+0	-2.7615e+0	1.2733e+0

Table 4.15: of CFX Boundary Flow values

➤ Analysis on wind speed of 5.0 m/s

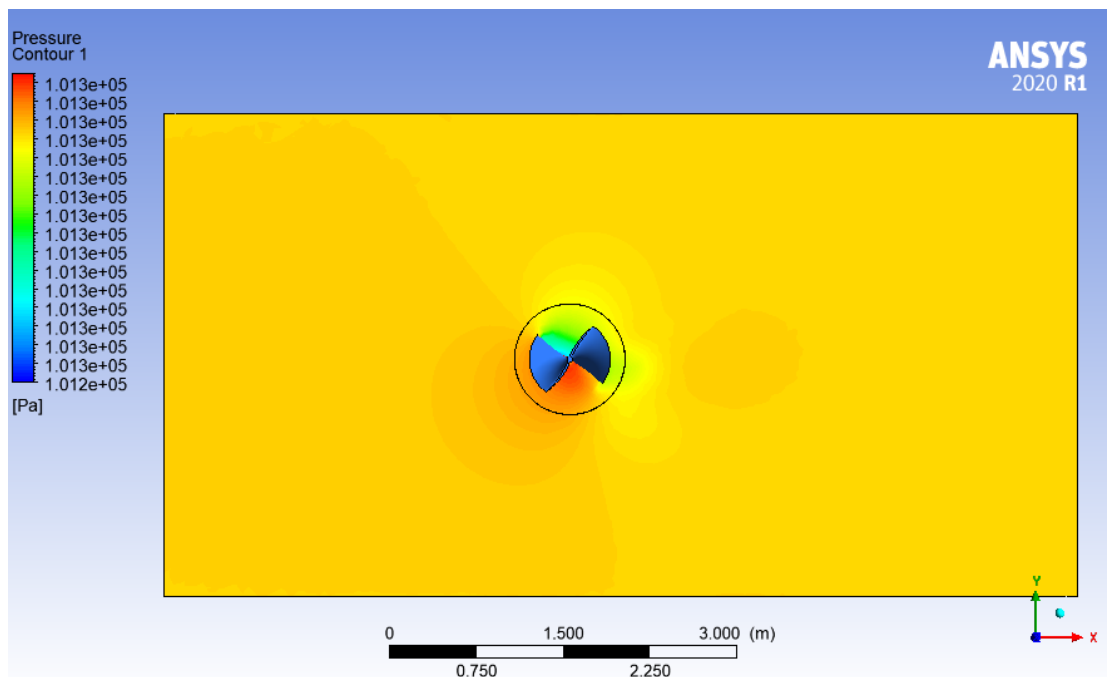


Fig 4.45: Pressure Contour (5 m/s) CFX pre

Maximum Pressure	1.013e+00 Pa
Minimum Pressure	1.012e+00 Pa
Wind speed	5 m/s

LOCATION	TYPE	MASS FLOW	MOMENTUM		
			X	Y	Z
Inlet (Stator)	Boundary	8.3822e+1	1.4339e+6	4.7121e-8	-9.7533e-8
ROTOR Default (ROTOR)	Boundary	0.0000e+0	2.0461e+1	8.3100e-1	7.2199e-1
opening (Stator)	Boundary	-8.3823e+1	-1.4339e+6	6.2500e-1	2.4001e+0
Copy of Copy of Domain Interface 1 Side 1 (ROTOR)	Domain Interface	-4.9453e-1	2.9092e+0	-1.3225e+0	-7.2404e+4
Copy of Copy of Domain Interface 1 Side 2 (Stator)	Domain Interface	4.9460e-1	2.0330e+0	2.2596e-1	7.2010e+4
Copy of Domain Interface 1 Side 1 (ROTOR)	Domain Interface	-1.8616e-1	5.5804e-1	-1.3405e+0	7.2602e+4
Copy of Domain Interface 1 Side 2 (Stator)	Domain Interface	1.8617e-1	9.2343e-1	2.7187e-2	-7.2390e+4
Domain Interface 1 Side 1 (ROTOR)	Domain Interface	6.8014e-1	8.9730e+0	3.7907e+1	-3.6791e+0
Domain Interface 1 Side 2 (Stator)	Domain Interface	-6.8025e-1	-1.6878e+1	-1.0337e+1	3.6721e+0

Table 4.16: of CFX Boundary Flow values

➤ Analysis on wind speed of 7.5 m/s

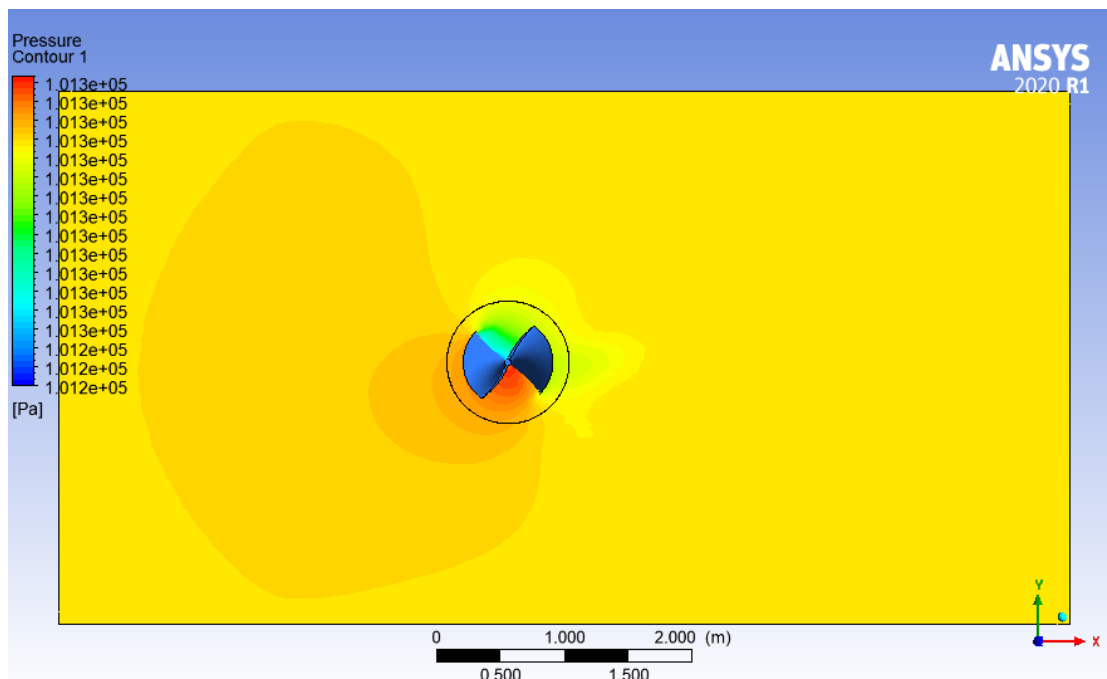


Fig 4.46: Pressure Contour (7.5 m/s) CFX pre

Maximum Pressure			1.0013e+00 Pa		
Minimum Pressure			1.012e+00 Pa		
Wind speed			7.5 m/s		
LOCATION	TYPE	MASS FLOW	MOMENTUM		
			X	Y	Z
Inlet (Stator)	Boundary	1.2573e+2	1.4344e+6	3.3695e-8	1.6564e-8
ROTOR Default (ROTOR)	Boundary	0.0000e+0	2.5941e+1	5.4894e+0	5.3924e-1
opening (Stator)	Boundary	-1.2573e+2	-1.4341e+6	5.0000e-1	1.5407e+0
Copy of Copy of Domain Interface 1 Side (ROTOR)	Domain Interface	-7.1313e-1	3.9840e+0	-1.4128e+0	-7.2405e+4
Copy of Copy of Domain Interface 1 Side 2 (Stator)	Domain Interface	7.1325e-1	3.3380e+0	-1.6008e-2	7.2011e+4
Copy of Domain Interface 1 Side 1 (ROTOR)	Domain Interface	-4.2943e-1	2.1315e+0	-2.1306e+0	7.2603e+4
Copy of Domain Interface 1 Side 2 (Stator)	Domain Interface	4.2946e-1	2.5027e+0	6.3134e-2	-7.2391e+4
Domain Interface 1 Side 1 (ROTOR)	Domain Interface	1.1428e+0	-3.2735e+0	4.4007e+1	-4.1645e+0
Domain Interface 1 Side 2 (Stator)	Domain Interface	-1.1429e+0	-2.6968e+1	-1.4984e+1	4.1564e+0

Table 4.17: of CFX Boundary Flow values

➤ Analysis on wind speed of 10 m/s

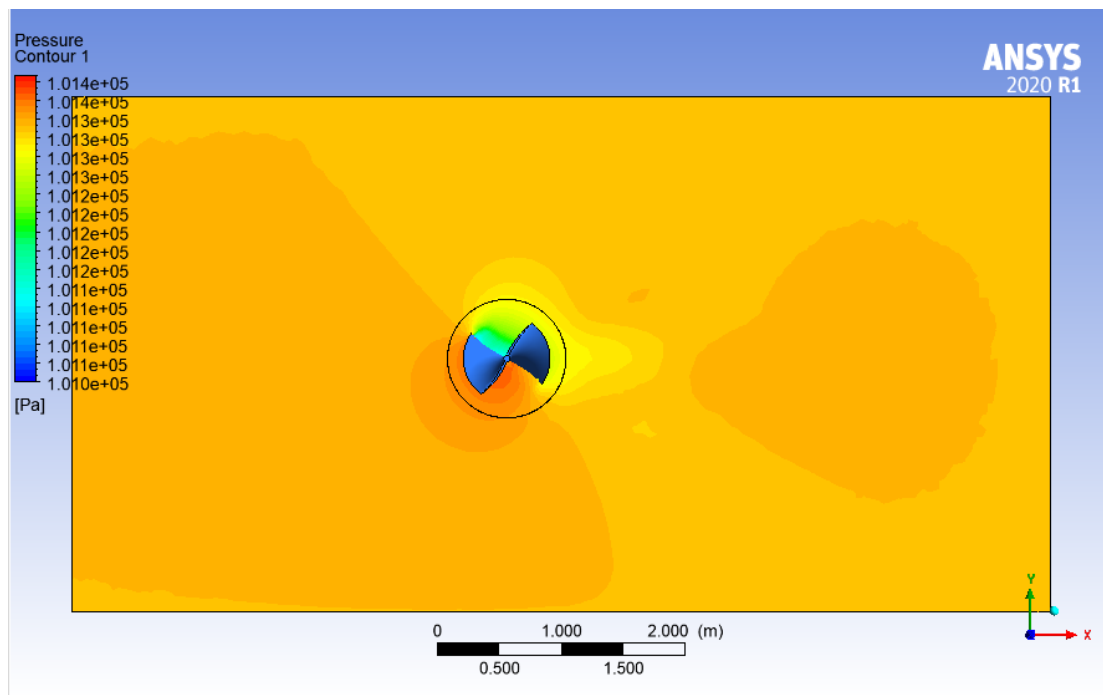


Fig 4.47: pressure contour (10 m/s) CFX pre

Maximum Pressure		1.014e+05 Pa			
Minimum Pressure		1.010e+05 Pa			
Wind speed		10 m/s			
LOCATION	TYPE	MASS FLOW	MOMENTUM		
			x	y	z
Inlet (Stator)	Boundary	1.6765e+2	1.4352e+6	4.1140e-8	1.6059e-8
ROTOR Default (ROTOR)	Boundary	0.0000e+0	6.7467e+1	2.6970e+0	-2.8691e-2
opening (Stator)	Boundary	-1.6764e+2	-1.4352e+6	7.5000e-1	2.0717e+0
Copy of Copy of Domain Interface 1 Side 1 (ROTOR)	Domain Interface	-7.9886e-1	6.8026e+0	-4.3561e+0	-7.2405e+4
Copy of Copy of Domain Interface 1 Side 2 (Stator)	Domain Interface	7.9884e-1	7.0857e+0	-1.8272e-2	7.2011e+4
Copy of Domain Interface 1 Side 1 (ROTOR)	Domain Interface	-7.7643e-1	6.4216e+0	-5.8597e+0	7.2601e+4
Copy of Domain Interface 1 Side 2 (Stator)	Domain Interface	7.7642e-1	7.8397e+0	3.0042e-1	-7.2388e+4
Domain Interface 1 Side 1 (ROTOR)	Domain Interface	1.5758e+0	-1.2786e+1	7.4385e+1	-1.5554e+0
Domain Interface 1 Side 2 (Stator)	Domain Interface	-1.5760e+0	-6.4382e+1	-4.5408e+1	1.5464e+0

Table 4.18: of CFX Boundary Flow values

➤ Analysis on wind speed of 12.5 m/s

Maximum Pressure	1.014e+05 Pa
Minimum Pressure	1.009e+05 Pa
Wind speed	5 m/s

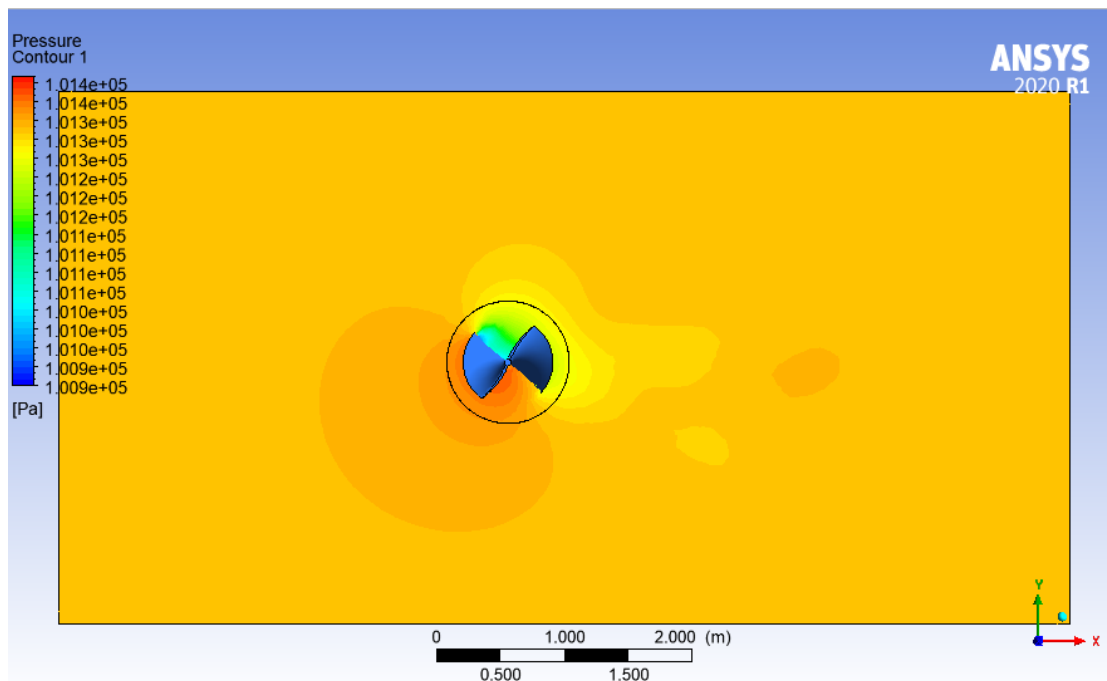


Fig 4.48: Pressure Contour (12.5 m/s) CFX pre

LOCATION	TYPE	MASS FLOW	MOMENTUM		
			x	y	z
Inlet (Stator)	Boundary	2.0956e+2	1.4361e+6	2.9947e-8	3.5599e-9
ROTOR Default (ROTOR)	Boundary	0.0000e+0	9.5085e+1	1.2145e+1	1.8159e+0
opening (Stator)	Boundary	-2.0956e+2	-1.4361e+6	8.7500e-1	2.3805e+0
Copy of Copy of Domain Interface 1 Side 1 (ROTOR)	Domain Interface	-5.9705e-1	7.2923e+0	-4.0403e+0	-7.2403e+4
Copy of Copy of Domain Interface 1 Side 2 (Stator)	Domain Interface	5.9698e-1	7.1260e+0	3.4696e-2	7.2009e+4
Copy of Domain Interface 1 Side 1 (ROTOR)	Domain Interface	-9.1594e-1	9.9217e+0	-6.6869e+0	7.2599e+4
Copy of Domain Interface 1 Side 2 (Stator)	Domain Interface	9.1595e-1	1.1485e+1	3.6583e-1	-7.2386e+4
Domain Interface 1 Side 1 (ROTOR)	Domain Interface	1.5133e+0	-4.4473e+1	8.5850e+1	8.0473e+0
Domain Interface 1 Side 2 (Stator)	Domain Interface	-1.5133e+0	-9.0691e+1	-7.0970e+1	-8.0343e+0

Table 4.19: of CFX Boundary Flow values

➤ Analysis on wind speed of 15 m/s

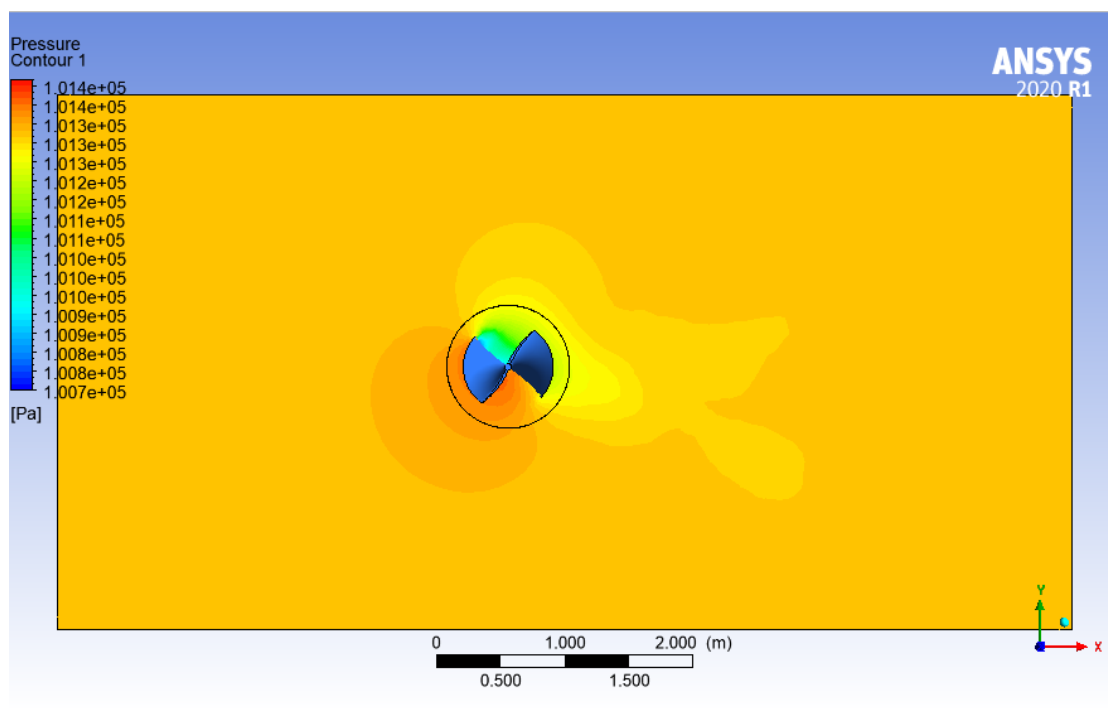


Fig 4.49: Pressure contour (15 rad/s) CFX pre

Maximum Pressure	1.014e+05 Pa
Minimum Pressure	1.007e+05 Pa
Wind speed	15 m/s

LOCATION	TYPE	MASS FLOW	MOMENTUM		
			x	y	z
Inlet (Stator)	Boundary	2.5147e+2	1.4373e+6	9.0128e-9	-3.5166e-8
ROTOR Default (ROTOR)	Boundary	0.0000e+0	9.6394e+1	2.8531e+1	1.7686e+1
opening (Stator)	Boundary	-2.5147e+2	-1.4372e+6	6.2500e-1	3.0203e+0
Copy of Copy of Domain Interface 1 Side 1 (ROTOR)	Domain Interface	-3.5448e-1	6.5442e+0	-9.4750e-1	-7.2792e+4
Copy of Copy of Domain Interface 1 Side 2 (Stator)	Domain Interface	3.5454e-1	5.1262e+0	1.4033e-1	7.2389e+4
Copy of Domain Interface 1 Side 1 (ROTOR)	Domain Interface	-5.4320e-1	7.3702e+0	-1.7697e+0	7.2785e+4
Copy of Domain Interface 1 Side 2 (Stator)	Domain Interface	5.4322e-1	8.2235e+0	6.4579e-2	-7.2381e+4
Domain Interface 1 Side 1 (ROTOR)	Domain Interface	8.9799e-1	-9.2833e+1	9.9202e+1	1.4885e+1
Domain Interface 1 Side 2 (Stator)	Domain Interface	-8.9801e-1	-1.0415e+2	-5.6551e+1	-1.4854e+1

Table 4.20: of CFX Boundary Flow values

➤ **Analysis on wind speed of 17.5 m/s**

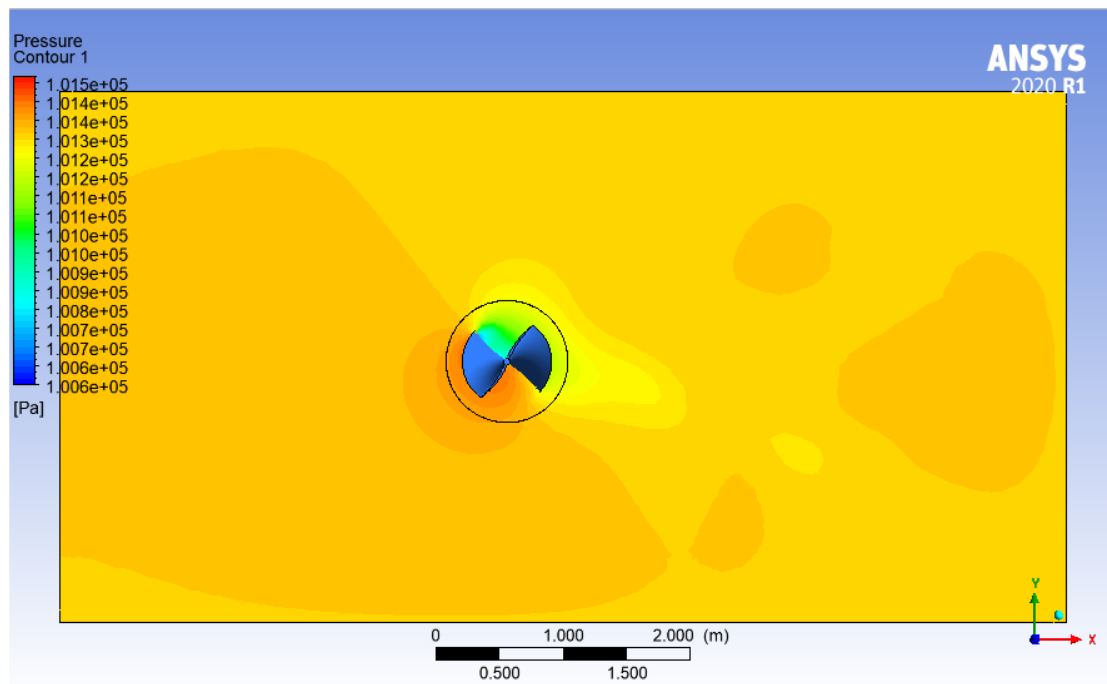


Fig 4.50: Pressure Contour (17.5 Rad/s)

Maximum Pressure			1.015e+05 Pa		
Minimum Pressure			1.006e+05 Pa		
Wind speed			17.5 m/s		
LOCATION	TYPE	MASS FLOW	MOMENTUM		
			x	y	z
Inlet (Stator)	Boundary	2.9338e+2	1.4386e+6	1.5007e-8	-7.7846e-10
ROTOR Default (ROTOR)	Boundary	0.0000e+0	1.4953e+2	8.9405e+0	1.5968e+1
opening (Stator)	Boundary	-2.9338e+2	-1.4386e+6	-5.0000e-1	2.9040e+0
Copy of Copy of Domain Interface 1 Side 1 (ROTOR)	Domain Interface	-7.2841e-1	1.2135e+1	-5.7137e+0	-7.2403e+4
Copy of Copy of Domain Interface 1 Side 2 (Stator)	Domain Interface	7.2844e-1	1.2039e+1	1.4845e-1	7.2009e+4
Copy of Domain Interface 1 Side 1 (ROTOR)	Domain Interface	-9.6595e-1	1.3880e+1	-8.9184e+0	7.2590e+4
Copy of Domain Interface 1 Side 2 (Stator)	Domain Interface	9.6596e-1	1.6979e+1	2.7592e-1	-7.2378e+4
Domain Interface 1 Side 1 (ROTOR)	Domain Interface	1.6944e+0	-9.8772e+1	1.3052e+2	2.1612e+1
Domain Interface 1 Side 2 (Stator)	Domain Interface	-1.6944e+0	-1.5302e+2	-1.0080e+2	-2.1603e+1

Table 4.21: of CFX Boundary Flow values

➤ Analysis on wind speed of 20 m/s

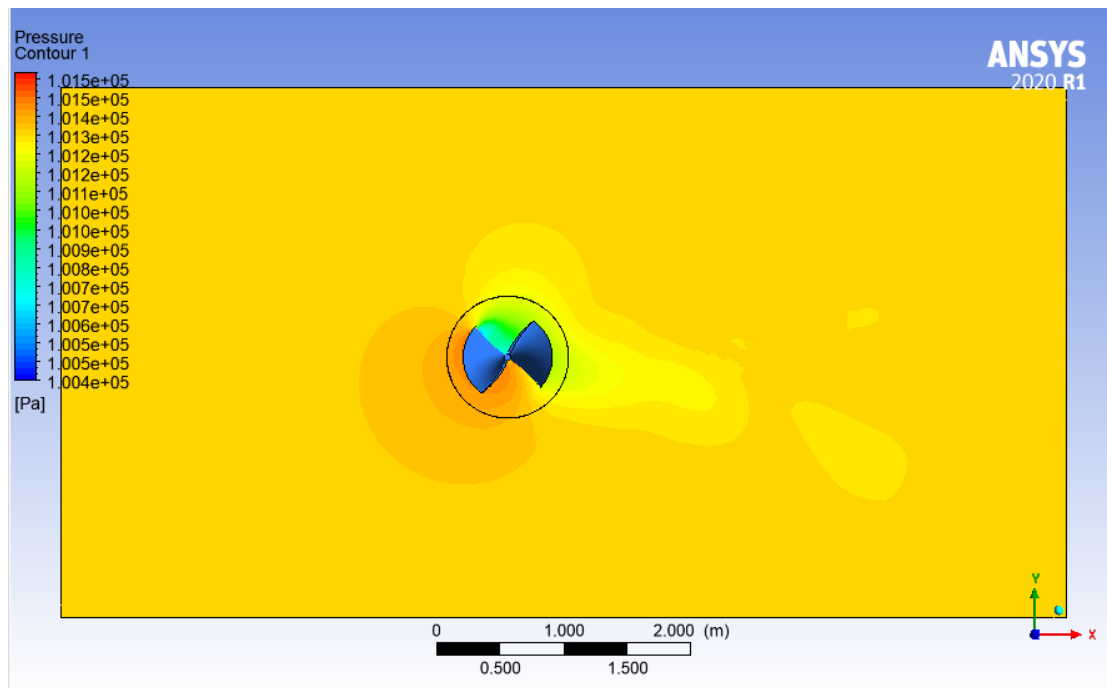


Fig 4.51: Pressure contour (20 m/s)

Maximum Pressure			1.015e+05 Pa		
Minimum Pressure			1.004e+05 Pa		
Wind speed			20 m/s		
LOCATION	TYPE	MASS FLOW	MOMENTUM		
			x	y	z
Inlet (Stator)	Boundary	3.3529e+2	1.4402e+6	2.3829e-8	1.5824e-9
ROTOR Default (ROTOR)	Boundary	0.0000e+0	1.6608e+2	6.9244e-1	2.9311e+1
opening (Stator)	Boundary	-3.3528e+2	-1.4401e+6	-7.1250e+0	-3.1292e+0
Copy of Copy of Domain Interface 1 Side 1 (ROTOR)	Domain Interface	-6.7344e-1	1.3139e+1	-5.6779e+0	-7.2402e+4
Copy of Copy of Domain Interface 1 Side 2 (Stator)	Domain Interface	6.7344e-1	1.3089e+1	1.1586e-1	7.2008e+4
Copy of Domain Interface 1 Side 1 (ROTOR)	Domain Interface	-9.0311e-1	1.4741e+1	-8.7297e+0	7.2583e+4
Copy of Domain Interface 1 Side 2 (Stator)	Domain Interface	9.0309e-1	1.8173e+1	9.2593e-2	-7.2371e+4
Domain Interface 1 Side 1 (ROTOR)	Domain Interface	1.5771e+0	-1.1732e+2	1.6281e+2	2.6428e+1
Domain Interface 1 Side 2 (Stator)	Domain Interface	-1.5771e+0	-1.7585e+2	-9.4047e+1	-2.6392e+1

Table 4.22: of CFX Boundary Flow values

➤ **Analysis on wind speed of 22.5 m/s**

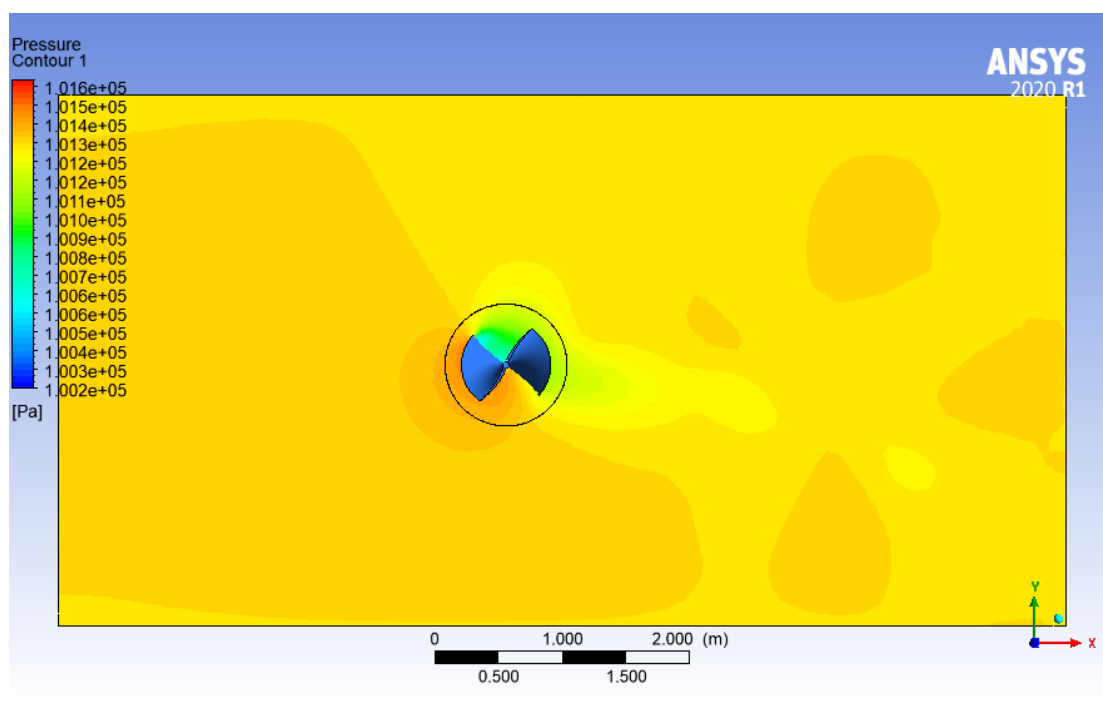


Fig 4.52: Pressure Contour (22.5 m/s)

Maximum Pressure			1.014e+05 Pa		
Minimum Pressure			1.010e+05 Pa		
Wind speed			22.5 m/s		
LOCATION	TYPE	MASS FLOW	MOMENTUM		
			x	y	z
Inlet (Stator)	Boundary	3.7720e+2	1.4420e+6	8.2885e-9	-2.3122e-9
ROTOR Default (ROTOR)	Boundary	0.0000e+0	2.0297e+2	-2.2760e+1	3.4699e+1
opening (Stator)	Boundary	-3.7719e+2	-1.4419e+6	-3.1250e+0	-2.3675e+1
Copy of Copy of Domain Interface 1 Side 1 (ROTOR)	Domain Interface	-8.9018e-1	1.7864e+1	-1.0564e+1	-7.2404e+4
Copy of Copy of Domain Interface 1 Side 2 (Stator)	Domain Interface	8.9020e-1	1.9599e+1	9.1756e-2	7.2010e+4
Copy of Domain Interface 1 Side 1 (ROTOR)	Domain Interface	-1.1252e+0	1.9437e+1	-1.4635e+1	7.2578e+4
Copy of Domain Interface 1 Side 2 (Stator)	Domain Interface	1.1252e+0	2.5442e+1	1.8029e-1	-7.2366e+4
Domain Interface 1 Side 1 (ROTOR)	Domain Interface	2.0170e+0	-1.3269e+2	2.0051e+2	3.2694e+1
Domain Interface 1 Side 2 (Stator)	Domain Interface	-2.0170e+0	-2.2052e+2	-1.1738e+2	-3.2657e+1

Table 4.23: of CFX Boundary Flow values

➤ Analysis on wind speed of 25 m/s

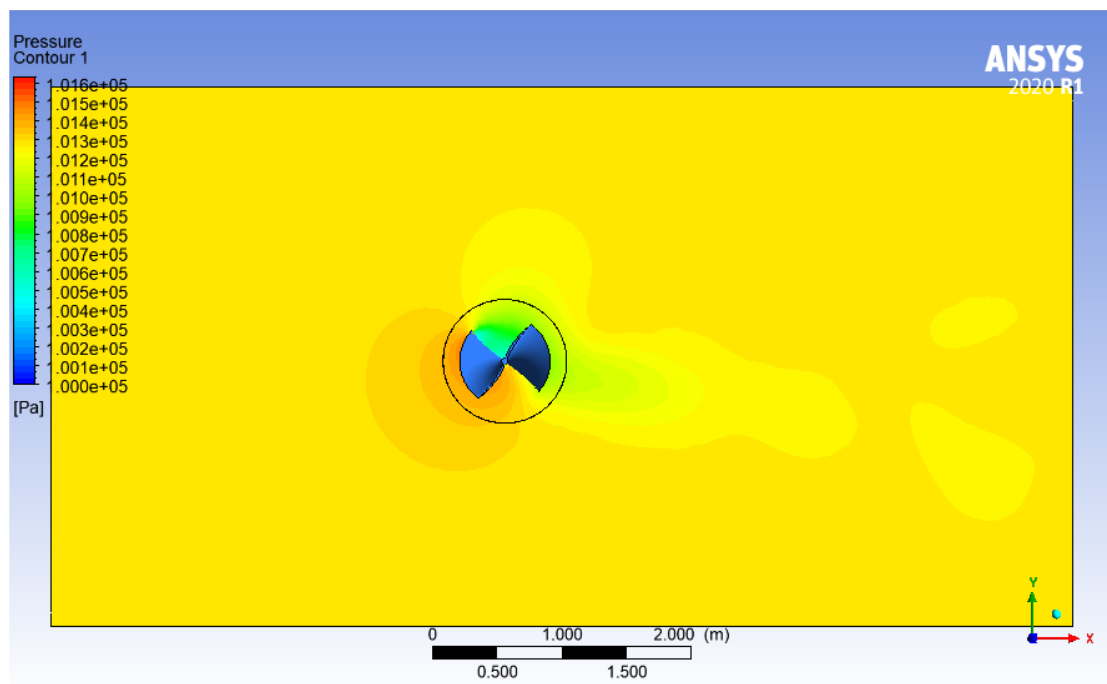


Fig 4.53: Pressure contour (25 m/s)

Maximum Pressure			1.016+05 Pa		
Minimum Pressure			1.000+05 Pa		
Wind speed			25 m/s		
LOCATION	TYPE	MASS FLOW	MOMENTUM		
			x	y	z
Inlet (Stator)	Boundary	4.1911e+2	1.4440e+6	2.1595e-9	-9.5025e-9
ROTOR Default (ROTOR)	Boundary	0.0000e+0	2.2344e+2	-4.3312e+1	4.4722e+1
opening (Stator)	Boundary	-4.1911e+2	-1.4438e+6	7.7625e+1	-5.0579e+1
Copy of Copy of Domain Interface 1 Side 1 (ROTOR)	Domain Interface	-9.9966e-1	2.1995e+1	-1.3153e+1	-7.2404e+4
Copy of Copy of Domain Interface 1 Side 2 (Stator)	Domain Interface	9.9966e-1	2.4590e+1	9.8589e-2	7.2010e+4
Copy of Domain Interface 1 Side 1 (ROTOR)	Domain Interface	-1.1979e+0	2.2738e+1	-1.7281e+1	7.2571e+4
Copy of Domain Interface 1 Side 2 (Stator)	Domain Interface	1.1979e+0	3.0069e+1	5.0931e-2	-7.2358e+4
Domain Interface 1 Side 1 (ROTOR)	Domain Interface	2.1993e+0	-1.4501e+2	2.4955e+2	2.9140e+1
Domain Interface 1 Side 2 (Stator)	Domain Interface	-2.1993e+0	-2.5568e+2	-1.0555e+2	-2.9103e+1

Table 4.24: of CFX Boundary Flow values

❖ **COLLECTIVE RESULT OF MOMENTUM**

SL NO	ANGULAR VELOCITY	WIND SPEED (m/s)	MOMENT			TORQUE (Rotation about z axis)	
			X	Y	Z		
1	10 rad/s (95.493 RPM)	2.5	1.231	4.678	.8718	0.45547	
2		5	20.461	.83100	.72199	7.16135	
3		7.5	25.941	5.489	.53924	9.07935	
4		10	67.467	2.697	-.02869	23.6134	
5		12.5	95.085	12.145	1.8159	33.2797	
6		15	96.394	28.531	17.686	43.5015	
7		17.5	149.29	8.9405	15.968	52.2515	
8		20	166.08	.69244	29.311	58.128	
9		22.5	202.97	202.97	-22.760	34.699	71.0395
10		25	223.44	223.44	-43.312	44.722	78.2040

Table 4.25: Multiple Wind velocities with a constant Angular velocity of 10rad/s

4.2.3 CALCULATING THE EFFICIENCY

As mentioned above the efficiency is calculated according to the value of the Coefficient of Power or C_p

$$\text{Power co-efficient, } C_p = T\omega / \left(\frac{1}{2} \rho AV^3 \right)$$

Taking **12.5 m/s** wind speed as an example;

- Torque T = Moment about x direction * Turbine Radius
 = 95.085 N * .35 m
 = 33.27975 Nm

- Angular velocity $\omega = 10 \text{ rad/s}$
 = 95.493 RPM * Turbine Radius
 = 95.493 * .35
 = 33.42255 m/s

- For constant Wind speed 12m/s
 \Rightarrow Wind power = $0.5 * 1.225 * \text{Blade swept area} * 12.5^3$
 = $0.5 * 1.225 * (.847 * 2) * 12.5^3$
 = 2026.513672 watt.

$$C_p = \frac{33.27957 * 33.42255}{2026.513672} = .548870$$

i.e., Efficiency in terms of Coefficient of power can be expressed as,

$$\text{Efficiency} = 54.88\%$$

Similarly, the efficiencies of all the Analysis are found out:

SL NO	ANGULAR VELOCITY	WIND SPEED (m/s)	MOMENT			TORQUE (Rotation about z axis)	Efficiency
			X	Y	Z		
1	10 rad/s (95.493 RPM)	2.5	1.231	4.678	.8718	0.45547	88.82
2		5	20.461	.83100	.72199	7.16135	22.19
3		7.5	25.941	5.489	.53924	9.07935	69.32
4		10	67.467	2.697	-.02869	23.6134	76.06
5		12.5	95.085	12.145	1.8159	33.2797	54.88
6		15	96.394	28.531	17.686	33.3779	32.20
7		17.5	149.29	8.9405	15.968	52.2515	31.40
8		20	166.08	.69244	29.311	58.128	23.40
9		22.5	202.97	-22.760	34.699	71.0395	20.08
10		25	223.44	-43.312	44.722	78.2040	16.22

Table 4.26: Multiple turbine efficiency with constant Angular velocity of 10rad/s

CHAPTER 5 CONCLUSION

This data analysis on the HELICAL SAVONIUS WIND TURBINE revealed much information about the efficiency of the design. The efficiency will vary in a real-life simulation as some of the characteristics, such as, temperature, irregular airflow, extreme turbulence, humidity etc. were assumed to be in ideal condition, it is also to be noted that the efficiency calculated here is the efficiency of this particular design, this drag type wind turbine still lacks some key features in terms of efficiency but still it can be upgraded. The major advantage of this particular design is that, even though the turbine is drag type, its airfoil inclusion resulted in an increase in efficiency and can endure the stress and strain of normal winds of up-to 25-30 m/s based on our analysis. However, some key parts are to be reinforced such as, the edge of the blade and the area near to that of the shaft as they experience a lot of strain and stress. It should also be noted that the efficiency that we have got here through ANSYS CFX for the wind speed of 2.5 m/s is hypothetical. The reason we believe so is because of how low the adjacent values are. We believe that the cause for this is that because of the fixed angular velocity of 10 rad/s which cannot be achieved by a speed of mere 2.5m/s wind speed.

The graphical depiction of the efficiencies of the wind turbine is as shown below:

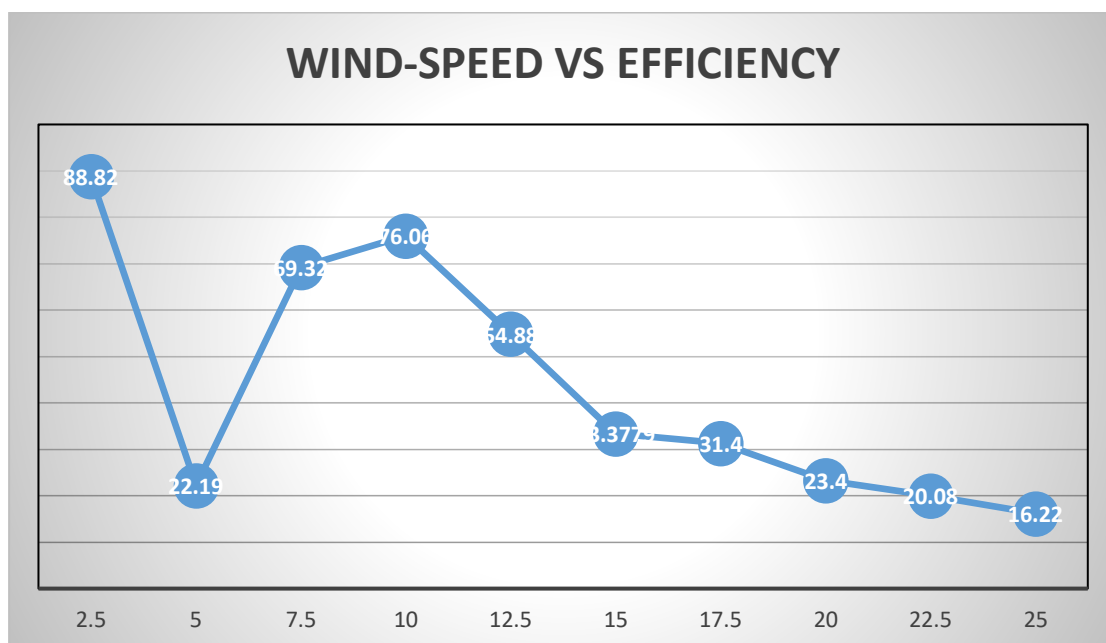


Fig 5.1: Graphical Representation of Efficiency

From the graph we can clearly see that there exists a progressive increment in the wind turbine efficiency from the wind speed of 5m/s to 10m/s and decreases gradually as the speed increases, the reason for such a behavior is because of the fact that the rotation of the turbine which is fixed does not compensate for the wind energy that it receives.

Another observation from these experiments is that, the pressure difference that happens from the maximum to minimum is not that of a huge value, which concludes that, the airfoil addition to this drag type wind turbine helps in maintaining the flow of the wind rather than making it uneven or disruptive.

The loss of efficiency from the velocity point of 12.5 can be minimized by the addition of a gear system which helps in the completer utilization of the rotational energy provided by the wind turbine.

We can conclude that, even though the efficiency of the turbine is not on par with that of Horizontal axis wind turbines, it could still be applicable for small scale uses, like Highways and places where wind velocities are lower than usual, like that of cities and near forest areas with lot of obstructions. The design also gives an aesthetically pleasing value to the environment.

REFERENCES

- [1]. **N.H.Mahmoud, el-Haroun E.Wahba M, H.Nasef**, *An Experimental Study On Improvement Of Savonius Rotor Performance*. September 2012 (journal)
- [2]. **S P Venkitesan, S. Senthamizh Selvan, Yugandhar sai**, *Analysis of The Blade Profile of The Savonius Wind Turbine Using Computational Fluid Dynamics*, May 15 2019 (journal)
- [3]. **Burçin Deda Altan & Mehmet Atılğan**, *A Study on Increasing the Performance of Savonius Wind Rotors*, 20 May 2012 (journal)
- [4]. **B Anggara, I Widiastuti and H Saputro**, *Numerical Study of Savonius Wind Turbine with Additional Fin Blade Using Computational Fluid Dynamic*, 18 April 2018 (journal)
- [5]. **P.Karthikeyan, P.Dineshkumar, R.Gokul, G.Tamilvanan**, *Design And Development Of Enlil Turbine For Highways Electrification*, March 2019 (journal)
- [6]. **Eddahmani Aymane, Dr. Hassan Darhmaoui, Dr. Naeem sheikh**, *Savonius Vertical Wind Turbine: Design, Simulation, And Physical Testing*: May 2017 (journal)
- [7]. **David-Elie Levy and Avraham Seifert**, *Simplified Dragonfly Airfoil Aerodynamics at Reynolds Numbers Below 8000*, 2009 (journal)
- [8]. **Umunna j Reuben, Koju Hiroaki, Miyamoto Shohe**. *Airfoil Considerations in The Design of High Performance, Low Reynolds Number Propellers*: September 2018 (journal)
- [9]. **Young-Moon Kim, Ki-Pyo You, and Jang-Youl You**, *Characteristics of Wind Velocity and Temperature Change Near an Escarpment-Shaped Road Embankment*, 20 July 2014 (journal)
- [10]. **Matej Zadavec and Matjaz Hriberšek**, *The Influence of Rotating Domain Size in A Rotating Frame of Reference Approach for Simulation of Rotating Impeller in A Mixing Vessel*, august 2007 (journal)
- [11]. <https://solidwize.com/wp-content/uploads/2013/07/7-Understanding-the-Wind-Power-Equation.pdf> (Online-journal)